

Section 8d



AFEAS

Alternative Fluorocarbons Environmental Acceptability Study

The West Tower, Suite 400 1333 H Street N.W. Washington, D.C. 20005
• Tel: 202-898-0906 Fax: 202-789-1206 •

24 March 1994

Document Processing Center (TS-790)
Office of Pesticides and Toxic Substances
U.S. Environmental Protection Agency
401 M Street SW
Washington, DC 20460

Contains No CBI

REC'D
OFFICE OF POLLUTION
PREVENTION AND TOXIC
SUBSTANCES
31 MAR 30 PM 2:51

Re: 8(d) Health and Safety Reporting Rule (Notification/Reporting), OPTS-84024A;
FRL-3528-4; Significant New Use Rule and Addition to Health and Safety Data Reporting
Rule, OPTS-50574B; FRL-3743-6

COMPOUND	TSCA CHEMICAL SUBSTANCE INVENTORY NAME	CAS NUMBER
HCFC-21	Methane, dichloro-fluoro-	75-43-4
HCFC-22	Methane, chloro-difluoro-	75-45-6
HCFC-142b	Ethane, 1-chloro-1,1-difluoro-	75-68-3
HFC-152a	Ethane, 1,1-difluoro-	75-37-6
HCFC-133a	Ethane, 2-chloro-1,1,1-trifluoro-	75-88-7
HCFC-123	Ethane, 2,2-dichloro-1,1,1-trifluoro-	306-83-2
HFC-125	Ethane, pentafluoro-	354-33-6
HFC-134a	Ethane, 1,1,1,2-tetrafluoro-	811-97-2
HCFC-132b	Ethane, 1,2-dichloro-1,1-difluoro	1649-08-7
HCFC-141b	Ethane, 1,1-dichloro-1-fluoro-	1717-00-6
HCFC-124	Ethane, 2-chloro-1,1,1,2-tetrafluoro	2873-89-0

86940000213
TO
86940000222

Dear Coordinator:

As required under the subject TSCA 8(d) rule published at 54FR8484, the Alternative Fluorocarbons Environmental Acceptability Study (AFEAS) submits on behalf and at the request of its sponsors the following information on studies to investigate the potential atmospheric environmental effects of the subject 8(d) chemicals. AFEAS is a consortium of 12 fluorocarbon manufacturers organized to fund environmental studies on HCFCs and HFCs. The AFEAS companies are:

AFEAS Member Companies: Akzo Chemicals International BV (Neth.), Allied-Signal Inc. (USA), Asahi Glass Co., Ltd. (Japan), Ausimont S.p.A. (Italy), Daikin Industries, Ltd. (Japan), E.I. du Pont de Nemours & Co., Inc. (USA), Elf Atochem S.A. (France), Hoechst AG (Germany), ICI Chemicals & Polymers, Ltd. (UK), LaRoche Chemicals Inc. (USA), Rhône-Poulenc Chemicals Ltd. (UK), and Solvay S.A. (Belgium).

0 0 0 3

Akzo Chemicals BV
AlliedSignal Inc.
Asahi Glass Co., Ltd.
Ausimont S.p.A.
Daikin Industries, Ltd.
E.I. du Pont de Nemours & Co., Inc.
Elf Atochem S.A. / Elf Atochem North America
Hoechst AG
ICI Chemicals & Polymers, Ltd.
LaRoche Chemicals Inc.
Rhône-Poulenc Chemicals, Ltd.
Solvay S.A.

AFEAS has recently approved for funding the following reportable projects:

- Principal Investigator: T.L. Bott
Stroud Water Research Center, 512 Spencer Road, Avondale, Pennsylvania 19311
Title: Incorporation into Biomass AFEAS Ref. #SP91-18.13/BP93-21
- Principal Investigator: R. Kannuck, P. Rardon, and W. Kenyon
DuPont Haskell Laboratory, P.O. Box 50 Elkton Road, Newark, Delaware 19714-0050
Title: Trifluoroacetic Acid: Terrestrial Plant Toxicity AFEAS Ref. #SP91-18.14/BP93-14
- Principal Investigator: T.L. Bott
Stroud Water Research Center, 512 Spencer Road, Avondale, Pennsylvania 19311
Title: Effects on Normal Acetate Metabolism AFEAS Ref. #SP91-18.15/BP93-20
- Principal Investigator: S.E. Schwarzbach, J.P. Skorupa, and J. Sefchick
U.S. Fish and Wildlife Service, Sacramento Field Office, 3310 El Camino Avenue – Suite 130, Sacramento, California 95825
Title: Review of Evaporative Concentration Potential of Conservative Soluble Tracers in Selected Wetland Systems AFEAS Ref. #SP91-18.16/BP93-22
- Principal Investigator: P. Newman, M.R. Schoeberl, and R.B. Rood
NASA Goddard Space Flight Center, Greenbelt, Maryland
Title: Field Support for the Airborne Southern Hemisphere Ozone Experiment and the Measurements for Assessing the Effects of Stratospheric Aircraft Mission (ASHOE/MAESA) AFEAS Ref. #P93-41b,c

The following AFEAS-sponsored projects have been completed; the final reports are provided for:

- Principal Investigator: O. Rattigan and R.A. Cox **86940000213**
University of Cambridge, Lensfield Road, Cambridge CB2 1EW, UK ✓
Title: Spectra and Photochemistry of Degradation Products of HCFCs and HFCs
AFEAS Ref. #P90-007



AFEAS
Alternative Fluorocarbons Environmental Acceptability Study

0 0 0 4

- Principal Investigator: R. Zellner, A. Hoffmann, V. Mörs, and W. Malm
 Universität Göttingen, 37077 Göttingen, Germany
 Title: Time Resolved Studies of Intermediate Products in the Oxidation of HCFCs and HFCs
 86940000214 AFEAS Ref. #P91-068 ✓
- Principal Investigator: J.M. Lobert, T.J. Baring – University of Colorado, Boulder, Colorado; J.H. Butler, S.A. Montzka, R.C. Myers, and J.E. Elkins – NOAA/CMDL, Boulder, Colorado
 86940000215 AFEAS Ref. #P91-068 ✓
- Principal Investigator: E.C. Tuazon and R. Atkinson, Statewide Air Pollution Research Center, University of California, Riverside, California 92521
 Title: Experimental Investigation of the Products Formed from the Tropospheric Reactions of Alternative Fluorocarbons
 86940000216 AFEAS Ref. #P91-082 ✓
- Principal Investigator: C. George, J.Y. Saison, J.L. Ponche, P. Mirabel
 Université Louis Pasteur, Strasbourg, France
 Title: Kinetics of Mass Transfer of COF₂, CF₃COF, and CF₃COCl at the Air/Water Interface
 AFEAS Ref. #P92-089 ✓
- Principal Investigator: K.-D. Asmus
 Hahn-Meitner-Institut Berlin, Glienicke Strasse 100, D-14109 Berlin, Germany
 Title: Exploratory Study on the Possible Degradation of Trifluoroacetic Acid by Semi-conducting Material
 86940000217
 86940000218 AFEAS Ref. #P93-110 ✓
- Principal Investigator: H. Sidebottom
 University College Dublin, Department of Chemistry, Dublin, Ireland
 Title: STEP-Halocside/AFEAS Workshop on Kinetics and Mechanisms for the Reactions of Halogenated Organic Compounds in the Troposphere
 86940000219 AFEAS Ref. #SP91-15 ✓
- Principal Investigator: R. Thompson
 Brixham Environmental Laboratory, Zeneca Ltd., Brixham, Devon UK
 86940000220
 86940000221
 86940000222
 1. Title: Sodium Trifluoroacetate: Determination of its Effect in Soil on Seed Germination and Early Plant Growth of Wheat
 AFEAS Ref. #SP91-18.6 ✓
 2. Title: Sodium Trifluoroacetate: Determination of its Effect in Soil on Seed Germination and Early Plant Growth of Sunflower and Mung Bean
 AFEAS Ref. #SP91-18.6 ✓
 3. Title: Sodium Trifluoroacetate: Toxicity to Duckweed
 AFEAS Ref. #SP91-18.7 ✓

You may contact me at (202) 898-0906 if you have any questions regarding this submission.

Sincerely,

Katie D. Smythe

Katie D. Smythe
 AFEAS Program Administrator



AFEAS
Alternative Fluorocarbons Environmental Acceptability Study

0 0 0 5

UV Absorption Cross-Sections and Atmospheric Photolysis rates of CCl₃CHO, CCl₂FCHO and CClF₂CHO

O.V. Rattigan, O. Wild and R.A. Cox

Centre for Atmospheric Science, Department of Chemistry, University of Cambridge, Lensfield Road, Cambridge CB2 1EW, UK.

Introduction

Halogenated aldehydes are produced in the degradation of hydrochlorofluorocarbons (HCFC's)¹ which are considered as potential replacements for CFC's. In the atmosphere the removal of these aldehydes can occur in a number of ways including photolysis, reaction with the hydroxyl radical, uptake into clouds followed by rainout and deposition to the ocean. An accurate knowledge of the absorption cross-section is required in order to estimate the photolysis lifetime. In the troposphere temperatures fall with altitude therefore we need to determine the temperature dependence of the absorption cross-section. In this work the absorption cross-sections for CCl₃CHO, CCl₂FCHO and CClF₂CHO have been determined over the wavelength range 200-400 nm at temperatures in the range 298-240 K. The absorption cross-section for CCl₃CHO is in good agreement with previous measurements by Libuda et al.². The values obtained by Gillotay et al.² are higher by approximately 10%. Gillotay et al.³ also determined the temperature dependence of the absorption cross-section for CCl₃CHO.

Experimental

Absorption cross-section measurements were made using a dual beam diode array spectrometer which has been described in detail previously⁴. CCl₃CHO was obtained from Fluka with a stated purity of 99%. CClF₂CHO was prepared by dehydration of the hydrate CClF₂CH(OH)₂ with concentrated sulphuric acid⁵ and collected at 198 K. The infrared spectrum was in excellent agreement with Yamada et al.⁵. CCl₂FCHO was prepared according to the method of Yamada et al.⁶. Heating the polymerised sample provided a vapour pressure of approximately 3.0 Torr at 298 K sufficient for spectral measurements.

Results

(i) Room Temperature

Measurements of CCl₃CHO, CCl₂FCHO and CClF₂CHO absorption spectra were made in the wavelength range 200-380 nm at several pressures in the range 0.20-10.0 Torr. The absorbance showed good agreement with the Beer Lambert Law provided the absorbance was less than 0.80. The absorption cross-section data are shown in Figs. 2-4. All three aldehydes show strong absorption in the region 230-380 nm with maximum absorption cross-sections of 10.4 x 10⁻²⁰ cm² molecule⁻¹.



$13.8 \times 10^{-20} \text{ cm}^2 \text{ molecule}^{-1}$ and $16.4 \times 10^{-20} \text{ cm}^2 \text{ molecule}^{-1}$ for CCl_3CHO , CCl_2FCHO and CClF_2CHO respectively. The band maxima showed a shift to longer wavelengths on substitution of Cl by F.

(ii) Temperature Dependence

Absorption measurements were also made at several temperatures in the range 298-240 K. At each temperature at least 5 spectra were recorded and the data averaged to produce the absorption cross-section at that temperature. The spectra illustrated in Figs. 2-4 show a decline in the cross-section in the long wavelength tail of the absorption band, at wavelengths $> 330 \text{ nm}$, and a corresponding increase in the cross-section around the band maxima with decreasing temperature. The standard deviation on the absolute values for CCl_3CHO at 298 K were approximately 3% for wavelengths $< 340 \text{ nm}$ increasing to 50% near 355 nm. At 243 K the standard deviations were 5% increasing to 50% at 350 nm.

Discussion

The halogenated acetaldehydes show characteristic absorption in the region 240-340 nm with band maxima around 290 nm which is attributed to the $n \rightarrow \Pi^*$ transition of the carbonyl group. However, it appears that substitution of Cl by F shifts the band centre to longer wavelengths. Thus for CCl_3CHO the $n \rightarrow \Pi^*$ band has a maximum at 289.4 nm, in CCl_2FCHO the band centre is at 290.6 nm and in CClF_2CHO the band maximum is at 300 nm. Libuda et al.² have also measured the UV absorption cross-section for CCl_3CHO using a diode array detector. They report a maximum cross-section at 290 nm of $9.73 \times 10^{-20} \text{ cm}^2 \text{ molecule}^{-1}$ in good agreement with a value of $10.4 \times 10^{-20} \text{ cm}^2 \text{ molecule}^{-1}$ from the present work. Gillotay et al.³ determined the absorption cross-section for CCl_3CHO . The shape of the spectrum is in good agreement with the present work although their cross-section at the band centre is higher by approximately 10%. There are no previous measurements of the absorption cross-sections for CCl_2FCHO and CClF_2CHO with which to compare. The shape of the spectra are typical of acetaldehydes. The absorption spectrum for CClF_2CHO shows structure similar to that observed in the spectrum of CH_3CHO ². All three aldehydes showed a distinct variation in the absorption cross-section with temperature, see Figs. 2-4. The decrease in the cross-section in the wings of the absorption bands is compensated for by an increase at the band maxima with declining temperatures due to a reduction in the population of the vibrational and rotational levels of the ground electronic state of the molecules at the lower temperatures⁷. The magnitude of the temperature dependence for CCl_3CHO is in good agreement with recent results by Gillotay et al.³. The best fit to the temperature dependence for the halogenated aldehydes was obtained by plotting $\log_{10} \sigma$ versus temperature using a linear least squares analysis routine. Table 1 shows the room temperature cross-sections for CCl_3CHO together with the recommended temperature coefficients from the present work. Cross-sections at any temperature can then be calculated from the following expression: $\log_{10} \sigma = \log_{10} \sigma_{298} + B[T - 298]$.

Photolysis Lifetimes

The absorption cross-sections for CCl_3CHO , CCl_2FCHO and CClF_2CHO were used to calculate atmospheric photolysis lifetimes. These calculations were carried out

using the Cambridge two dimensional model⁷. Atmospheric conditions appropriate to a Northern Hemisphere Spring were used and assuming a photodecomposition quantum efficiency of unity. Table 2 shows the calculated lifetimes due to photolysis and reaction with OH for conditions appropriate to 30° N and 8.75 km. The results show that photolysis is the major removal process for the halogenated aldehydes in the troposphere for example the photolysis lifetime for CCl₃CHO is approximately a factor of 30 faster than the reaction with the OH radical. In the case of the fluorinated aldehydes CCl₂FCHO and CClF₂CHO photolysis is at least two orders of magnitude faster than reaction with the OH radical. These results indicate that in the troposphere the halogenated aldehydes CCl₃CHO, CCl₂FCHO and CClF₂CHO produced from the photo-oxidation of HCFC's will be removed primarily by photolysis. However, if the photolysis quantum yield is significantly less than unity then the photolysis lifetimes will be longer and reaction with the OH radical may therefore become important. Therefore there is a need to determine accurately the photolysis quantum yield for the halogenated aldehydes.

Acknowledgements

We thank the Alternative Fluorocarbon Environment Acceptability Study (AFEAS) and the UK Department of the Environment for financial support. O.R. thanks the Commission of the European Communities for a post doctoral fellowship award. Thanks are due to Donncha Scollard, University College Dublin, Ireland, for providing the sample of CCl₂FCHO.

References

- 1) Scientific Assessment of Stratospheric Ozone, W.M.O. Report No. 20, Volume 2, (1989).
- 2) H.G. Libuda, F. Zabel, and K.H. Becker, "UV Spectra of some Organic Chlorine and Bromine Compounds of Atmospheric Interest", Paper presented to the STEP-HALOCSIDE/AFEAS Workshop, Dublin, May, (1991).
- 3) D. Gilliotay, P.C. Simon and L. Dierickx, "UV Absorption Cross-Sections of some Carbonyl Compounds and their Temperature Dependence", Paper presented at the Quadrennial Ozone Symposium, University of Virginia, June, (1992).
- 4) O. Rattigan, E. Lutman, R.L. Jones, R.A. Cox, K. Clemitshaw and J. Williams, J. Photochem. Photobiol. A: Chem., **66**, 313, (1992).
- 5) B. Yamada, R.W. Campbell and O. Vogl, J. Polymer Sci., **15**, 1123, (1977).
- 6) B. Yamada, R.W. Campbell and O. Vogl, Polymer Sci., **9**, 23, (1977).
- 7) H. Okabe, "Photochemistry of Small Molecules", Wiley, New York, (1978).
- 8) R.S. Harwood and J. Pyle, Quart. J. Roy. Met. Soc., **103**, 319, (1977).

Table 1 Absorption cross-section data for CCl_3CHO .

Wavelength/nm	$\sigma_{298}/10^{-20} \text{ cm}^2 \text{ molecule}^{-1}$	$B/10^{-4} \text{ K}^{-1}$
200	115.1	3.53
210	48.19	7.66
220	10.92	12.8
230	2.034	38.0
240	0.774	50.5
250	1.827	9.20
260	3.977	1.06
270	6.722	-1.88
280	9.318	-2.32
290	10.32	-2.09
300	9.019	-2.02
310	6.074	1.72
320	3.063	7.63
330	1.121	12.7
340	0.194	39.8
350	0.020	61.2

Note: The B values refer to the temperature dependence obtained from a plot of $\log_{10} \sigma$ versus temperature.

Table 2 Lifetimes due to photolysis and reaction with OH

	J/hrs	$\tau_{\text{OH}}/\text{hrs}$
CCl_3CHO	3.8	130
CCl_2FCHO	1.3	200
CClF_2CHO	<1	270

Calculations were carried out for 30°N and 8.75 km using the Cambridge 2-d model

0009

final report

FINAL REPORT for period 1/7/90-30/6/92

TO SPA-AFEAS INC.

on contract CTR90-2/P90-007

**SPECTRA AND PHOTOCHEMISTRY OF DEGRADATION PRODUCTS OF
HYDROCHLOROFLUOROCARBONS AND HYDROFLUOROCARBONS**

BY

O. RATTIGAN and R.A. COX

UNIVERSITY OF CAMBRIDGE

DEPARTMENT OF CHEMISTRY

LENSFIELD ROAD

CAMBRIDGE CB2 1EW

UK



86940000213

TABLE OF CONTENTS

	PAGE
SUMMARY	2
1. INTRODUCTION	3
2. EXPERIMENTAL DETAILS	4
3. RESULTS	
3.1. Acetyl halides	6
3.2. Halogenated aldehydes	7
3.3. Carbonyl chloride	8
3.4. Formyl fluoride	8
3.5. Peroxyacetyl nitrates	8
3.6. Trifluoroacetic acid	9
3.7. Photo-oxidation of HFC 134a	9
4. DISCUSSION	10
5. ATMOSPHERIC REMOVAL RATES	
5.1. Photolysis Rates	16
5.2. Comparison with removal by OH and hydrolysis	18
6. CONCLUSION	19
REFERENCES	21
TABLES	25
FIGURES	37
Appendix 1	57

SUMMARY

This is the final report for work sponsored by SPA-AFEAS INC., under contract CTR90-2/P90-007 from 1/7/1990 to 30/6/1992 on the Spectra and Photochemistry of the Degradation Products of Hydrochlorofluorocarbons and Hydrofluorocarbons. This report contains the absorption cross-section measurements of

- (1) Acetyl halides; CF_3COCl , CF_3COF and CH_3COF
- (2) Halogenated aldehydes; CCl_3CHO , CCl_2FCHO and CClF_2CHO
- (3) Carbonyl chloride (COCl_2)
- (4) Formyl fluoride (HCOF)
- (5) $\text{CF}_2\text{C}(\text{O})\text{O}_2\text{NO}_2$
- (6) CF_3COOH

It also includes the final progress report for work carried out from 1/4/92-30/6/92 *ie*

- (7) Temperature dependent cross-section measurements of CCl_2FCHO
- (8) Studies on the photo-oxidation of HFC 134a.
- (9) Analysis of spectra and preparation of final report.

Absorption cross-sections for CF_3COCl , CF_3COF , CH_3COF , CF_3COOH , CCl_3CHO , CClF_2CHO , CCl_2FCHO , $\text{CClF}_2\text{C}(\text{O})\text{O}_2\text{NO}_2$, COCl_2 and HCOF have been measured in the wavelength region 200-370 nm, using a dual beam diode array spectrometer. The temperature dependence of the absorption cross-sections was investigated for CF_3COCl , CF_3COF , CCl_3CHO , CClF_2CHO and CCl_2FCHO . Absorption over most of the wavelength range showed a distinct temperature dependence, with a significant decline in the cross-section in the long wavelength tail with decreasing temperature. From the calculated atmospheric photolysis lifetimes it was concluded that in the troposphere photolysis is an important removal process for CF_3COCl , CCl_3CHO , CClF_2CHO , CCl_2FCHO and $\text{CClF}_2\text{C}(\text{O})\text{O}_2\text{NO}_2$ but is unimportant for CF_3COF , CF_3COOH , CH_3COF , HCOF and COCl_2 .

The chlorine initiated photooxidation of HFC 134a ($\text{CF}_3\text{CH}_2\text{F}$) has been studied in the temperature range 235-320 K and 1 atmosphere total pressure using UV absorption. Trifluoroacetyl fluoride (CF_3COF) and formyl fluoride (HCOF) were observed as the

major products. Infrared analysis of the reaction mixture also showed carbonyl fluoride (COF_2) as a major product. By measurement of the yields of HCOF and CF_3COF as a function of oxygen concentration, the rate of the unimolecular decomposition of the alkoxy radical, CF_3CHFO was determined relative to its reaction with O_2 :



Inclusion of other recently published results leads to the following recommended expression for the rate constant ratio k_7/k_8 :

$$k_7/k_8 = 8.7 \times 10^{-26} \exp(4305/T) \text{ cm}^3 \text{ molecule}^{-1}$$

1. INTRODUCTION

Significant increases in the use of selected hydrochlorofluorocarbons (HCFCs) and hydrofluorocarbons (HFCs) are expected to occur over the next few decades following the phase out of CFC's. Unlike the CFC's removal of the HCFCs and HFCs in the troposphere can occur by reaction with the hydroxyl radical¹. Several types of photochemically active products may be formed following the initial attack of the HCFCs¹. Although the reaction of the hydroxyl radical with HCFCs has been the subject of several recent studies²⁻⁵ the subsequent fate of the primary products is still uncertain. Once formed in the troposphere these products may be removed in a number of ways including photolysis, uptake into clouds and subsequent rainout, deposition to the ocean and reaction with the hydroxyl radical¹.

The objective of this study was to determine the UV-visible absorption cross-sections for a number of degradation products of the HCFCs and HFCs, so that their removal due to atmospheric photolysis could be determined. Temperatures in the troposphere decrease by approximately 6-7 K per 1 km rise in altitude. Previous work in this laboratory^{6,7,8} has shown that the UV absorption cross-sections of halogenated carbonyls and aldehydes also vary significantly with temperature. Therefore, in order to accurately estimate the removal rate due to photolysis of the HCFC and HFC oxidation products their UV absorption cross-sections have been determined as a function of temperature.

HFC 134a ($\text{CF}_3\text{CH}_2\text{F}$) is a proposed replacement for difluorodichloromethane (CFC 12) which is widely used as a refrigerant and in air conditioning systems. In the troposphere OH initiated oxidation of HFC 134a leads to the formation of the oxy radical CF_3CHFO . Subsequently, this radical may either react with molecular oxygen to form CF_3COF and HO_2 , (7), or undergo unimolecular decomposition to CF_3 and HCOF , (8):



The primary product distribution from the oxidation of HFC 134a therefore depends on the relative rates of reactions (7) and (8). The UV absorption cross-sections for CF_3COF and HCOF have been measured in this study and this information has been used to determine the yields of these products in the chlorine photosensitized oxidation of HFC 134a^{9,10}. Measurement of the yields as a function of $[\text{O}_2]$ and temperature gave information on the reaction mechanism and enabled a determination of the rate constant ratio k_7/k_8 in the temperature range 235-320 K. During the course of this work a number of other studies of the photooxidation of HFC 134a have been carried out¹¹⁻¹⁴ which have greatly aided in the understanding of the complex reaction scheme and in the determination of the kinetic parameters.

Recently, the results from this work have been used in two-dimensional numerical model studies^{9,15} and the fraction of CF_3COF (which may subsequently hydrolyse to trifluoroacetic acid) formed from the degradation of HFC 134a in the troposphere has been calculated⁹.

2. EXPERIMENTAL

2.1. Apparatus

The apparatus, illustrated schematically in Fig. 1, consisted of a dual beam diode array spectrometer. A collimated beam from a deuterium lamp (Hamamatsu 30 watt, L 1636) was passed through a beam splitter (Oriel Scientific, model 78150) and the two beams (reference and sample) were collected in optical fibre couplers (Oriel Scientific model 77800) either directly (reference) or after passage through a 1 meter long jacketed quartz cell (sample). The temperature of the cell could be regulated in the range 298-230 K by

0 0 1 4

flowing ethanol through the inner jacket from a thermostatically controlled cooling unit. Evacuated double-end window assemblies prevented frosting on the optical faces at the low temperatures. The light beams from the two optical fibres were directed one above the other into the 500 μm wide inlet slit of a 275 mm Czerny-Turner spectrograph (Acton Research Corporation 'Spectropro 275') using an optical fibre adapter (Princeton Instruments model OFA X1.5). The spectrograph contained three indexable holographic gratings mounted on a turret under direct software control. Generally a 600g/mm grating giving a spectral resolution of 1.2 nm and a spectral range of 75 nm was used to disperse the beams onto two 512 channel unintensified silicon diode arrays (Reticon). However, in the case of HCOF a 2400g/mm grating with a spectral resolution of 0.3 nm (FWHH) was also used and a 150g/mm grating with a spectral resolution of 3.0 nm (FWHH) and a spectral range of 300 nm was used to record spectra for $\text{CF}_2\text{ClC(O)O}_2\text{NO}_2$. The detector function was controlled by an SI-180 O-SMA detector controller (Spectroscopy Instruments GmbH) which incorporated a 14 bit ADC coupled to a Dell 316SX computer. Software packages were used for linearisation of the wavelength scale, for background subtraction and averaging of the data and for calculation of the absorbance using the reference spectrum to correct for changes in the source lamp intensity. The main limitation in the accuracy in the absorbance measurements was the drift with time of the baseline, due apparently to inhomogeneities in the source output affecting the reference and sample beams differently. This limited the accuracy of measurements to ± 0.0005 absorbance units, corresponding to a cross-section of approximately $10^{-23} \text{ cm}^2 \text{ molecule}^{-1}$ for the partial pressures used.

Gases were introduced to the sample cell from a conventional Pyrex glass vacuum line, fitted with Youngs greaseless taps. Pressures were measured on calibrated Baratron gauges (100 Torr MKS 222 A or 1000 Torr MKS 122 AA).

2.2. Preparation of samples

CF_3COCl (97%), CF_3COF (97%), CH_3COF (97%) and CF_3COOH (99.5%) were obtained from Fluorochem Ltd. COCl_2 (99%) was obtained from Matheson. CCl_3CHO was obtained from Fluka with a stated purity of 99% but contained traces of the hydrate $\text{CCl}_3\text{CH(OH)}_2$. It was transferred under a nitrogen atmosphere to a trap on the vacuum line. All the samples were degassed and trap to trap distilled prior to use. The spectrum for CH_3COF was found to change with time, possibly due to hydrolysis on the cell walls to form acetic acid. A fresh sample was used each time for absorption measurements. Because

0 0 1 5

of this instability the temperature dependence of the absorption cross-section was not investigated.

CClF_2CHO was prepared by dehydration of the hydrate $\text{CClF}_2\text{CH}(\text{OH})_2$ with concentrated sulphuric acid¹⁶ and collected at 198 K. Several successive distillations of the product were carried out. The infrared spectrum was in excellent agreement with Yamada et al.¹⁶.

A sample of CCl_2FCHO polymer was obtained from Howard Sidebottom, University College Dublin. The sample was prepared according to the method of Yamada et al.¹⁷. Heating the polymer provided a vapour pressure of approximately 3.0 Torr at 298 K sufficient for spectral measurements.

Formyl fluoride was prepared by the reaction of formic acid with benzoyl chloride using dry KHF_2 at 333 K¹⁸. The formyl fluoride was first purified by passing through a trap at 255 K to remove benzoyl chloride vapours and then trapped at 78 K. Several successive distillations of the formyl fluoride were carried out. The IR spectrum was in excellent agreement with that of Morgan et al.¹⁹.

3. RESULTS

3.1. Acetyl halides

3.1.1. Room Temperature

Measurements of CF_3COCl , CF_3COF , CH_3COF were made in the wavelength range 200-370 nm at pressures in the range 0.20-20.0 Torr. The absorbance showed good agreement with the Beer Lambert Law provided the absorbance was < 0.80 . Inaccuracies in the cross-section measurements in the short wavelength region (< 220 nm) arose because of the low light levels transmitted by the optical fibres at shorter wavelengths. In the longer wavelength region, at vapour pressures > 10 Torr, a small residual absorbance (< 0.001 Absorbance units) was detected for all the samples up to 370 nm which generally increased with increasing partial pressure. This was thought to be due to the presence of a low level of scattered UV light of shorter wavelengths scattered within the spectrograph and was therefore subtracted out from all the spectra. Absorption cross-section data are illustrated in Figs. 2-4. Absolute cross-sections averaged over 5 nm intervals are shown in Tables 1-3.

CF₃COCl has a strong absorption band in the 200-215 nm region and a second somewhat weaker broad absorption band between 215 and 330 nm with a maximum absorption cross-section at 255 nm of $6.80 \times 10^{-20} \text{ cm}^2 \text{ molecule}^{-1}$, (Fig. 2). CF₃COF has a broad absorption band between 200 and 300 nm with a maximum absorption cross-section at 214 nm of $13.8 \times 10^{-20} \text{ cm}^2 \text{ molecule}^{-1}$, (Fig. 3). CH₃COF appears to have two overlapping absorption bands in the UV, the first one with a maximum absorption cross-section at 207 nm of $12.4 \times 10^{-20} \text{ cm}^2 \text{ molecule}^{-1}$, and a second band appearing as a shoulder near 260 nm and extending out to 310 nm (Fig. 4).

3.1.2. Temperature Dependence

Absorption measurements of CF₃COCl and CF₃COF were also made at several temperatures in the range 298-233 K. At each temperature at least five spectra were recorded and the data averaged to produce the absorption cross-section at that temperature. The spectra show a definite temperature dependence for both molecules. The spectra for CF₃COCl show a decline in the cross-section over the absorption band 215-330 nm, the decline being more pronounced in the long wavelength tail at wavelengths > 290 nm. The temperature dependence also extends into the shorter wavelength region of the spectrum particularly at wavelengths < 215 nm (Fig 2). In the case of CF₃COF the decline is apparent in the wings of the absorption band, the cross-sections show an increase with decreasing temperature around the band maximum (Fig. 3). A more detailed investigation was undertaken for CF₃COCl. Measurements of the cross-section were carried out at six different temperatures in the range 296 K to 227 K. Fig. 5 shows a plot of log₁₀ (cross-section) versus temperature (K) in the wavelength range 290-315 nm. The data shows a good linear fit over the entire temperature range. The slopes of the plots increase with increasing wavelength reflecting the increased temperature dependence at the longer wavelengths.

3.2. Halogenated aldehydes

3.2.1. Room Temperature

Measurements of CCl₃CHO, CCl₂FCHO and CF₂ClCHO absorption spectra were made in the range 200-380 nm at several pressures in the range 0.20-10.0 Torr at room temperature. The absorbance showed good agreement with the Beer Lambert Law provided the absorbance was less than 0.80. A plot for CF₂ClCHO is illustrated in Fig. 6. The

absorption cross-section data are shown in Figs. 7-9. Absolute cross-sections averaged over 5 nm intervals are listed in Tables 4-6. All three aldehydes show strong absorption in the region 230-380 nm with a maximum absorption at 289 nm for CCl_3CHO , 290 nm for CCl_2FCHO and 300 nm for CClF_2CHO . The magnitude of the cross-section at the absorption maximum increased on substitution of Cl by F, see Tables 4-6.

3.2.2. Temperature Dependence

Absorption measurements were also made at several temperatures in the range 298-240 K. At each temperature at least 5 spectra were recorded and the data averaged to produce the absorption cross-section at that temperature. Figs. 7-9 illustrate the temperature dependence of the cross-sections for CCl_3CHO , CCl_2FCHO and CClF_2CHO . The spectra show a small but definite temperature dependence. The spectra show a decline in the cross-section at the long wavelength tail of the absorption band, at wavelengths > 330 nm and a corresponding increase around the band maxima with decreasing temperature.

3.3. Carbonyl chloride (COCl_2)

COCl_2 absorbs strongly in the 200-215 nm region and has a second weaker broad absorption band from 215-305 nm with a maximum absorption cross-section at 233 nm of $13.7 \times 10^{-20} \text{ cm}^2 \text{ molecule}^{-1}$ (Fig. 10).

3.4. Formyl fluoride (HCOF)

Absorption measurements were made in the wavelength range 220-280 nm using a 600g/mm grating with a spectral resolution of 1.2 nm (FWHH). The spectrum shows fine structure in this region and is illustrated in Fig. 11. Absorption measurements were also carried out at several temperatures in the range 298-230 K. The absorption cross-section did not show any variation with temperature. A spectrum was also recorded using a 2400g/mm grating with a spectral resolution of 0.3 nm (FWHH) and is shown in Fig. 12.

3.5. Peroxyacetyl nitrates

Preparation of the peroxy nitrates $\text{CF}_3\text{CCl}_2\text{O}_2\text{NO}_2$ and $\text{CFCl}_2\text{CH}_2\text{O}_2\text{NO}_2$ was attempted by the chlorine initiated photooxidation of HCFC 123 and HCFC 141b respectively in the presence of NO_2 . Complications occurred due to the reaction of Cl with NO and NO_2 and

the halogenated products. This appeared to be due to the slow reactions of Cl with the HCFCs²⁰. Experiments were then carried out using the aldehyde CF₂ClCHO in order to obtain a spectrum of CF₂ClC(O)O₂NO₂. Experiments were carried out at room temperature with the ratio of [CF₂ClCHO]/[NO₂] of approximately 5.0 so as to minimise the formation of ClNO₂. A 150g/mm grating with a spectral range of 300 nm and a spectral resolution of 3.0 nm (FWHH) was used. The residual spectra were obtained after stripping of absorbances due to Cl₂, CF₂ClCHO, NO₂ and ClNO₂. Absorption cross-sections for CF₂ClC(O)O₂NO₂ were calculated based on the amount of NO₂ consumed. The spectrum is illustrated in Fig.13. However there is considerable uncertainty in the absolute cross-section (Table 9) and the spectral shape because of the need to correct for several absorbing species.

3.6. Trifluoroacetic acid

CF₃COOH exhibits a single absorption band with a broad maximum near 215 nm and extending out to approximately 275 nm (Fig. 14). Absolute cross-sections averaged over 5 nm intervals are shown in Table 10.

3.7. Photooxidation of HFC 134a

For the photooxidation study mixtures of CF₃CH₂F (8-12 Torr), Cl₂ (1.0 Torr, 5% in N₂) and O₂ (20-730 Torr) were made up to a total pressure of 760 Torr using N₂ (17-731 Torr) and premixed for several hours. Irradiation in the wavelength range 300-400 nm using Philips TL/09 Lamps was used to drive the Cl atom initiated photooxidation of HFC 134a. At regular time intervals prior to and during this photolysis, UV spectra of the reaction mixture were recorded. Fig.15 shows three sequential spectra taken following 111, 171 and 243 seconds of irradiation. As can be seen from these spectra, there is a buildup of absorption around 230 nm, attributable to product formation and a reduction of absorption around 300 nm attributable to chlorine consumption, with increasing irradiation time.

Spectral stripping routines were applied to the sequential spectra for the identification and quantification of products formed during the photooxidation. CF₃COF and HCOF reference spectra reported above were used, accounting for the temperature dependence of the CF₃COF spectrum. However, owing to the very weak UV absorption at wavelengths available to this study of HFC 134a, consumption of the hydrofluorocarbon could not be monitored. Yields of the two main products were therefore expressed in terms of the

molecular chlorine consumed, given that the experimental conditions were arranged such that chlorine atoms were converted stoichiometrically into CF_3CHFO_2 radicals. Chlorine cross-sections were taken from the current NASA evaluation²¹. A graph of product formation against chlorine consumption gave the chlorine based yield as the gradient, and the small non-zero intercept, where present, was attributed to differential baseline shifting of the sample and reference beams and neglected. Errors on individual yields were taken from these graphs and combined with a $\pm 5\%$ uncertainty in cross-sections. Typically, this resulted in a total error on the yield of $\pm 8\%$. Following spectral stripping of Cl_2 , HCOF and CF_3COF , the baseline of UV absorption showed no additional significant absorbance.

Experiments were carried out at four different temperatures in the range 320-235 K and at various oxygen partial pressures. Chlorine based yields of HCOF and CF_3COF obtained are shown in Table 12. As can be seen from Table 12, with the exception of the 235 K data, the combined yield of CF_3COF and HCOF is in excess of the amount of chlorine consumed (ie the total product yield > 2.0). Not all spectra were analysed for the CF_3COF yield, however, since this quantity proved to be difficult to ascertain and of limited use in extracting branching ratios. This is discussed further below.

In addition to the UV yield analysis, qualitative experiments to determine the composition of the reaction mixture following photolysis were carried out using IR spectroscopy. A spectrum of a typical photolysed mixture of HFC 134a, Cl_2 , O_2 and N_2 is shown in Fig.16. In addition to the major products, absorptions attributable to COF_2 , HF and SiF_4 were observed. The yield of HCOF was found to agree with that observed in the UV.

4. DISCUSSION

4.1. UV Absorption cross-sections

4.1.1. Room Temperature

The absorption spectra of the halogenated carbonyls CX_3CXO show strong absorption in the UV, and by analogy with the aldehydes and ketones, bands due to the $n \rightarrow \pi^*$ electronic transition of the $\text{C}=\text{O}$ group are expected. It appears that substitution of the halogen on the carbonyl carbon $\text{X}-\text{C}=\text{O}$ has the effect of shifting the absorption to shorter wavelengths. In CH_3COF , Fig. 4, the $n \rightarrow \pi^*$ band appears as a shoulder at 260 nm on the more intense absorption band centred around 208 nm. This may be compared to CH_3CHO

where the $n \rightarrow \Pi^*$ band centre is at 290 nm²². Substitution of the halogen on the *B*-*C* atom also modifies the absorption spectrum significantly. Thus CF_3COCl , Fig. 2, has an absorption band, believed to be due to the $n \rightarrow \Pi^*$ transition, centred at 255 nm whereas in CF_3COF , Fig. 3, the band is blue shifted to 214 nm. In the halogenated aldehydes the band centre is around 290 nm. However it appears that substitution of Cl by F shifts the band centre to longer wavelengths⁷. Thus CCl_3CHO , Fig. 5, the $n \rightarrow \Pi^*$ band has a maximum at 289 nm, in CCl_2FCHO the maximum is at 291 nm and in CClF_2CHO the band maximum is at 300 nm. Libuda *et al.*²² and Gillotay *et al.*²³ have recently measured the UV absorption spectrum for CCl_3CHO . Libuda *et al.*²² used a diode array detector and report a maximum cross-section of $9.73 \times 10^{-20} \text{ cm}^2 \text{ molecule}^{-1}$ at 290 nm compared to $11.6 \times 10^{-20} \text{ cm}^2 \text{ molecule}^{-1}$ at 288 nm obtained by Gillotay *et al.*²³ in a dual-beam apparatus with a photomultiplier detector system. Our value of $10.4 \times 10^{-20} \text{ cm}^2 \text{ molecule}^{-1}$ at 289 nm is approximately midway between these two measurements.

The COCl_2 spectrum shows two overlapping absorption bands indicating that two or more electronic transitions are involved. The more energetic one is possibly due to a $\Pi \rightarrow \Pi^*$ transition and the band centred at 233 nm and extending out to 305 nm possibly due to the $n \rightarrow \Pi^*$ of the C=O bond. The absorption cross-sections are in good agreement with earlier workers^{24,25} and also with the more recent measurements of Gillotay *et al.*²³ and Meller *et al.*²⁶.

HCOF shows considerable fine structure in the UV absorption spectrum from 220 to 260 nm. The UV absorption spectrum shows good agreement with previous measurements by Giddings and Innes²⁷ although there is some ambiguity concerning the absolute magnitude of their cross-section data. Similar structure has been observed in the UV spectra for HCOCl ²⁸ and HCOH ²⁹ which is likely due to the resolution of vibrational structure in these simple molecules. The band centre shows a shift to shorter wavelengths in the series HCOH , HCOCl , HCOF possibly reflecting the increased electronegativity trend. This is in contrast to the aldehydes where the band maximum shows a shift to longer wavelengths with increased fluorination.

Meller *et al.*²⁶ also measured the UV absorption cross-sections of CF_3COCl and CF_3COF at room temperature. Their results are in excellent agreement with the data from the present study. Jemi-Alade *et al.*³⁰ have measured the absorption spectrum of CF_3COCl between 220 and 290 nm, as part of their work on the chlorine initiated oxidation of hydrohalocarbons. The shape of their absorption spectrum closely resembles that obtained in the present work, and they report a cross-section of $6.72 \times 10^{-20} \text{ cm}^2 \text{ molecule}^{-1}$ at 250

nm which is in excellent agreement with a value of $6.80 \times 10^{-20} \text{ cm}^2 \text{ molecule}^{-1}$ from the present work.

There are no previous spectra for $\text{CF}_2\text{ClC}(\text{O})\text{O}_2\text{NO}_2$ with which to compare. However the spectrum is typical of a peroxyacetyl nitrate with a steady increasing absorption towards shorter wavelengths and a cut off at 310 nm. Compared to peroxyacetyl nitrate³¹ the cross-sections are approximately a factor of 2 larger at wavelengths $< 260 \text{ nm}$ increasing to almost a factor of 10 at 300 nm.

Basch *et al.*³² previously recorded the absorption spectrum of CF_3COOH at 298 K as part of their work on the electronic spectra of a series of amides, acids and acyl fluorides. They observed two distinct spectra depending on the vapour pressure used. At low pressures of about 1 Torr a sharply structured spectrum characteristic of the monomer was observed, whereas at relatively higher pressures, the spectrum consisted of a broad continuous band with a maximum around 210 nm. The shape of their second spectrum closely resembles that obtained in the present study and at the pressures of around 10 Torr used in this work our spectrum is probably due to the dimer species. Basch *et al.*³² have not reported absolute UV cross-section data for CF_3COOH however, from their published spectrum we estimate a cross-section of $1.12 \times 10^{-19} \text{ cm}^2 \text{ molecule}^{-1}$ at the band maximum for the dimer species. This is approximately 40% larger than our measured value of $7.8 \times 10^{-20} \text{ cm}^2 \text{ molecule}^{-1}$.

4.1.2. Temperature dependencies

CF_3COCl , CF_3COF , CCl_3CHO , CF_2ClCHO and CFCl_2CHO all showed a significant variation in the absorption cross-section with temperature, Figures 2, 3 and Figures 7-9, which was different for all the compounds. The variation was more pronounced in the long wavelength tail but the temperature dependence also extended into the shorter wavelength absorption bands, Figures 2 and 7. Gillotay *et al.*²³ have recently measured the temperature dependence of the UV cross-sections for COCl_2 , CCl_3COCl and CCl_3CHO . They observed similar temperature dependencies of the cross-sections in all cases i.e. a decrease in the cross-section with decreasing temperature in the tail of the absorption bands whereas only a relatively minor change in the cross-sections with temperature was observed at the band maxima. The magnitude of the temperature dependence for CCl_3CHO matches well with that of the present study.

For CF_3COCl a more detailed study of the temperature dependence of the absorption cross-section between 296 K and 227 K was undertaken. The temperature dependence for

CF₃COCl is illustrated in Fig. 5 where log₁₀ σ is plotted against temperature for selected wavelengths in the tail of the UV absorption band. The intercepts and slopes of these plots, obtained by linear regression analysis, are given in Table 11. In general the slopes of these plots, B values, increase with increasing wavelength reflecting the increased importance of the temperature dependence at longer wavelengths.

The temperature coefficients obtained from the plot of log₁₀ σ vs T can be used to obtain cross-sections outside the experimental range by extrapolation. This is particularly important for the purposes of calculating the photodissociation rate of CF₃COCl at temperatures relevant to the upper atmosphere. The linearity in the plot in Fig. 5 suggests that the cross-section can be calculated for any temperature from the equation:

$$\log_{10} \sigma = \log_{10} \sigma_{298} + B[T-298]$$

It is believed that the decrease in cross-section with decreasing temperature is due to a reduction in the population of the vibrational and rotational levels of the ground electronic state of the molecule at the lower temperatures³³. The total integrated absorption in a single band remains constant, the decrease in the cross-section in the wings of the absorption band is compensated for by an increase at the band maximum. This is apparent in CF₃COF, CCl₃CHO, CF₂ClCHO and CFCl₂CHO, Fig. 3 and Figs. 7-9, where there is little overlap of the two absorption bands, but not in CF₃COCl, Fig. 2, due to the predominant influence of the tail of the strong absorption band centred at < 200 nm. A similar effect has been observed in the spectra for HNO₃ and CH₃ONO₂³⁴ which also have two overlapping absorption bands.

4.2. Photooxidation of HFC 134a

On photolysis of CF₃CH₂F/Cl₂/O₂ mixtures the following reactions take place:



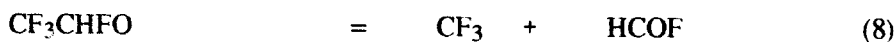
The experimental conditions were selected such that rapid conversion of the alkyl radical, CF_3CHF , into peroxy radicals CF_3CHFO_2 ensued, reaction (3). The peroxy radicals then self-react leading to the formation of molecular products or CF_3CHFO radicals.



Reaction of CF_3CHFO_2 with NO (6) has been found to be rapid^{35,36} and in the troposphere it is likely to dominate over the self-reaction.



The alkoxy radicals, CF_3CHFO , produced in the above reactions may either react with oxygen, or undergo unimolecular decomposition:



The final product distribution reflects this branching. Analysis of the measured product yields in terms of the CF_3CHFO rate constant ratio k_7/k_8 was carried out using two separate techniques⁹.

4.2.1. Arithmetic derivation of k_7/k_8

The branching ratio for the nonterminating channel of the CF_3CHFO_2 radical self-reaction is defined as $\alpha = k_4/(k_4 + k_5)$. Similarly, the branching ratio for the CF_3CHFO radical reaction with oxygen is defined as β .

$$\beta = k_7[\text{O}_2] / (k_7[\text{O}_2] + k_8)$$

The existence of total product yields in excess of the chlorine consumption in the present study (see Table 12) is evidence for the further production of these products via secondary chemistry or the regeneration of Cl_2 . Wallington et al³⁷ have shown that CF_3O radicals

0 0 2 9

react with HFC 134a in this photooxidation to form CF_3OH and with excess HFC 134a (10 Torr) used in the present study this is the most probable fate of CF_3O leading to the regeneration of CF_3CHFO_2 radicals.



This reaction thus leads to the production of CF_3CHFO_2 radicals without the concomitant consumption of Cl_2 . CF_3OH was observed to decay in the dark to give COF_2 and HF³⁷; products observed in the IR spectrum of the photolysed mixture in the present study.



and the reaction of HF with the cell walls is the most probable source of SiF_4 .

A chain reaction is therefore taking place, wherein both products CF_3COF and HCOF are formed and CF_3CHFO_2 is regenerated. A relationship between the yield of HCOF and α and β was derived:

$$1/y(\text{HCOF}) = \{(1+\alpha)/2\alpha\}[\text{O}_2] \{k_7/k_8\} + \{(1-\alpha\theta)/2\alpha\}$$

where θ is the fractional efficiency of production of CF_3O radicals from CF_3 .

A plot of $1/y(\text{HCOF})$ vs $[\text{O}_2]$ at 293 K is shown in Fig 17 which shows good linearity and lends confidence to the analysis technique. Using values of α from the work of Wallington et al ¹¹, values of θ and k_7/k_8 have been calculated.

A similar approach was taken to try to quantify the CF_3COF yield in terms of α and β . However, unlike HCOF , this compound is formed in small amounts in a number of different channels in the photooxidation of HFC 134a. The sensitivity of the yield to changes in α and β is consequently reduced. Furthermore, because of the difficulties in stripping the smooth spectrum of this compound off the composite UV spectrum of the products the uncertainty in the CF_3COF yield was somewhat larger than that in HCOF , where its structured spectrum greatly facilitates spectral stripping. Hence no meaningful estimates of branching ratios could be produced from the CF_3COF yields.

0 0 2 5

4.2.2. Kinetic Modelling

A computer simulation of the experimental system was also carried out using the FACSIMILE program. The kinetic model used was based on a reaction mechanism similar to that used by Wallington *et al.*¹¹.

The unknown rate coefficients, k_8 (unimolecular decomposition of CF_3CHFO) and k_1 (the rate of Cl_2 photolysis) were obtained by fitting computer-generated concentration-time data for Cl_2 , HCOF , CF_3COF and other products, to experimental data obtained in 16 experiments covering a range of temperatures and O_2 partial pressures. The values of k_8 obtained from the simulation are plotted in Arrhenius form in Fig 18 and are listed in table 13, together with the data from the arithmetic treatment. The agreement between the values obtained from the two methods is good.

Table 13 shows the Arrhenius parameters for reaction (8) obtained from the various studies. The unimolecular decomposition k_8 was calculated in each case using the expression: $k_7 = 6.0 \times 10^{-14} \exp(-925/T) \text{ cm}^3 \text{ molecule}^{-1} \text{ s}^{-1}$ as used in this study. All values except those of Maricq and Szente¹² are close to the high pressure limit according to the data of Wallington *et al.*¹¹ Nevertheless the A-factors are all significantly lower than the typical value of $10^{13} - 10^{14} \text{ s}^{-1}$, expected for a radical decomposition at the high pressure limit³⁸. This suggests that the reaction may not be as close to the high pressure limit as the data of Wallington *et al.*¹¹ indicate. Further experimental investigation of the pressure dependence is clearly needed to establish this.

The recommended expression $k_8 = 6.9 \times 10^{-11} \exp(-4960/T) \text{ s}^{-1}$ in Table 13 is based on the mean of the experimental values at 293 K and the E/R values from Wallington *et al.*¹¹, Tuazon and Atkinson¹³ and the present work, excluding the data at 235 K. The temperature dependence obtained from the present work if the 235 K data are included, and from the lower pressure data of Maricq and Szente¹², both lead to unrealistically low A-factors and are therefore not included in the evaluation.

5. ATMOSPHERIC REMOVAL RATES

5.1. Photolysis Rates

Photodissociation of the HCFC degradation products is possible following absorption in their UV absorption spectra. The solar radiation is strongly attenuated in the UV at

wavelengths 220-290 nm by absorption due to ozone. Two spectral regions therefore play a major role in the photolysis of the HCFC and HFC oxidation products. The first region, around 200 nm becomes more important at higher altitudes, above 25 km, whereas the second region > 290 nm is dominant below 20 km³⁹. Fig. 19 shows a plot of solar flux⁴⁰ versus wavelength at 300 mbar (upper troposphere) which clearly illustrates that wavelengths greater than 290 nm have the major contribution to photolysis in the troposphere.

CF₃COF, CH₃COF, HCOF, COCl₂ and CF₃COOH, (Tables 2,3,7,8 and 10), absorb strongly in the middle UV with little or no significant absorption beyond 300 nm. Therefore, photodissociation is likely to be unimportant for these compounds in the troposphere. However, CF₃COCl and the halogenated aldehydes have significant absorption at wavelengths > 300 nm, (Tables 1, 4-6), and photodissociation is a potentially important removal process.

The absorption cross-section measurements were used to calculate atmospheric photolysis lifetimes for CH₃COF, CF₃COF, CF₃COCl, CF₃COOH, CCl₃CHO, CCl₂FCHO and CF₂ClCHO. These calculations were carried out using the Cambridge two-dimensional model⁴¹. An albedo of 0.35 was used and a photodecomposition quantum efficiency of unity was assumed.

Table 14 shows the tropospheric lifetimes with respect to photolysis, reaction with OH and physical removal for CH₃COF, CF₃COF, CF₃COOH, CF₃COCl and CCl₃CHO. The photolysis lifetimes for CH₃COF, CF₃COF and CF₃COOH are relatively long *eg* CH₃COF 41 yrs, CF₃COF 3 x 10³ yrs and CF₃COOH 6 x 10³ yrs. Photolysis will therefore be unimportant for these compounds in the lower atmosphere and other possible removal processes such as reaction with hydroxyl radicals and physical removal therefore need to be considered.

The photolysis lifetimes for CF₃COCl, CCl₃CHO, CCl₂FCHO and CClF₂CHO are relatively shorter than those for CH₃COF, CF₃COF and CF₃COOH and photolysis is a potentially important removal process for CF₃COCl, CCl₃CHO, CCl₂FCHO and CClF₂CHO, see Tables 14 and 15.

Gillotay *et al.*²³ have calculated the photolysis lifetime for COCl₂ at various altitudes for SZAs of 0° and 60°. Since the absorption cross-section show a cut off at 305 nm photolysis in the troposphere was found to be relatively unimportant (photolysis lifetime

>100 yrs). HCOF absorbs further in the UV than COCl_2 and thus is expected to be stable with respect to photolysis in the troposphere.

The absorption cross-sections for $\text{CF}_2\text{ClC(O)O}_2\text{NO}_2$ are a factor of 2 larger than that of peroxyacetyl nitrate at wavelengths < 260 nm and approximately an order of magnitude at 300 nm. see Table 9. Therefore, since the photolysis lifetime for peroxyacetyl nitrate in the troposphere is 96 days³¹ the lifetime for $\text{CF}_2\text{ClC(O)O}_2\text{NO}_2$ is expected to be at least a factor of 2 shorter *ie* < 45 days.

5.2. Comparison with removal by OH and hydrolysis

The photolysis lifetimes were calculated using the UV absorption cross-sections determined in the present study. OH lifetimes were calculated at 30° N using the Cambridge two-dimensional model⁴¹. For CH_3COF no rate data for the reaction with OH have been reported, thus the value for the reaction of OH with CH_3COCl ⁴² ($k = 0.91 \times 10^{-14} \text{ cm}^3 \text{ molecule}^{-1} \text{ s}^{-1}$) has been used. Because of the lack of Henry's Law solubility data for the HCFC and HFC oxidation products the removal rate by cloud water or deposition to the ocean is difficult to assess. Wine and Chameides¹ suggested that the hydrolysis lifetimes for acid halides are dominated by transport to the marine environment and cloudy regions and are of the order of 1-2 months. Worsnop *et al.*⁴³ were unable to determine any significant uptake of gaseous acetyl halides into droplets and thus removal by rainout was expected to be unimportant. However, recent modifications to their apparatus suggested that the removal rate of COCl_2 , CF_3COCl and CF_3COF due to hydrolysis in cloud water is of the order of 1-2 months⁴⁴.

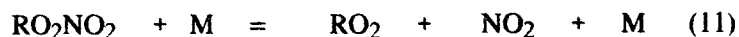
Therefore, since photolysis and reaction with OH are very slow for CH_3COF and CF_3COF . (Table 14), then transport to the marine environment and cloudy regions with physical removal is likely to be the major loss process in the troposphere. Hydrolysis products include CH_3COOH and HF from CH_3COF and CF_3COOH and HF from CF_3COF . The results from the present study suggest that photolysis of these acids is relatively unimportant and physical removal processes will therefore dominate.

For CF_3COCl both photolysis (lifetime 1 month) and physical removal processes (1-2 months) are the main loss processes. Hydrolysis of CF_3COCl will form CF_3COOH and HCl. These acids HCl and CF_3COOH are water soluble and will be removed in precipitation.

Photolysis and reaction with hydroxyl radicals, (Table 15) are the main loss processes for the halogenated aldehydes. Provided the photolysis quantum yield for the halogenated aldehydes, CX_3CHO , is greater than or equal to that for CH_3CHO ⁴⁵ photolysis is likely to be their major fate in the troposphere⁷, see Table 15. The photolysis lifetimes vary from 3.4 hours for CCl_3CHO to less than 1 hour for $CClF_2CHO$. The corresponding lifetimes due to reaction with the hydroxyl radical are 130 hours and 270 hours respectively. The major photolysis products $COCl_2$, $COFCl$ and COF_2 ¹ are expected to be removed by hydrolysis in cloud water on a time scale of approximately 1-2 months⁴⁴.

$HCOF$ is stable with respect to photolysis in the troposphere. The reaction with OH has not been determined therefore the reaction with Cl ($k_{Cl} = 2 \times 10^{-15} \text{ cm}^3 \text{ molecule}^{-1} \text{ s}^{-1}$)¹¹ was used as an upper estimate for k_{OH} . This would predict a lifetime due to reaction with OH of approximately 16 yrs. Therefore, by analogy with CH_3COF , $HCOF$ is expected to be removed by hydrolysis in cloud water (lifetime of 1-2 months).

Peroxy nitrates are known to undergo thermal decomposition



into $RO_2 + NO_2$ ⁴⁶. However at higher altitudes where the temperatures are low the reaction may be sufficiently slow so that peroxy nitrates can act as longer lived reservoir compounds. This is particularly important in the case of acetyl peroxy nitrates because of the increased stability of the acyl radical. Kirchner *et al.*⁴⁶ studied the thermal decomposition of $CF_2ClC(O)O_2NO_2$ at 313 K using FTIR. They report a rate constant of $2 \times 10^{16} \exp(-116 \text{ kJ mol}^{-1}/RT) \text{ s}^{-1}$ at 1000 mbar. At 233 K this corresponds to a thermal lifetime of approximately 160 yrs. Therefore, in the upper troposphere photolysis is likely to be the main loss process for $CF_2ClC(O)O_2NO_2$ whereas at ground level thermal decomposition is likely to dominate.

6. CONCLUSION

The absorption cross-sections for CH_3COF , CF_3COOH , CF_3COCl , CF_3COF , CCl_3CHO , CF_2ClCHO , $CFCl_2CHO$, $CF_2ClC(O)O_2NO_2$, $COCl_2$ and $HCOF$ have been determined over the wavelength range 200-370 nm. A significant temperature dependence in the absorption cross-sections was observed for CF_3COCl , CF_3COF , CCl_3CHO , CF_2ClCHO and $CFCl_2CHO$ which was particularly pronounced in the long wavelength tail of their absorption spectra. The calculated atmospheric photolysis rates suggest that in the lower

atmosphere photolysis is an important removal process for CF_3COCl , CF_2ClCHO , CFCl_2CHO , CCl_3CHO and $\text{CF}_2\text{ClC(O)O}_2\text{NO}_2$ but that physical removal processes in cloudy regions and in the marine environment are more important for CH_3COF , CF_3COF , CF_3COOH , COCl_2 and HCOF .

The chlorine initiated photooxidation of HFC 134a ($\text{CF}_3\text{CH}_2\text{F}$) has been studied in the temperature range 235-320 K and 1 atmosphere total pressure using UV absorption. Trifluoroacetyl fluoride (CF_3COF) and formyl fluoride (HCOF) were observed as the major products. Infrared analysis of the reaction mixture also showed carbonyl fluoride (COF_2) as a major product. By measurement of the yields of HCOF and CF_3COF as a function of oxygen concentration, the rate of the unimolecular decomposition (k_8) of the alkoxy radical, CF_3CHFO was determined relative to its reaction with O_2 (k_7). Based on results from this study and elsewhere the following recommended expression for the rate constant ratio k_7/k_8 was obtained:

$$k_7/k_8 = 8.7 \times 10^{-26} \exp(4035/T) \text{ cm}^3 \text{ molecule}^{-1}$$

REFERENCES

- 1) Scientific Assessment of Stratospheric Ozone, World Meteorological Organisation Report No. 20, Volume 2, (1989).
- 2) R. Liu, R.E. Huie and M.J. Kurylo, *J. Phys. Chem.* **94**, 3247, (1990).
- 3) T. Gierczak, R. Talukdar, G.L. Vaghjiani, E.R. Lovejoy and A. R. Ravishankara, *J. Geophys. Res.*, **96**, 5001, (1991).
- 4) D.D. Nelson Jr., M.S. Zahniser and C.E. Kolb, *J. Phys. Chem.*, **96**, 249, (1992).
- 5) R. Talukdar, A. Mellouki, T. Gierczak, J.B. Burkolder, S.A. McKeen and A.R. Ravishankara, *J. Phys. Chem.*, **95**, 5815, (1991).
- 6) O. Rattigan, R.A. Cox and R.L. Jones, "The UV Absorption Cross-Sections of CF_3COCl , CF_3COF , CH_3COF and CCl_3CHO ", STEP-HALOCSIDE/AFEAS Workshop, Dublin, May (1991).
- 7) O.V. Rattigan, O. Wild and R.A. Cox, "UV Absorption Cross-Sections and Atmospheric Photolysis Rates of CCl_3CHO , CCl_2FCHO and CClF_2CHO ", Joint CEC/EUROTRAC Workshop LACTOZ-HALIPP Working group, Leuven, Belgium, September, (1992).
- 8) O.V. Rattigan, O. Wild, R.L. Jones and R.A. Cox, *J. Photochem. Photobiol. A: Chem.*, **73**, 1, (1993).
- 9) O.V. Rattigan, D.M. Rowley, O. Wild, R.L. Jones and R.A. Cox, "Photochemical Studies of 1,1,1,2 Tetrafluoroethane (HFC 134a)", STEP-HALOCSIDE/AFEAS Workshop, Dublin, 23-25 March, (1993).
- 10) O.V. Rattigan, D.M. Rowley, O. Wild, R.L. Jones and R.A. Cox, "Photochemical Studies of 1,1,1,2 Tetrafluoroethane (HFC 134a)", *J. Chem. Soc. Farad. Trans.* Manuscript in preparation.
- 11) T.J. Wallington, M.D. Hurley, J.C. Ball and E.W. Kaiser, *Environ. Sci. Tech.*, **26**, 1318, (1992).

- 12) M.M. Maricq and J.J. Szente, *J.Phys. Chem.*, **96**, 10862, (1992).
- 13) E. Tuazon and R. Atkinson, *J. Atm. Chem.*, **16(4)**, 301, (1993).
- 14) E. O. Edney and D.J. Driscoll, *Int. J. Chem. Kinet.*, **24**, 1067, (1992).
- 15) O.V. Rattigan, O. Wild, K. Law, R.L. Jones, J. Pyle and R.A. Cox, "Two-Dimensional Model Calculations of HCFCs, HFCs and their Degradation Products", AFEAS Workshop Proceedings, Brussels, September 22, (1992).
- 16) B. Yamada, R.W. Campbell and O. Vogl, *J. Polymer Sci.*, **15**, 1123 (1977).
- 17) B. Yamada, R.W. Campbell and O. Vogl, *Polymer Sci.*, **9**, 23, (1977).
- 18) G.A. Olah and S.J. Kuhn, *J. Am. Chem. Soc.*, **82**, 2380, (1960).
- 19) H.W. Morgan, P.A. Staats and J. H. Goldstein, *J. Chem. Phys.*, **25**, 337, (1956).
- 20) T.J. Wallington and M.D. Hurley, *Chem. Phys. Lett.*, **189**, 437, (1992).
- 21) W.B. DeMore et al. "Chemical Kinetics and Photochemical Data for Use in Stratospheric Modelling", NASA Evaluation No. 10, JPL Publication 92-20, Pasadena, CA., USA (1992).
- 22) H.G. Libuda, F. Zabel and K.H. Becker, "UV Spectra of some Organic Chlorine and Bromine Compounds of Atmospheric Interest", STEP-HALOCSIDE/AFEAS Workshop, Dublin, May (1991).
- 23) D. Gillotay, P.C. Simon and L. Dierickx, "UV Absorption Cross-Sections of some Carbonyl Compounds and Their Temperature Dependence", Quadrennial Ozone Symposium, University of Virginia, June (1992).
- 24) C.C Chou, G. Crescentini, H. vera Ruiz, W.S. Smith and F.S. Rowland "Stratospheric Photochemistry of CF₂O, CCIFC and CCl₂O" 173rd American Chemical Society Meeting, New Orleans L.A., (1977).
- 25) H.J. Okabe, *J. Chem. Phys.*, **66**, 2058, (1977).

- 26) R. Meller, D. Boglu and G.K. Moortgat, "UV Spectra of Several Halogenated Carbonyl Compounds and FTIR Studies on the Degradation of CF_3COCl , HCFC 123 and HFC 134a", STEP-HALOCSIDE/AFEAS Workshop, Dublin, May (1991).
- 27) L.E. Giddings Jr., and K.K. Innes, *J. Mol. Spectroscopy*, **6**, 528 (1961).
- 28) H.G. Libuda, F. Zabel, E.H. Fink and K.H. Becker, *J. Phys. Chem.* **94**, 5860, (1990).
- 29) J.D. Rogers, *J. Phys. Chem.*, **94**, 4011, (1990).
- 30) A.A. Jemi-Alade, P.D. Lightfoot, R. Lesclaux, *Chem. Phys. Lett.* **179**, 119 (1991).
- 31) G.I. Senum, Y.N. Lee and J.S. Gaffney, *J. Phys. Chem.*, **88**, 1269, (1984)
- 32) H. Basch, M.B. Robin and N.A. Kuebler, *J. Chem. Phys.*, **49**, 5007, (1968).
- 33) H.J. Okabe, "Photochemistry of small molecules", Wiley, New York. (1978).
- 34) O. Rattigan, E. Lutman, R.L. Jones, R.A. Cox, K. Clemitshaw and J. Williams. *J. Photochem. Photobiol. A: Chem.*, **66**, 313, (1992).
- 35) T.J. Wallington and O.J. Nielsen, *Chem. Phys. Lett.* **187**, 33, (1991).
- 36) J. Peeters and V. Pultau, " $\text{CF}_3\text{CHFO}_2 + \text{NO}$ ", CEC-AFEAS workshop, Leuven, September 1992.
- 37) T.J. Wallington, Private Communication.
- 38) S.W. Benson, "Thermochemical Kinetics", 2nd Ed., Wiley, New York, (1976).
- 39) F. Biaume, *J. Photochem.* **2**, 139, (1973).
- 40) D. Lary, PhD Dissertation, University of Cambridge, (1991).
- 41) K.S. Law, PhD Dissertation, University of Cambridge, (1992).

- 42 L. Nelson, I. Shanahan, H.W. Sidebottom, J. Treacy, and O.J. Nielsen, *Int. J. Chem. Kinet.* **22**, 577, (1990).
- 43) D.R. Worsnop, G.N. Robinson, M.S. Zahniser and C.E. Kolb, "Heterogeneous Chemistry of Alternative CFC Oxidation Intermediates" Paper presented at the STEP-HALOCSIDE/AFEAS Workshop, Dublin, May (1991).
- 44) W. DeBruyn, J.A. Shorter, P. Davidovits, D.R. Worsnop, M.S. Zahniser and C.E. Kolb, AFEAS Workshop Proceedings, September 22, Brussels, (1992).
- 45) D.L. Baulch, R.A. Cox, R.F. Hampson, Jr., J.A. Kerr, J. Troe and R.T. Watson, *J. Phys. Chem. Ref. Data*, **13**, 1259, (1984).
- 46) F. Kirchner, F. Zabel and K.H. Becker, "Thermal Stability of $\text{CClF}_2\text{CH}_2\text{O}_2\text{NO}_2$, $\text{CCl}_2\text{FCH}_2\text{O}_2\text{NO}_2$ and $\text{CClF}_2\text{C}(\text{O})\text{O}_2\text{NO}_2$ ". Paper presented at the STEP-HALOCSIDE/AFEAS Workshop, Dublin, May (1991).

Table 1 Absorption Cross-sections for CF₃COCl

Wavelength/nm	Cross-Section x 10 ²⁰ /cm ² molecule ⁻¹		
	296 K	253 K	233 K
200	37.98	33.83	31.88
205	14.75	12.81	12.02
210	3.526	2.678	2.560
215	1.041	0.711	0.695
220	1.106	0.910	0.834
225	1.687	1.621	1.578
230	2.871	2.744	2.674
235	4.009	3.966	3.874
240	5.092	5.074	4.975
245	5.972	5.947	5.845
250	6.571	6.520	6.414
255	6.796	6.676	6.553
260	6.606	6.433	6.317
265	5.967	5.742	5.625
270	5.126	4.890	4.785
275	4.217	3.978	3.878
280	3.111	2.901	2.817
285	2.166	1.985	1.914
290	1.386	1.249	1.197
295	0.809	0.706	0.668
300	0.425	0.358	0.334
305	0.198	0.159	0.145
310	0.077	0.056	0.048
315	0.024	0.016	0.012
320	0.007	0.005	0.004
325	0.002	0.001	0.001
330	0.000	0.000	0.000

0035

Table 2 Absorption Cross-section for CF₃COF

Wavelength/nm	Cross-Section x 10 ²⁰ /cm ² molecule ⁻¹	
	293 K	238 K
200	9.354	9.456
205	11.47	11.63
210	13.14	13.16
215	13.63	13.69
220	12.87	13.09
225	11.11	11.40
230	8.775	9.106
235	6.299	6.551
240	4.074	4.179
245	2.348	2.298
250	1.220	1.157
255	0.552	0.491
260	0.216	0.179
265	0.070	0.047
270	0.026	0.010
275	0.010	0.003
280	0.003	0.001
285	0.002	0.000
290	0.001	0.000
295	0.000	0.000

0 0 3 6

Table 3 Absorption Cross-section for CH₃ OF

Cross-section x 10²⁰/cm² molecule⁻¹

Wavelength/nm	296 K
200	11.26
205	12.16
210	11.96
215	10.53
220	8.345
225	5.974
230	3.829
235	2.186
240	1.135
245	0.566
250	0.311
255	0.206
260	0.158
265	0.120
270	0.090
275	0.056
280	0.029
285	0.016
290	0.008
295	0.004
300	0.002
305	0.001
310	0.000
315	0.000

Table 4 Absorption Cross-section for CCl_3CHO

Wavelength/nm	Cross-section x $10^{20}/\text{cm}^2 \text{ molecule}^{-1}$	
	296 K	243 K
200	115.1	110.7
205	86.14	81.89
210	48.19	43.20
215	23.88	20.32
220	10.92	9.179
225	4.759	3.527
230	2.034	1.264
235	0.944	0.430
240	0.774	0.418
245	1.135	0.882
250	1.827	1.633
255	2.799	2.659
260	3.977	3.910
265	5.360	5.388
270	6.722	6.878
275	8.012	8.368
280	9.318	9.625
285	10.08	10.35
290	10.32	10.62
295	9.886	10.06
300	9.019	9.245
305	7.671	7.602
310	6.074	5.942
315	4.572	4.446
320	3.063	2.790
325	1.901	1.741
330	1.121	0.951
335	0.498	0.322
340	0.194	0.114
345	0.086	0.043
350	0.020	0.004
355	0.002	0.000
360	0.000	0.000

Table 5 Absorption Cross-Section for CF₂CICHO

Wavelength/nm	Cross-section x 10 ²⁰ /cm ² molecule ⁻¹	
	298 K	245 K
240	0.384	0.417
245	0.703	0.751
250	1.184	1.276
255	1.910	2.021
260	2.875	3.082
265	4.181	4.451
270	5.802	6.154
275	7.623	8.108
280	9.651	10.29
285	11.61	12.32
290	13.48	14.37
295	14.74	15.59
300	15.67	16.70
305	15.49	16.08
310	15.18	15.99
315	13.22	13.80
320	11.63	12.13
325	9.367	10.03
330	6.553	6.583
335	4.800	4.840
340	2.784	2.944
345	1.516	1.393
350	0.730	0.599
355	0.113	0.070
360	0.034	0.024
365	0.011	0.007
370	0.000	0.000

0 0 3 9

Table 6 Absorption Cross-section for CCl_2FCHO

Cross-section x $10^{20}/\text{cm}^2$ molecule $^{-1}$		
Wavelength/nm	296 K	253 K
240	0.795	0.546
245	1.069	0.934
250	1.587	1.541
255	2.377	2.405
260	3.470	3.569
265	4.853	5.022
270	6.514	6.753
275	8.343	8.662
280	10.10	10.48
285	11.79	12.22
290	12.98	13.38
295	13.76	14.16
300	13.60	13.87
305	12.91	12.91
310	11.52	11.52
315	9.783	9.427
320	7.969	7.733
325	5.599	5.159
330	3.904	3.654
335	2.449	2.108
340	1.229	1.048
345	0.623	0.446
350	0.244	0.164
355	0.041	0.025
360	0.016	0.012
365	0.007	0.004
370	0.000	0.000

0 0 4 0

Table 7 Absorption Cross-section for HCOF

Wavelength/nm	Cross-section x $10^{20}/\text{cm}^2$ molecule $^{-1}$ 298 K
220-225	8.124
225-230	7.779
230-235	6.037
235-240	3.741
240-245	2.047
245-250	1.033
250-255	0.355
255-260	0.096
260-265	0.019
265-270	0.007
270-275	0.000

Table 8 Absorption Cross-section for COCl₂

Wavelength/nm	Cross-section x $10^{20}/\text{cm}^2$ molecule $^{-1}$ 296 K
200	26.20
205	17.67
210	12.15
215	10.23
220	10.41
225	11.78
230	13.17
235	13.60
240	12.82
245	11.08
250	8.837
255	6.582
260	4.538
265	2.772
270	1.690
275	0.936
280	0.419
285	0.171
290	0.060
295	0.019
300	0.005
305	0.001
310	0.0

Table 9
Absorption Cross-section for $\text{CF}_2\text{ClC}(\text{O})\text{O}_2\text{NO}_2$ and $\text{CH}_3\text{C}(\text{O})\text{O}_2\text{NO}_2$

Wavelength/nm	Cross-section $\times 10^{20}/\text{cm}^2 \text{ molecule}^{-1}$ at 298 K	
	$\text{CF}_2\text{ClC}(\text{O})\text{O}_2\text{NO}_2$	$\text{CH}_3\text{C}(\text{O})\text{O}_2\text{NO}_2^*$
225	82.49	55.0
230	68.66	39.9
235	53.95	29.0
240	41.37	20.9
245	31.43	15.0
250	23.04	10.9
255	17.34	7.90
260	12.78	5.70
265	9.836	4.04
270	7.349	2.79
275	6.112	1.82
280	4.897	1.14
285	3.180	0.716
290	2.348	0.414
295	1.618	0.221
300	0.999	0.105
305	0.531	0.000
310	0.000	

*Absorption cross-sections determined by Senum et al.²⁹

Table 10 Absorption Cross-Section for CF₃COOH

Cross-Section x 10 ²⁰ /cm ² molecule ⁻¹	
Wavelength/nm	296 K
200	5.201
205	6.484
210	7.229
215	7.585
220	7.760
225	7.209
230	6.025
235	4.463
240	2.892
245	1.685
250	0.870
255	0.390
260	0.155
265	0.050
270	0.013
275	0.006
280	0.000

Table 11 Temperature Dependence of CF₃COCl absorption cross-sections

Wavelength/nm	10 ²¹ (σ ₀ /cm ² molecule ⁻¹) ^a	(B/K ⁻¹ X 10 ³) ^b
290	6.866	1.028
300	1.346	1.672
305	0.424	2.253
310	0.070	3.487
315	0.0086	4.905
320	0.0042	6.370

^aIntercept and ^bslope obtained from a plot of $\log_{10} \sigma = \log_{10} \sigma_0 + BT$

0 0 4 3

Table 12: Yields of Products From HFC 134a Photooxidation

T/K	[O ₂]/10 ¹⁸ molec cm ⁻³	y(HCOF)	y(CF ₃ COF)
293	5.98	2.48	1.35
	9.89	1.96	1.87
	19.3	1.35	1.65
	24.0	1.15	1.85
235	0.822	0.98	na
	2.06	0.75	1.42
	3.25	0.60	1.26
	4.11	0.59	1.34
	4.77	0.60	na
	6.11	0.36	1.57
273	5.71	1.54	2.13
	10.59	1.07	1.67
	14.27	0.725	1.82
	17.73	0.754	1.75
318	9.78	3.78	na
	12.20	4.50	2.26
	17.80	3.12	na
	22.20	3.00	1.44

Table 13: Arrhenius parameters for the reaction $\text{CF}_3\text{CHFO} + \text{CF}_3 + \text{HCOF}$

$A / (\text{s}^{-1} \times 10^{-11})$	$(E/R) / \text{K}$	$k_{293} / (\text{s}^{-1} \times 10^{-4})$	Reference
45	5407	4.2	This work
16.7	5150	3.9	This work
3.6	4832	2.5	Wallington et al ¹¹
1.9	4760	1.7	Tuazon and Atkinson ¹³
0.0037	2200	4.0	Maricq and Szenté ¹²
6.9	4960	3.1	RECOMMENDED

0 0 4 5

Table 14 Tropospheric lifetimes for the acetyl halides

Removal	CH ₃ COF	CF ₃ COF	CF ₃ COCl	CCl ₃ CHO	CF ₃ COOH
photolysis	41 yrs	3000 yrs	33 days	3.4 hrs	> 6 x 10 ³ yrs
OH	3 yrs	-	-	7 days	*
hydrolysis	all 1-2 months				

Photolysis lifetimes are daily averaged tropospheric values

OH lifetime CH₃COF was calculated assuming k_{OH} CH₃COCl⁴² and an average OH concentration of 1×10^6 molecule cm⁻³.

* OH rate constant not determined.

Table 15 Lifetimes for halogenated aldehydes and carbonyl halides

Removal	CCl ₃ CHO	CCl ₂ FCHO	CClF ₂ CHO	HCOF	COCl ₂
OH	7 days	11 days	17 days	16 yrs*	--
Photolysis	3.4 hrs	1 hr	<1 hr	>7 x 10 ⁵ yrs	>100 yrs ⁺
Hydrolysis	1-2 Months				

* The OH lifetime HCOF was calculated assuming $k(Cl + HCOF)^{37} = 2 \times 10^{-15}$ cm³ molecule⁻¹ s⁻¹.

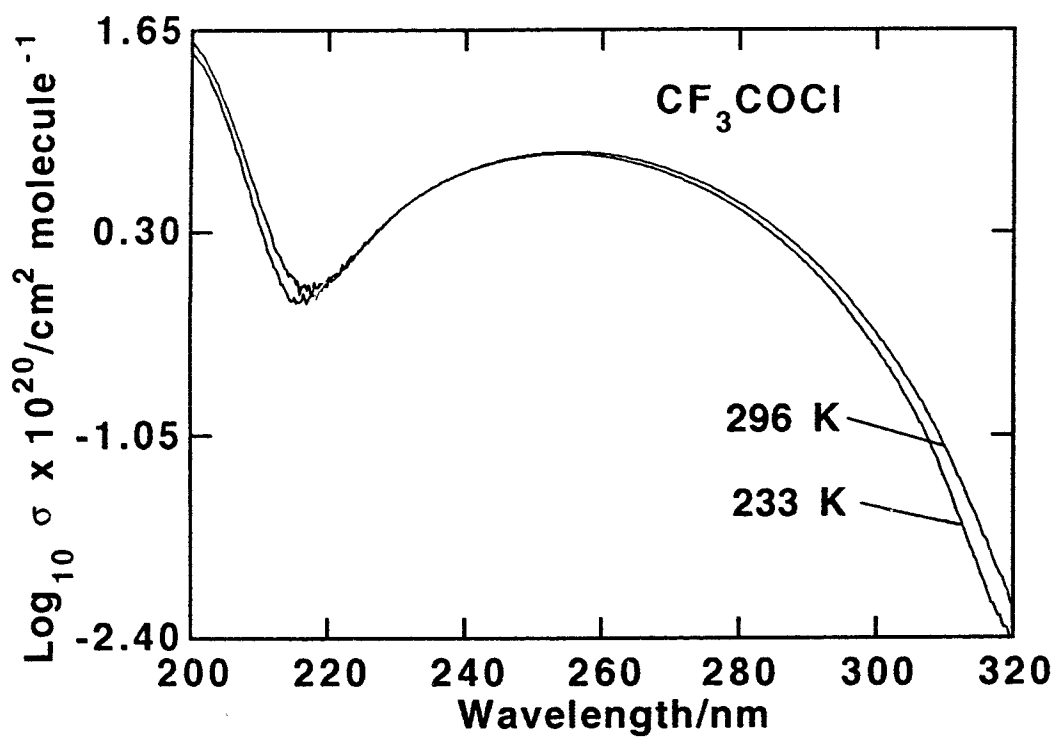
⁺ Estimated from Gillotay et al.²³

Figure Captions

- Figure 1: Schematic diagram of UV Diode array spectrometer.
- Figure 2: Absorption spectrum of CF_3COCl at 296 K and 233 K.
- Figure 3: Absorption spectrum of CF_3COF at 293 K and 239 K.
- Figure 4: Absorption spectrum of CH_3COF at 296 K.
- Figure 5: Plot of logarithm of the absorption cross-section at selected wavelengths against temperature for CF_3COCl . Lines show least squares linear regression slopes.
- Figure 6: Beer-Lambert law plot of CF_2ClCHO absorbance at 298 K.
- Figure 7: Absorption spectrum of CCl_3CHO at 296 K and 243 K.
- Figure 8: Absorption spectrum of CFCl_2CHO at 296 K and 253 K.
- Figure 9: Absorption spectrum of CF_2ClCHO at 298 K and 245 K.
- Figure 10: Absorption spectrum of COCl_2 at 296 K.
- Figure 11: Absorption spectrum of HCOF at 298 K and 1.2 nm resolution.
- Figure 12: Absorption spectrum of HCOF at 298 K and 0.3 nm resolution.
- Figure 13: Absorption spectrum of $\text{CF}_2\text{ClC(O)O}_2\text{NO}_2$ at 296 K and 3.0 nm resolution.
- Figure 14: Absorption spectrum of CF_3COOH at 296 K.
- Figure 15: Photolysis of $\text{CF}_3\text{CH}_2\text{F}/\text{Cl}_2/\text{O}_2$ mixtures at 295 K.
- Figure 16: Infrared spectrum of photolysed mixture of $\text{CF}_3\text{CH}_2\text{F}/\text{Cl}_2/\text{O}_2$.
- Figure 17: Plot of $(\text{HC(O)F yield})^{-1}$ vs $[\text{O}_2]$ at 293 K.
- Figure 18: Arrhenius plot for the CF_3CHFO radical decomposition.
- Figure 19: Plot of logarithm of the solar flux versus wavelength at 300 mbar.

0 0 4 7

Fig. 2



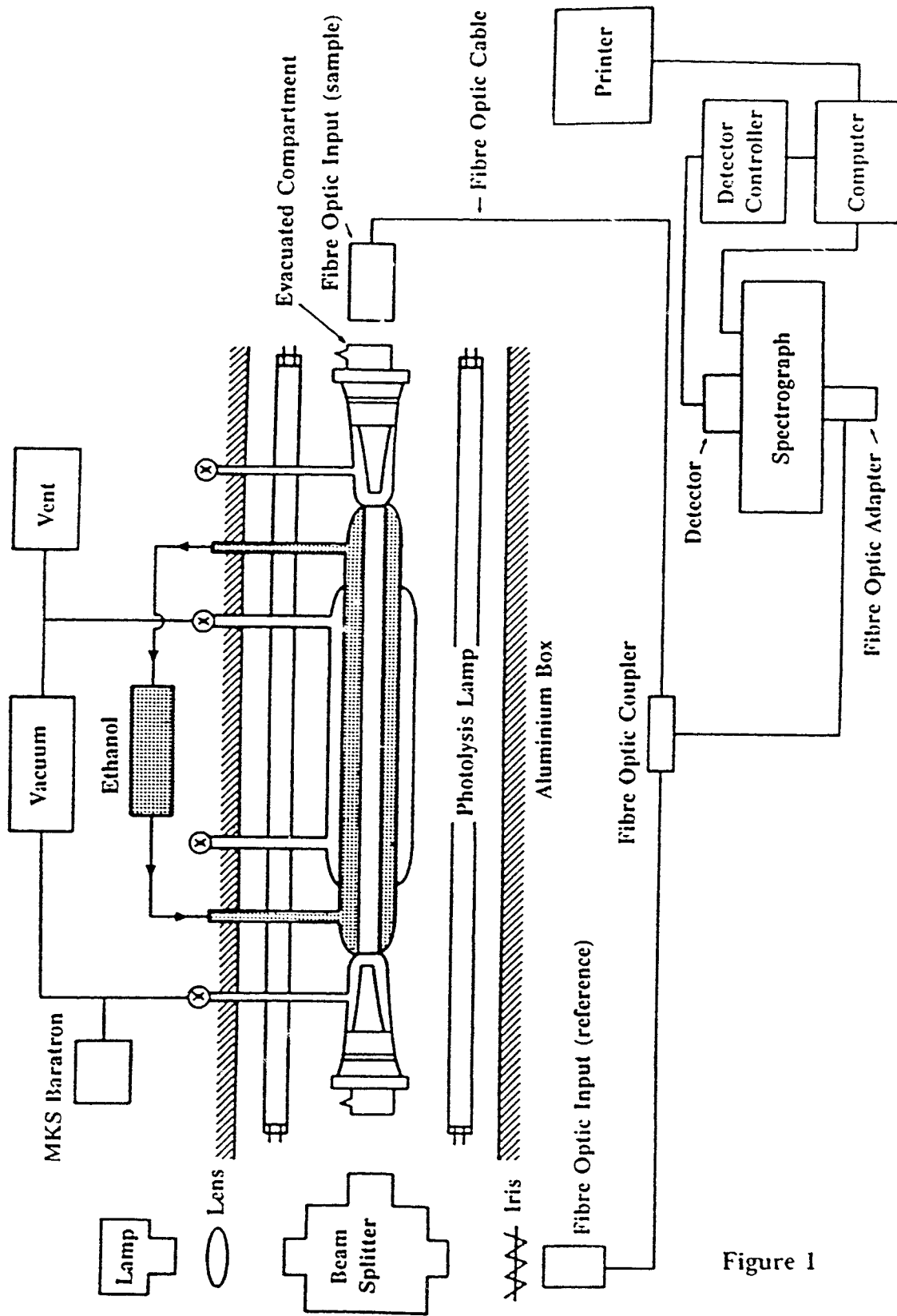
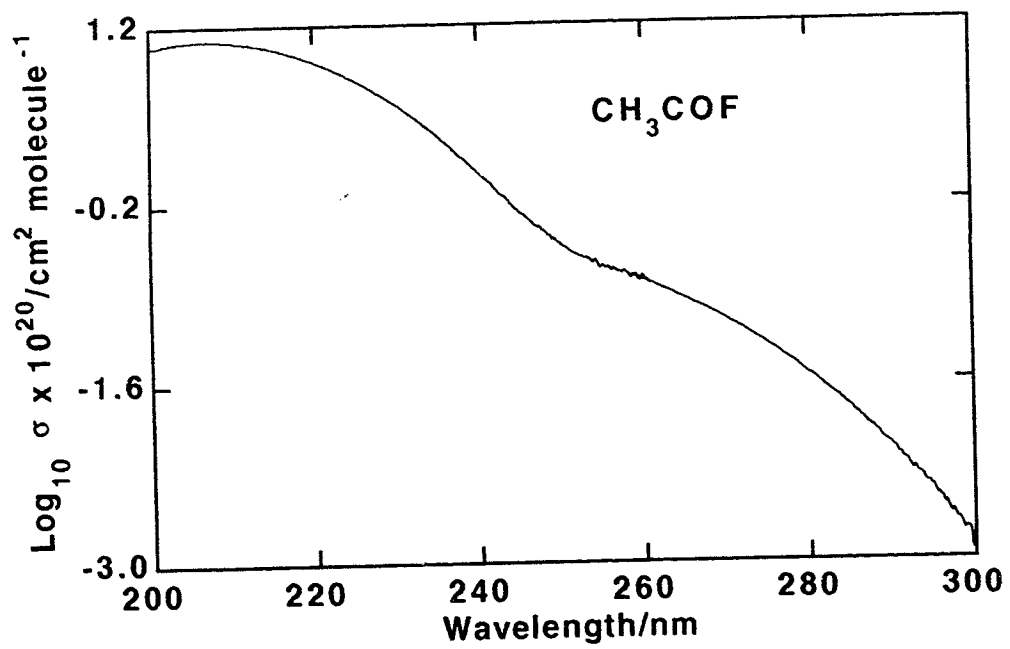


Figure 1

0 0 4 5

Fig. 4



0058

Fig. 3

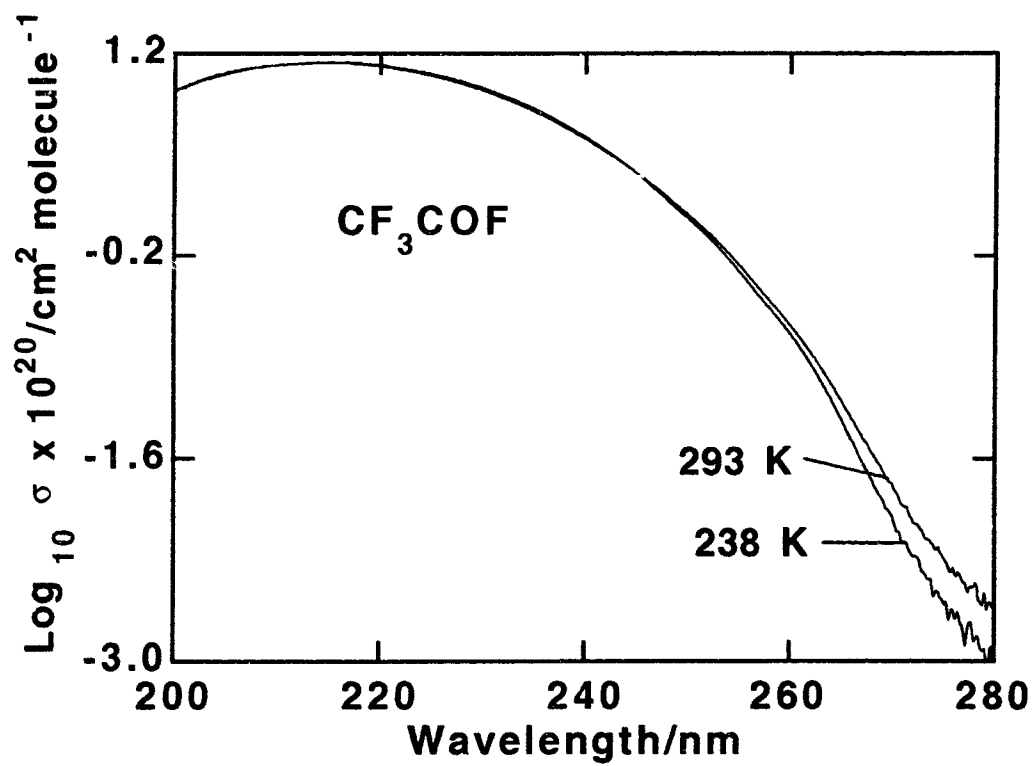
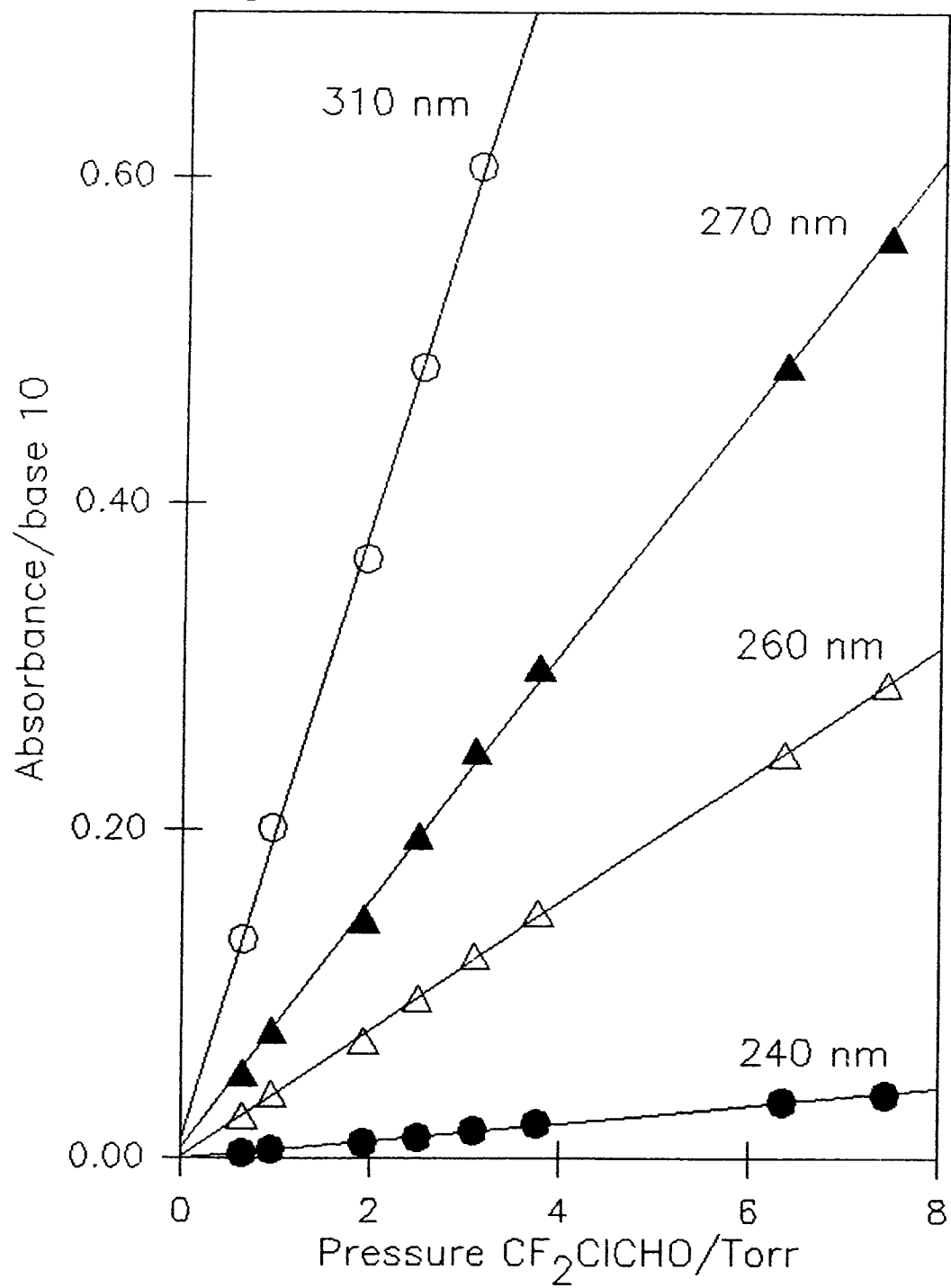
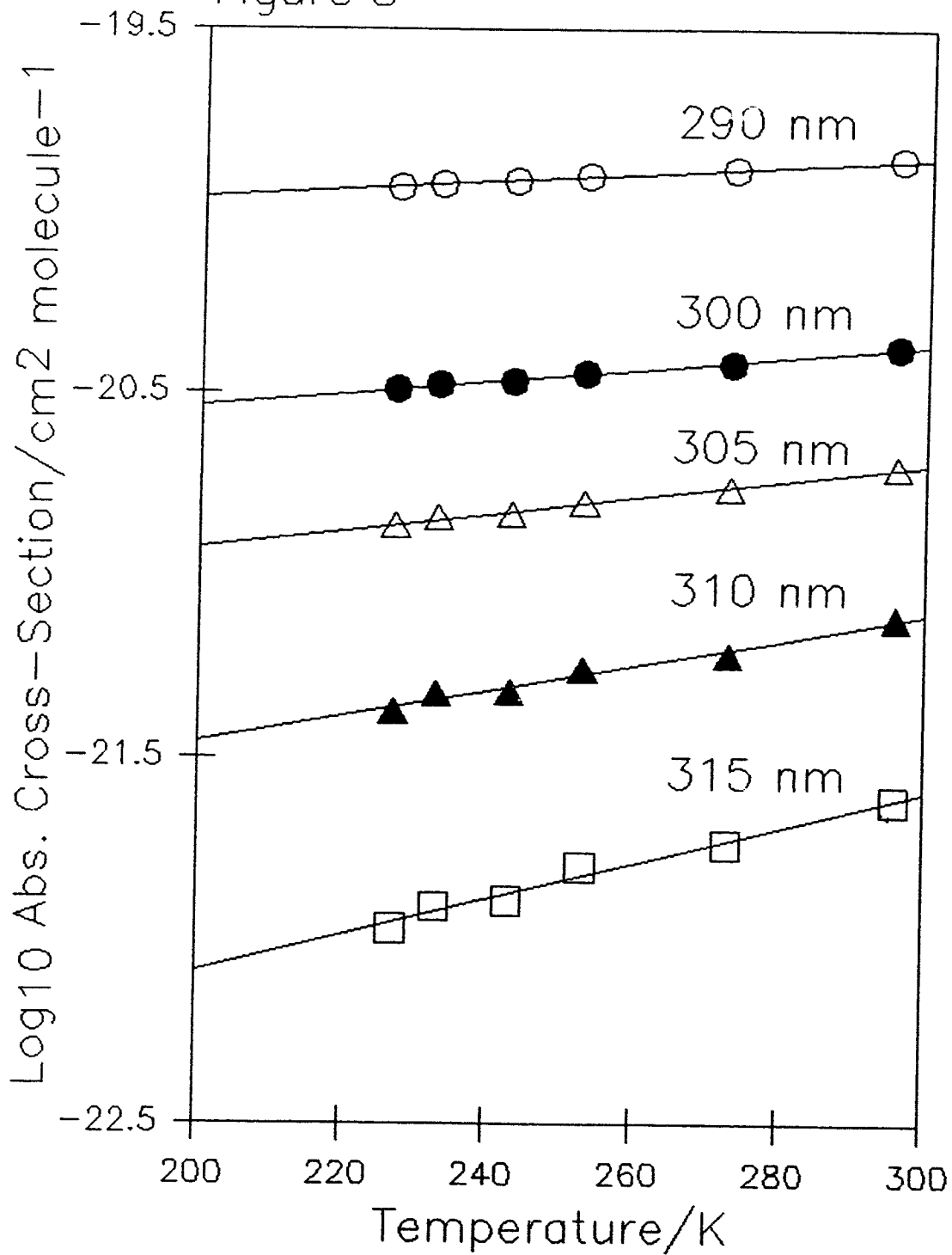


Figure 6



0052

Figure 5



0 0 5 3

Fig. 7

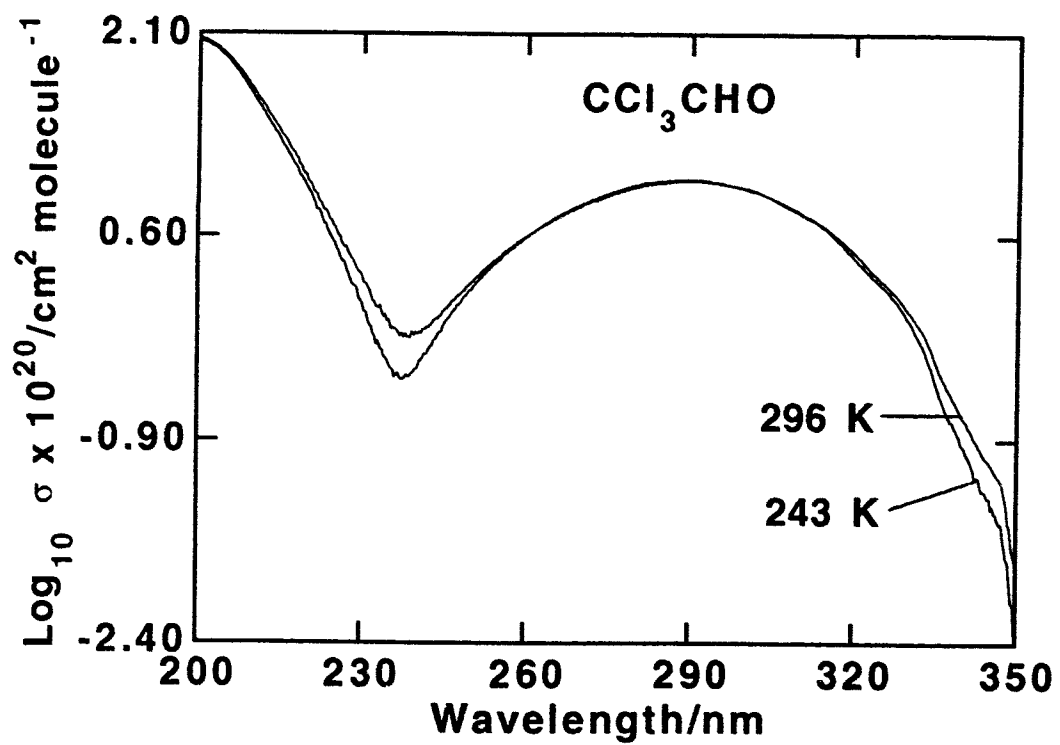
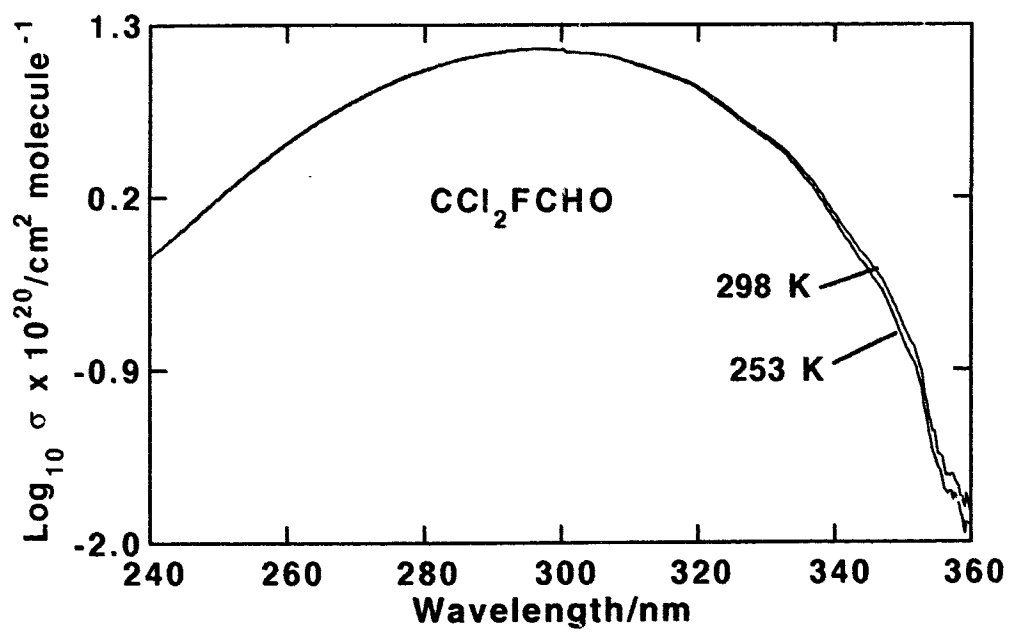


Fig. 8



0055

Fig. 9

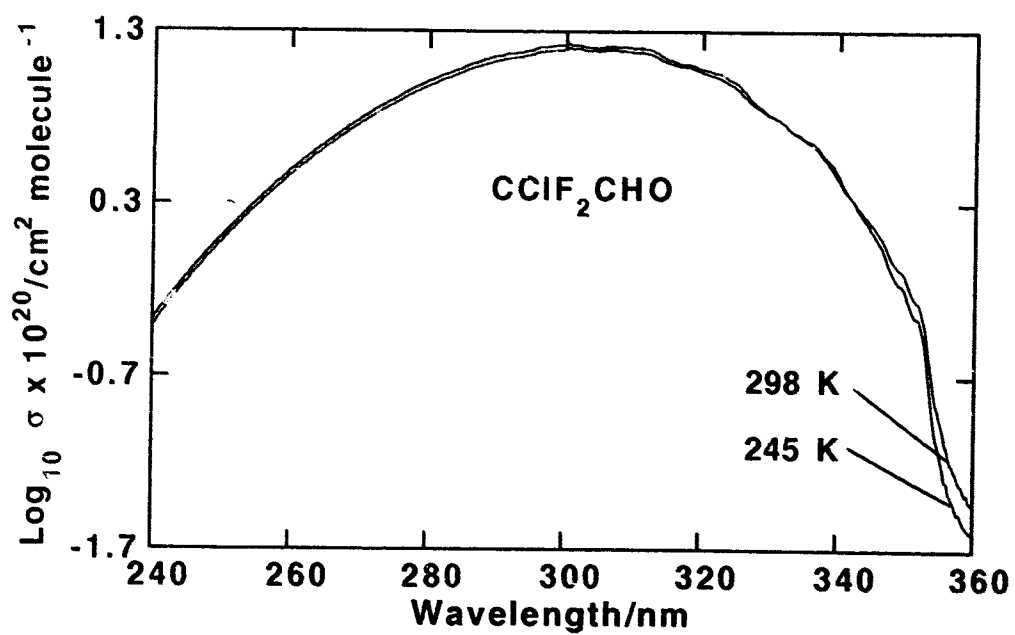


Fig. 10

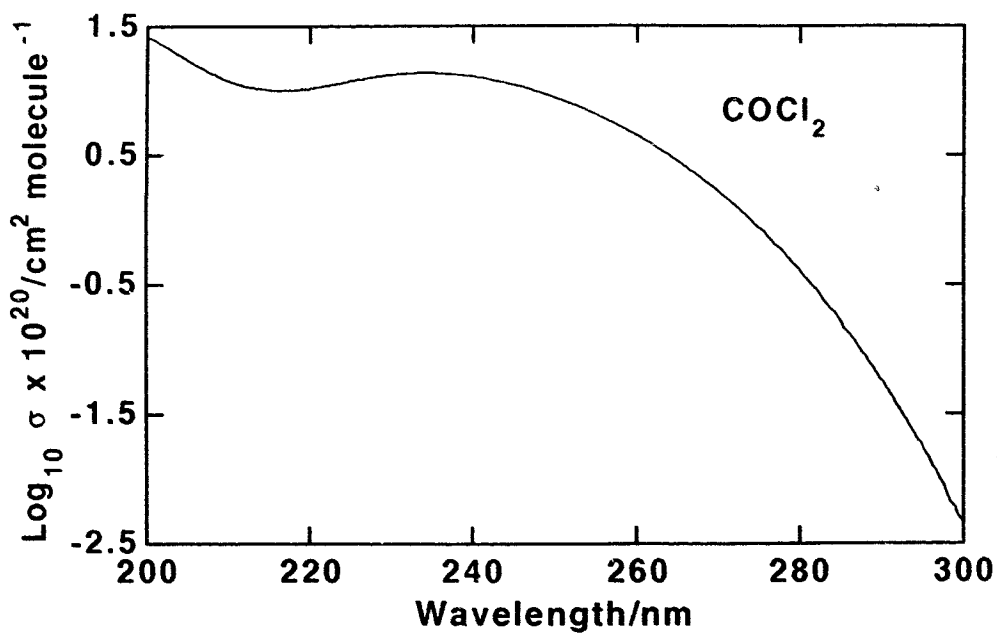
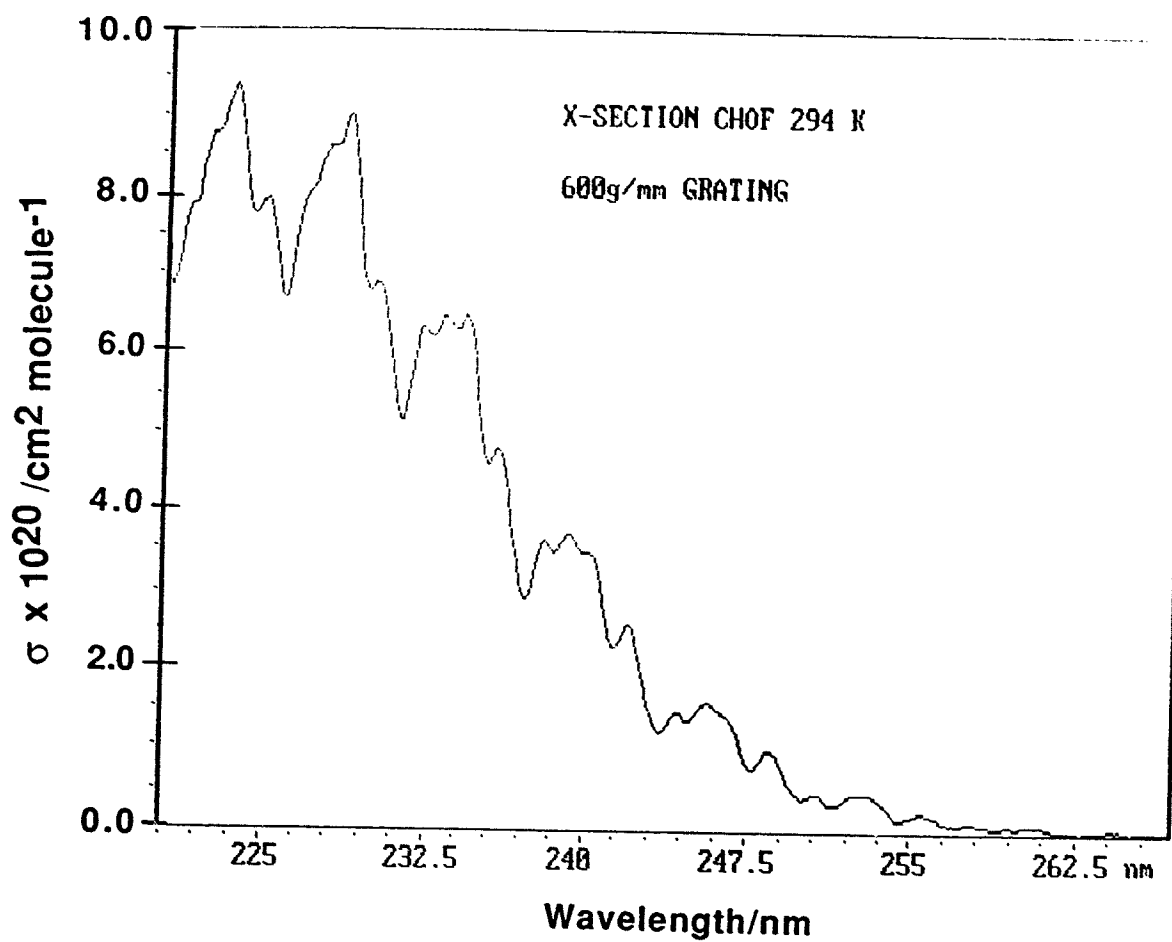
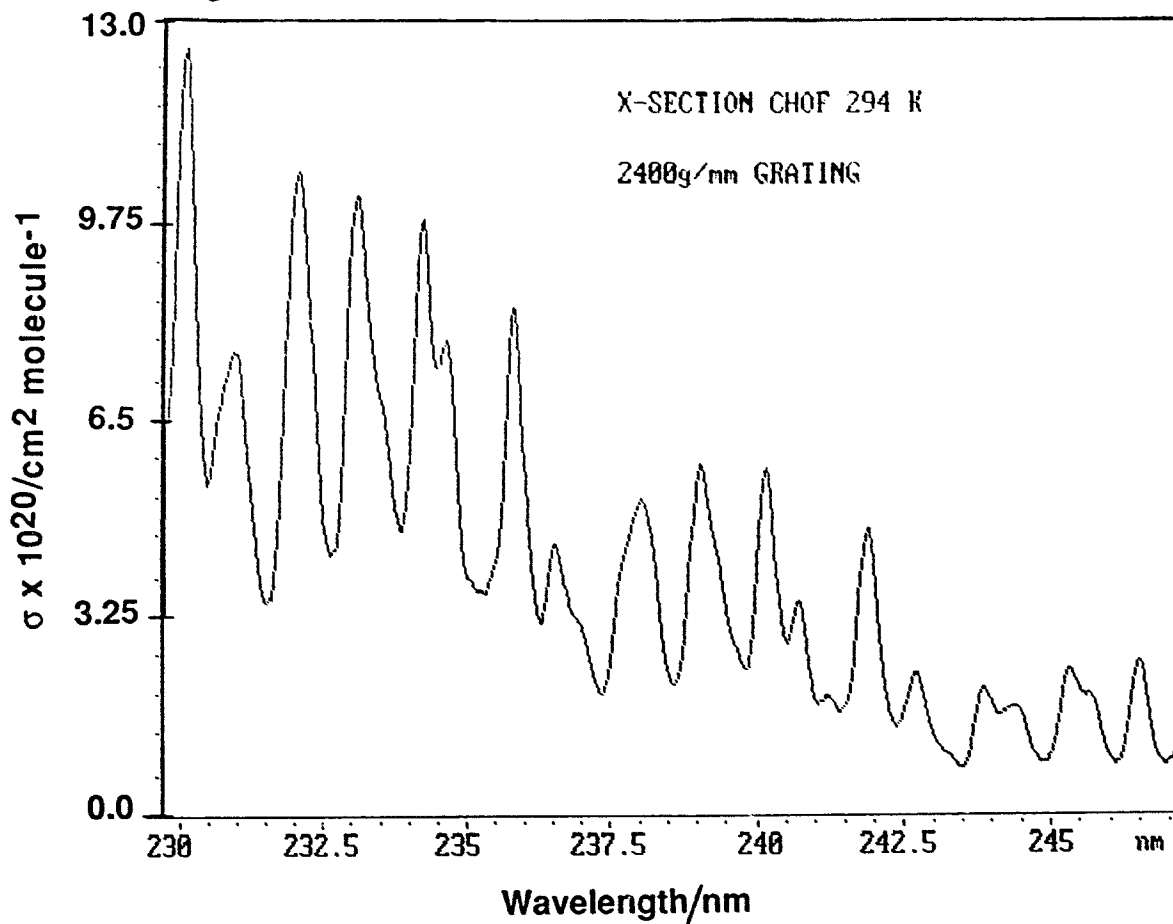


Figure 11



0058

Figure 12



0 0 . 5 9

Fig. 13

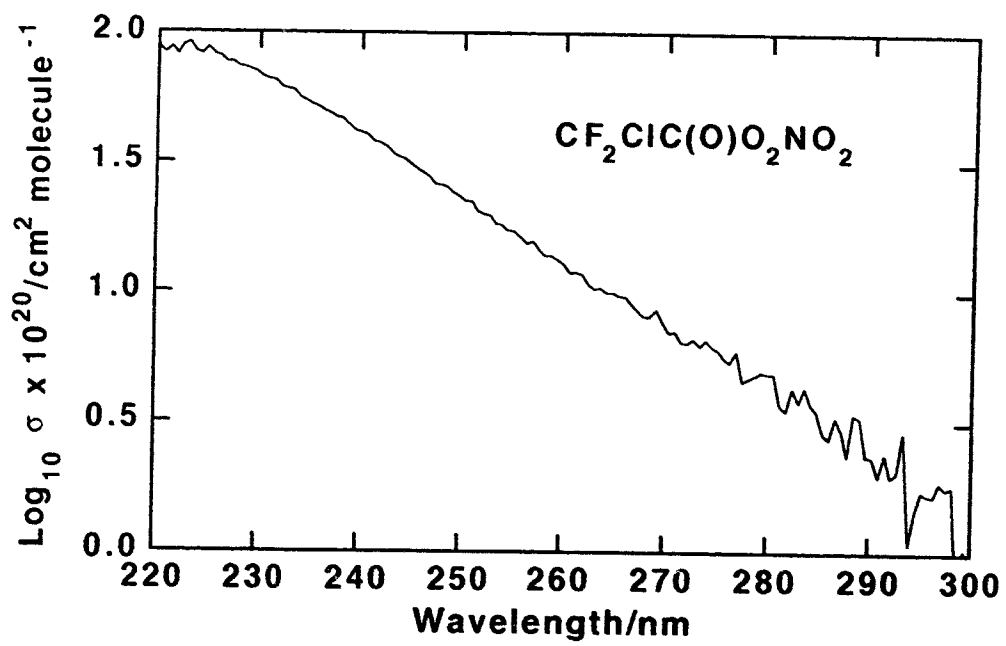


Fig. 14

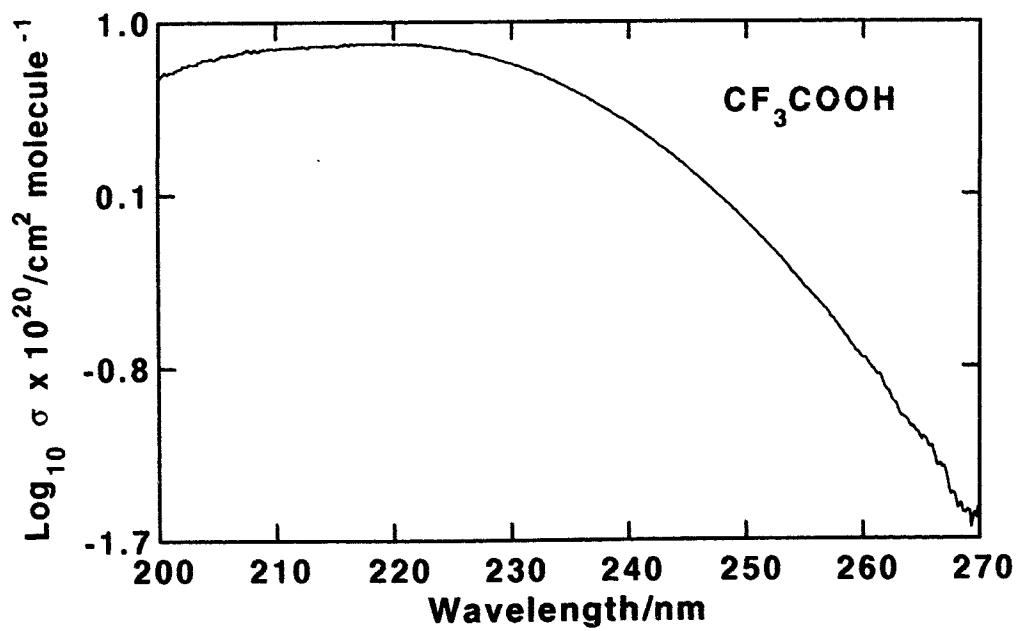
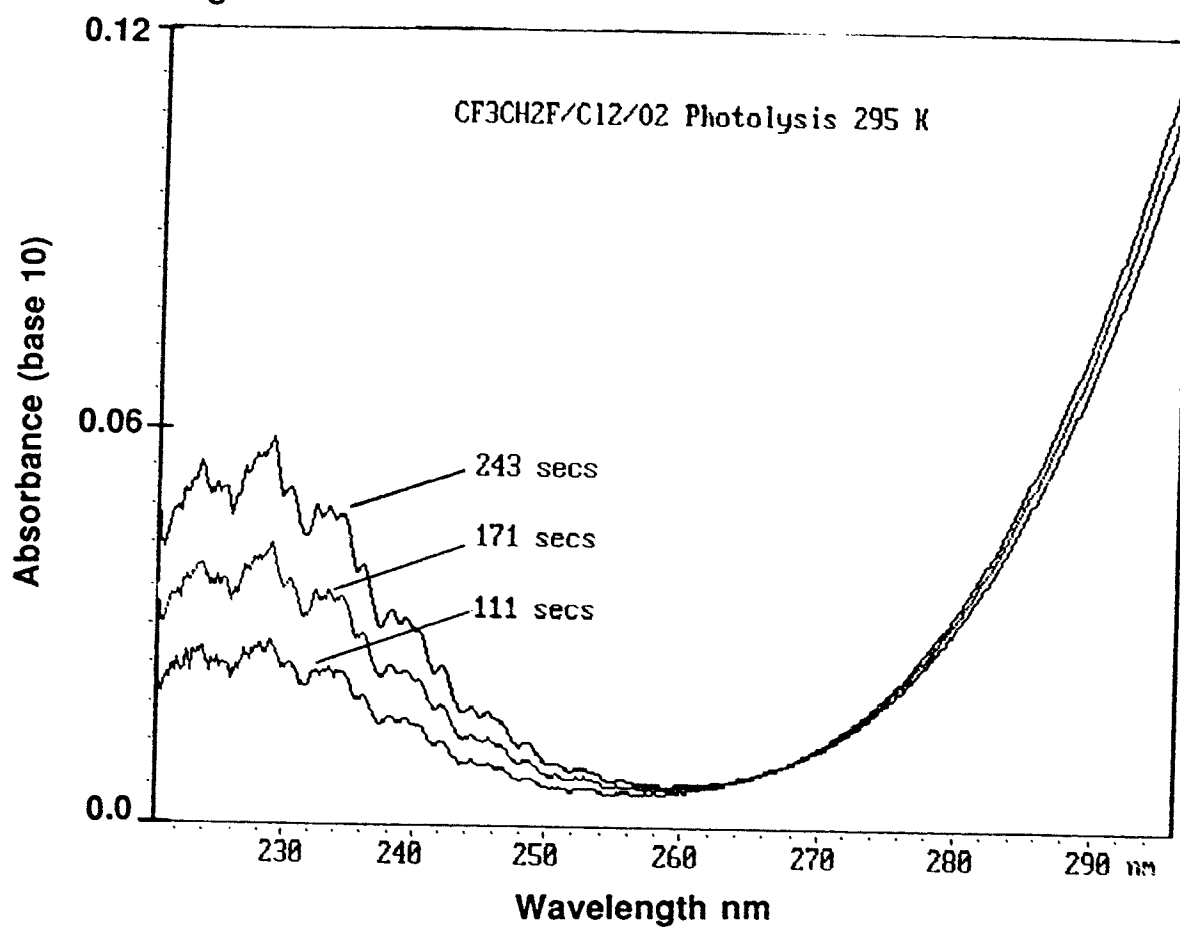
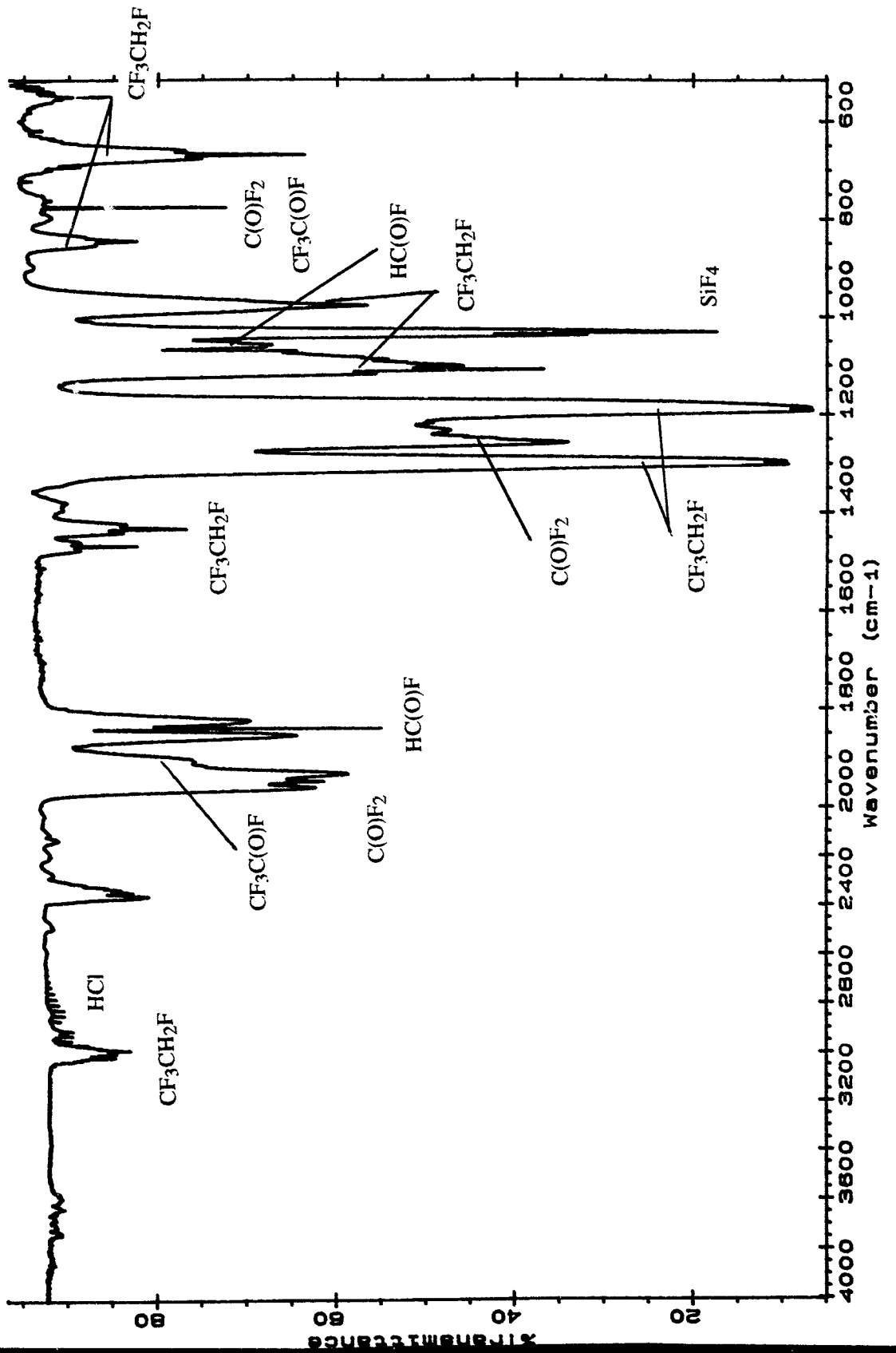


Figure 15



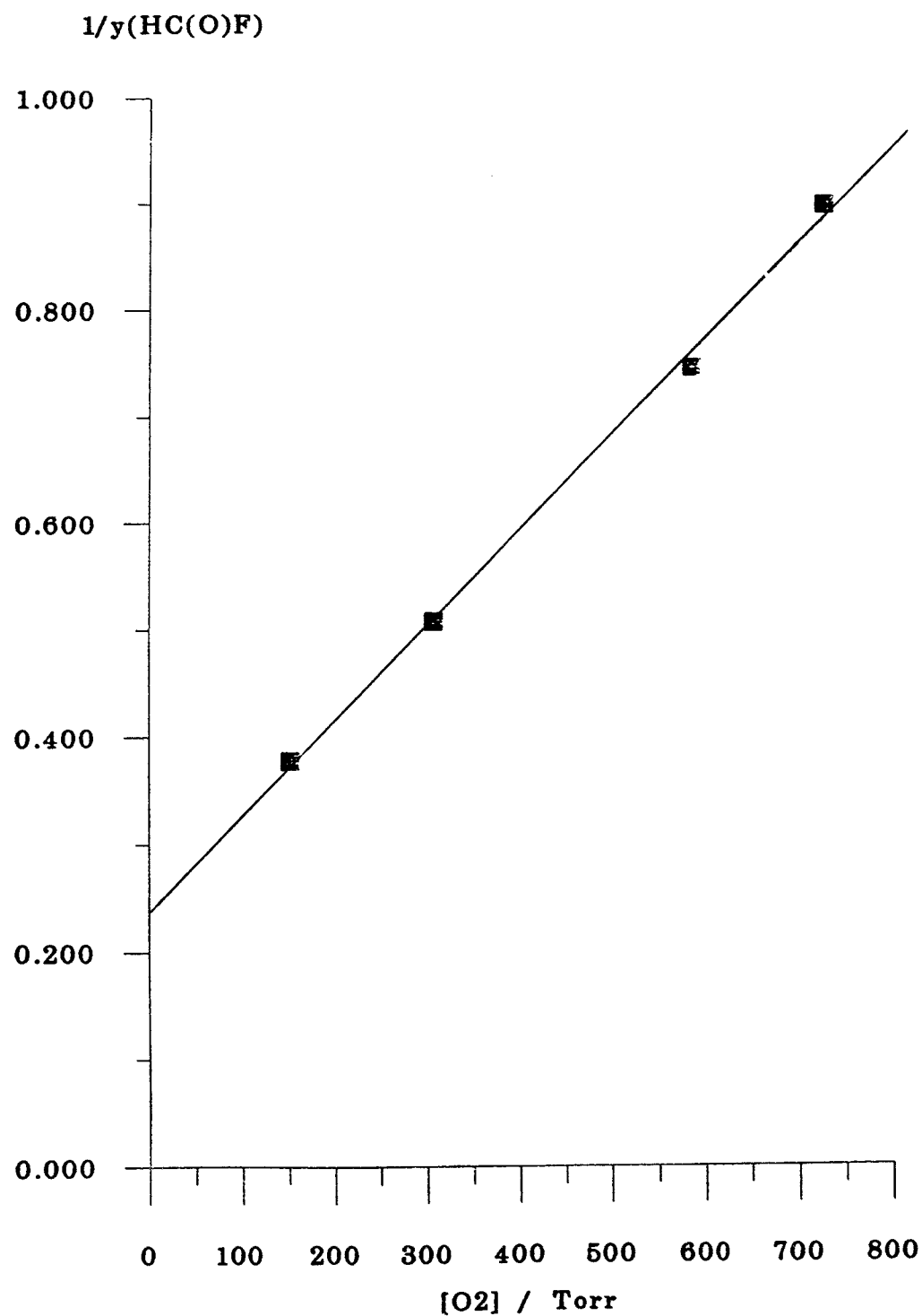
0 0 6 2

Fig. 16



0065

Figure 17: $1/y(\text{HC(O)F})$ vs $[\text{O}_2]$ at 293 K



0 0 6 4

Figure 18 : k5 from 2 analyses using
 $k_4 = (6.0 \times 10^{-14}) \exp(-925/T)$

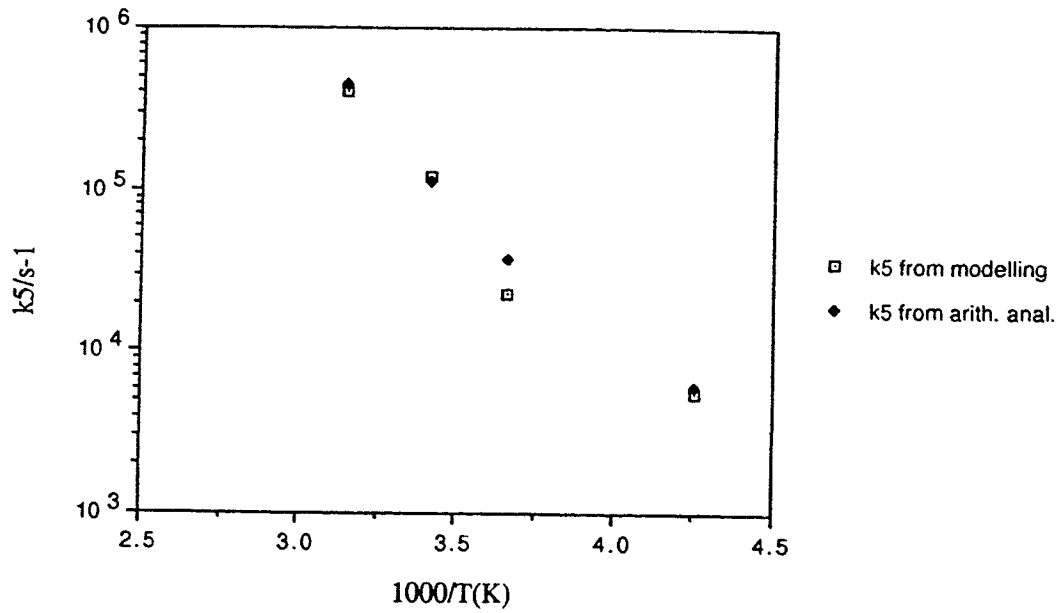
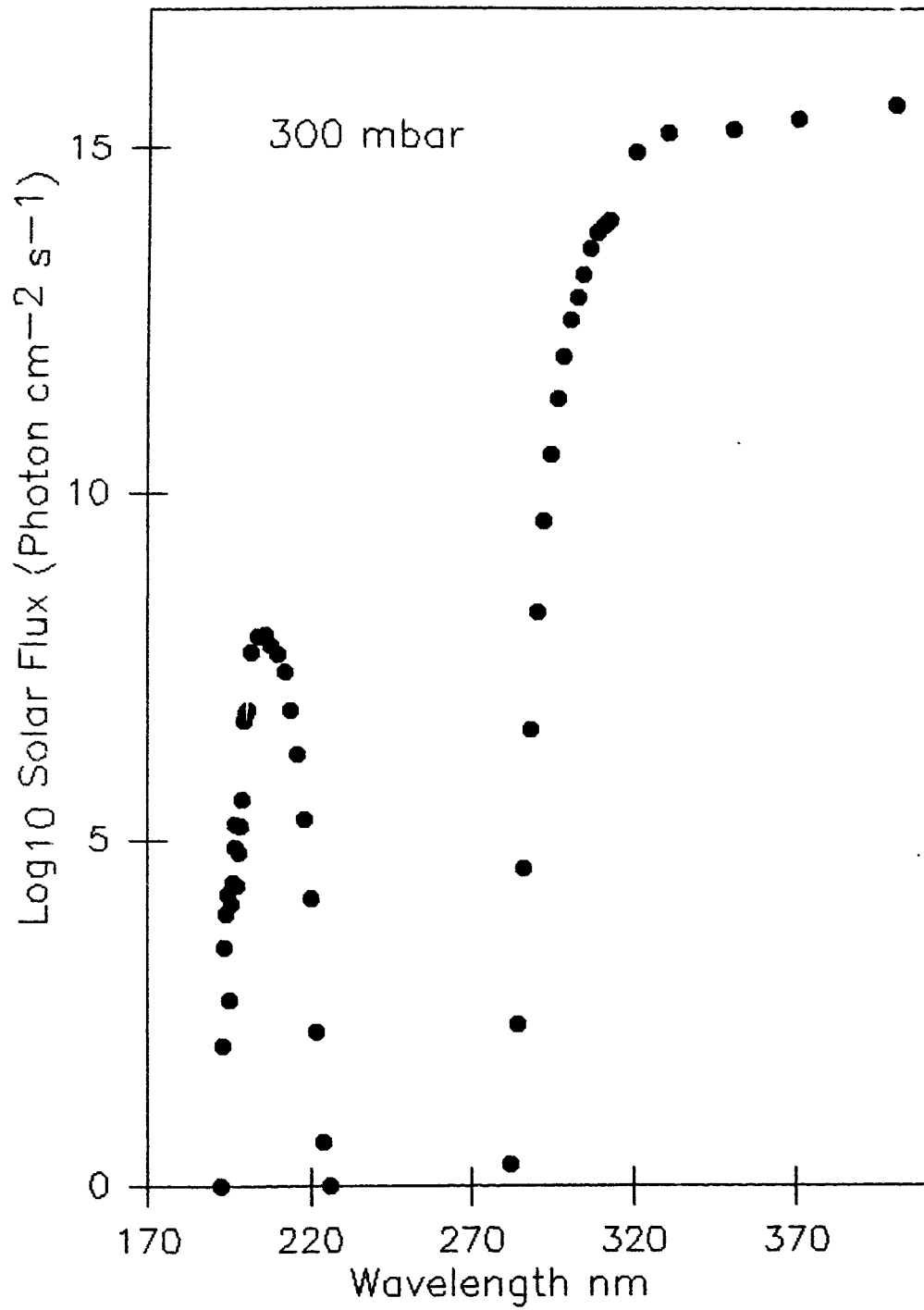


Figure 19



Appendix 1: Published Papers

- 1) O. Rattigan, E. Lutman, R.L. Jones, R.A. Cox, K. Clemitshaw and J. Williams, J. Photochem. Photobiol. A: Chem., **66**, 313, (1992).
- 2) O. Rattigan, E. Lutman, R.L. Jones, R.A. Cox, K. Clemitshaw and J. Williams, J. Photochem. Photobiol. A: Chem., **69**, 125, (1992).
- 3) O.V. Rattigan, O. Wild, R.L. Jones and R.A. Cox, J. Photochem. Photobiol. A: Chem., **73**, 1, (1993).
- 4) O.V. Rattigan, O. Wild and R.A. Cox, "UV Absorption Cross-Sections and Atmospheric Photolysis Rates of CCl_3CHO , CCl_2FCHO and CClF_2CHO ", CEC/EUROTRAC Workshop LACTOZ-HALIPP Working Group, Leuven, Belgium, September, (1992).

Fig. 1

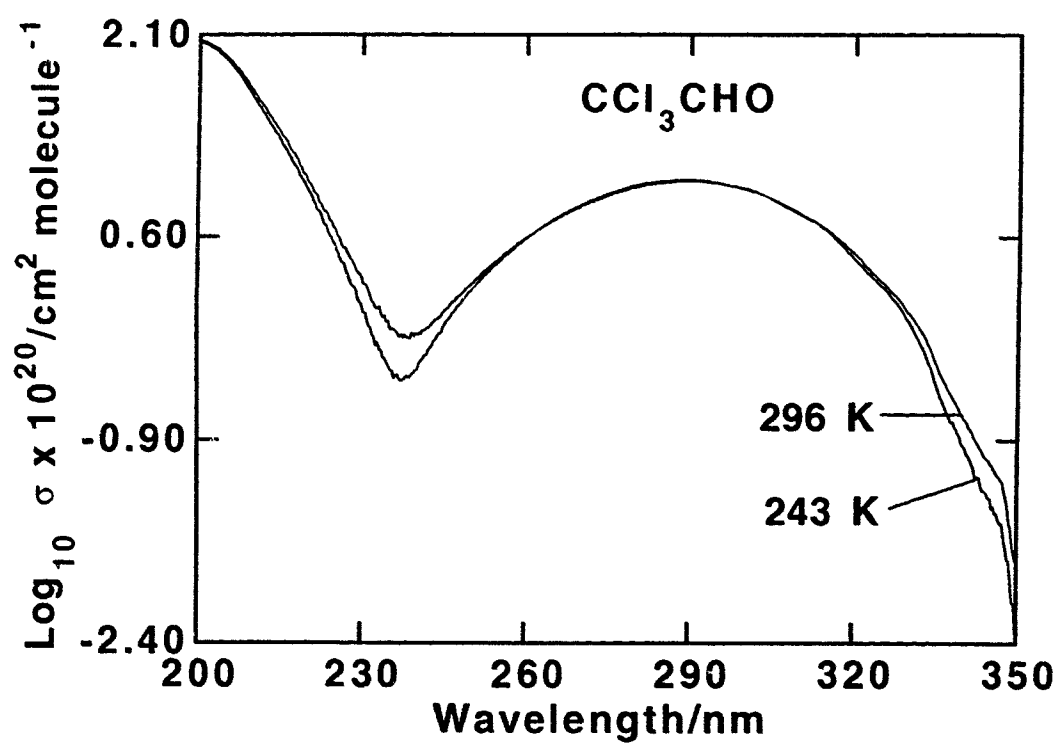
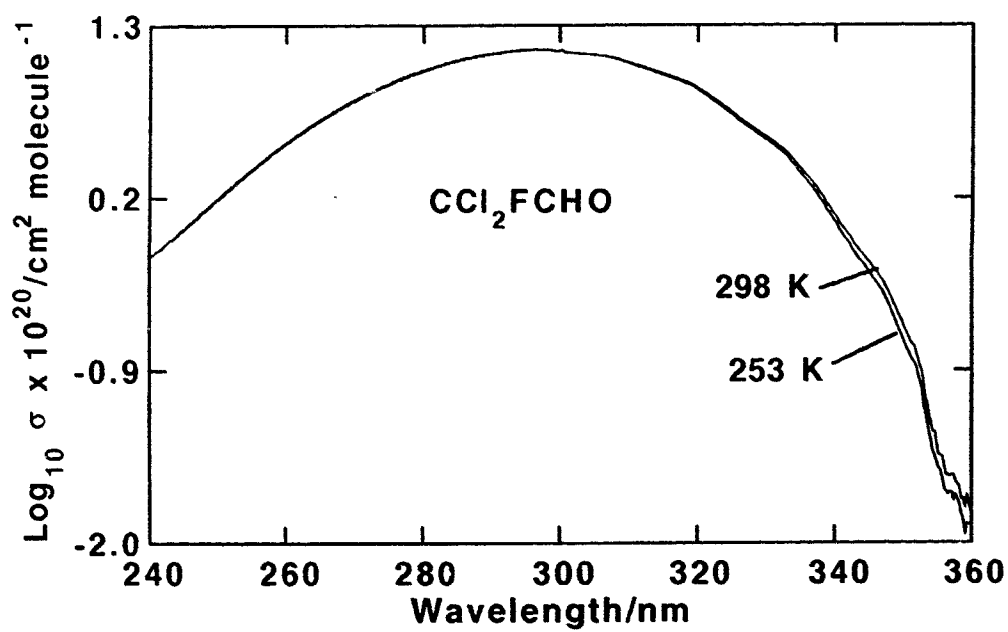


Fig. 2



0064

Corrigendum

J. Photochem. Photobiol. A: Chem., 66 (1992) 313-326

Temperature-dependent absorption cross-sections of gaseous nitric acid and methyl nitrate

O. Rattigan, E. Lutman, R. L. Jones, R. A. Cox, K. Clemitshaw and J. Williams

The intercepts and slopes in Table 3 obtained from the plot of $\log_{10} \sigma = \log_{10} \sigma_0 + BT$ in Fig. 7 are not the least squares linear regression values as stated on page 321. The correct values should be as follows:

TABLE 3

Temperature dependence of HNO₃ and CH₃ONO₂ absorption cross-sections

Wavelength (nm)	σ_0 ($\times 10^{21}$ cm ² per molecule) ^a		B ($K^{-1} \times 10^3$) ^b	
	HNO ₃	CH ₃ ONO ₂	HNO ₃	CH ₃ ONO ₂
270	5.63	8.91	1.56	1.41
280	4.33	4.92	1.38	1.70
290	1.89	2.18	1.71	2.00
300	0.71	0.62	1.86	2.58
310	0.14	0.129	2.61	3.23
320	0.0012	0.0035	7.77	6.56
330	0.0002	0.0004	7.90	7.38

^aIntercept

^bSlope of plot of $\log_{10} \sigma = \log_{10} \sigma_0 + BT$

As a consequence of this error, Table 4 should also be corrected. The correct Table 4 is shown below.

TABLE 4

Recommended cross-sections for HNO₃

Wavelength (nm)	Cross section at 298 K ($\times 10^{20}$ cm ² molecule ⁻¹)	B^a ($K^{-1} \times 10^3$)
190	1560.0	0
200	661.0	0
210	105.0	1.09
220	14.1	1.09
230	5.45	1.52
240	2.44	1.52
250	1.92	1.52
260	1.86	1.52
270	1.59	1.52
280	1.10	1.52
290	0.613	1.95
300	0.243	2.61
310	0.081	3.91
320	0.017	7.82
330	0.003	> 7.82

^aThe B values refer to the temperature dependence obtained from the equation $\log_{10} \sigma = \log_{10} \sigma_{298} + B(T - 298)$

not least because of the low vapour pressures of these compounds at temperatures relevant to the troposphere and lower stratosphere. Although the present work has provided improved accuracy of measurements of the HNO_3 and CH_3ONO_2 absorption cross-sections there is still a need for further improvement in the determination of the temperature dependences in the long-wavelength tail, particularly for HNO_3 in view of its importance with regard to stratospheric ozone depletion.

Acknowledgments

We thank the Alternative Fluorocarbon Environmental Acceptability Study (AFEAS) and the UK Department of the Environment for support. O.R. thanks the Commission of The European Communities for a post doctoral fellowship award.

References

- 1 S. Solomon, *Nature*, 347 (1990) 347.
- 2 F. Biaume, *Photochem.* 2 (1973-1974) 139.
- 3 W. B. DeMore, M. J. Molina, S. F. Sander, D. M. Golden, R. F. Hampson, M. J. Kurylo, C. J. Howard and A. R. Ravishankara, *JPL Publication 90-1*, 1990 (Jet Propulsion Laboratory, Pasadena, CA).
- 4 R. Atkinson, D. L. Baulch, R. A. Cox, R. F. Hampson, J. A. Kerr and J. Troe, *J. Phys. Chem. Ref. Data.*, 18 (1989) 881.
- 5 L. T. Molina and M. J. Molina, *J. Photochem.*, 15 (1981) 97.
- 6 H. Johnston and R. Graham, *J. Phys. Chem.*, 77 (1973) 62.
- 7 R. L. Jones, J. Austin, D. S. McKenna, J. G. Anderson, D. W. Fahey, C. B. Farmer, L. E. Heidt, K. K. Kelly, D. M. Murphy, M. H. Proffitt, A. F. Tuck and J. F. Vedder, *J. Geophys. Res.*, 94 (D9) (1989) 11529.
- 8 J. M. Roberts and R. W. Fajer, *Environ Sci. Technol.*, 23 (1989) 945.
- 9 W. D. Taylor, T. D. Allston, M. J. Moscato, G. B. Fazekas, R. Kozlowski and G. A. Takacs, *Int. J. Chem. Kinet.*, 12 (1980) 231.
- 10 M. P. Turberg, D. M. Giolando, C. Tilt, T. Soper, S. Mason, M. Davies, P. Klingensmith and G. A. Takacs, *J. Photochem. Photobiol. A: Chem.*, 51 (1990) 281.
- 11 R. Boschan, R. T. Merrow and R. W. Van Dolah, *Chem. Rev.*, 55 (1955) 485.
- 12 F. H. Verhoek and F. Daniels, *J. Am. Chem. Soc.*, 53 (1931) 1250.
- 13 J. G. Calvert and J. N. Pitts, Jr., *Photochemistry*, Wiley, New York, 1966.
- 14 D. Lary, *Ph.D. Dissertation*, University of Cambridge, 1991.

Temperature-dependent absorption cross-sections of CF_3COCl , CF_3COF , CH_3COF , CCl_3CHO and CF_3COOH

O. V. Rattigan, O. Wild and R. L. Jones

Centre for Atmospheric Science, Department of Chemistry, University of Cambridge, Lensfield Road, Cambridge CB2 1EW (UK)

R. A. Cox

NERC, Polaris House, North Star Avenue, Swindon SN2 1EU (UK)

(Received April 24, 1992; accepted February 11, 1993)

Abstract

Absorption cross-sections for CF_3COCl , CF_3COF , CH_3COF , CCl_3CHO and CF_3COOH have been measured in the wavelength region 200–360 nm, using a dual-beam diode-array spectrometer, with a spectral resolution (FWHM) of 1.2 nm. The temperature dependence of the absorption cross-sections was investigated for CF_3COCl , CF_3COF and CCl_3CHO . Absorption over most of the wavelength range showed a distinct temperature dependence, with a significant decline in the cross-section in the long wavelength tail with decreasing temperature. The calculated atmospheric photolysis lifetimes suggest that in the troposphere, photolysis is an important removal process for both CF_3COCl and CCl_3CHO but is unimportant for CF_3COF , CF_3COOH and CH_3COF .

1. Introduction

A significant increase in the use of selected hydrochlorofluorocarbons (HCFCs) and hydrofluorocarbons (HFCs) as replacements for the CFCs is expected to occur over the next decade. The removal of these compounds from the atmosphere initiated by hydroxyl radical attack is expected to lead to several types of photochemically active products [1]. These include hydroperoxides (ROOH) and peroxy nitrates (RO_2NO_2) formed by the reaction of RO_2 radicals with HO_2 and NO_2 respectively, and halogenated carbonyls formed by the oxidation of RO_2 (where R is a halogen-substituted alkyl radical).

Tropospheric removal of the halogenated carbonyls can occur in a number of ways including photolysis, hydrolysis and reaction with hydroxyl radicals [1]. Determination of the relative importance of these degradation pathways requires a knowledge of the atmospheric lifetime for each process. In order to assess the importance of photolysis the absorption cross-sections need to be determined. Furthermore, temperatures in the troposphere decrease by approximately 6–7 K per 1 km rise in altitude. It is therefore important to determine the absorption cross-sections of these halogenated carbonyls at atmospheric temperatures. Except for the recent work of Gillotay *et*

al. [2], previous measurements of the UV absorption cross-sections of the halogenated carbonyls [3–6] have been confined to room temperature.

In the present study, the absorption cross-sections for CF_3COCl , CF_3COF , CH_3COF , CCl_3CHO and CF_3COOH have been determined in the wavelength range 200–360 nm. The first four compounds are possible products arising from the oxidation of HCFC 123 (CF_3CHCl_2), HFC 134a ($\text{CF}_3\text{CH}_2\text{F}$), HFC 152a (CH_3CHF_2) and 1,1,1-trichloroethane respectively. CF_3COOH can be formed in the hydrolysis of CF_3COCl and CF_3COF , as well as in the reaction of CF_3CO_2 with HO_2 [1]. The temperature dependence of the absorption cross-sections for CF_3COCl , CF_3COF and CCl_3CHO has also been determined in the range 296–233 K.

2. Experimental details

Absorption measurements were made using a dual-beam diode-array spectrometer, illustrated schematically in Fig. 1. A collimated beam from a deuterium lamp (Hamamatsu 30 W, L 1636) was passed through a beam splitter (Oriel Scientific, model 78150) and the two beams (reference and sample) were collected in fibre-optic couplers

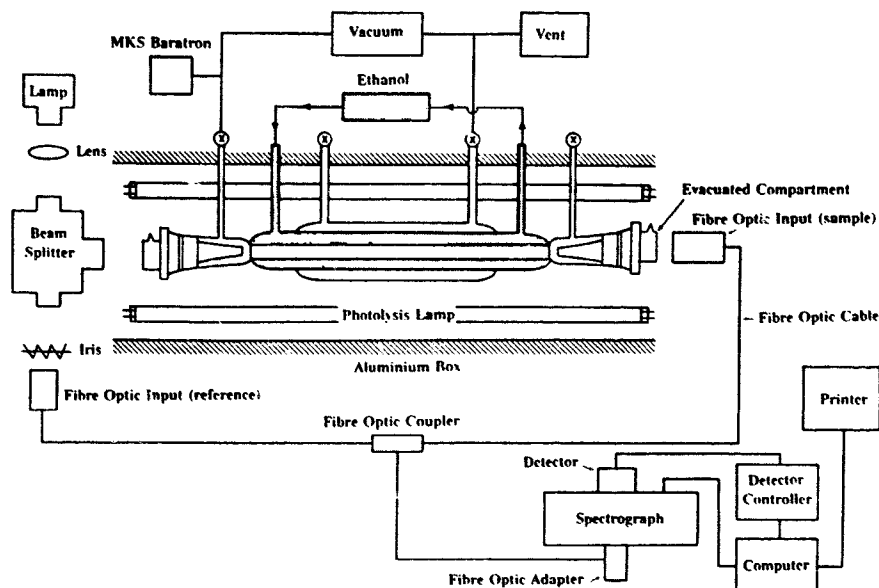


Fig. 1. Schematic diagram of UV diode-array spectrometer.

(Oriol Scientific, model 77800) either directly (reference) or after passage longitudinally through a 1 m long jacketed quartz cell (sample). The temperature of the cell could be regulated in the range 298–230 K by flowing ethanol through the inner jacket from a thermostatically-controlled cooling bath (Statim). Evacuated double end-window assemblies prevented frosting on the optical faces at low temperatures. The light beams from the fibre-optic couplers were directed one above the other into the 500 μm wide inlet slit of a 275 mm Czerny–Turner spectrograph (Acton Research Corporation, ‘Spectropro 275’). A 600 groove mm^{-1} holographic grating was used to disperse the beams, on to two 512 channel unintensified silicon diode arrays (Reticon). The detector function was controlled by an SI-180 O-SMA detector controller coupled to a Dell 316 SX computer. Software packages were used for linearisation of the wavelength scale, for background subtraction and averaging of the data, and for calculation of the absorbance using the reference spectrum to correct for changes in the source lamp intensity.

The main limitation in the accuracy of the absorbance measurements was the drift with time of the baseline, caused apparently by inhomogeneities in the source output affecting the reference and sample beams differently. This limited the accuracy of measurements to ± 0.0005 absorbance units, corresponding to a cross-section of approximately $10^{-23} \text{ cm}^2 \text{ molecule}^{-1}$ for the partial pressures used.

Gases were introduced to the cell from a conventional static vacuum system constructed of Pyrex glass employing Youngs greaseless taps. Pressures were measured using calibrated Baratron gauges (100 Torr MKS 222 A and 1000 Torr MKS 122 AA).

CF_3COCl (97%), CF_3COF (97%), CH_3COF (97%) and CF_3COOH (99.5%) were obtained from Fluorochem Ltd. CCl_3CHO was obtained from Fluka with a stated purity of 99% but contained traces of chloral hydrate ($\text{CCl}_3\text{CH}(\text{OH})_2$). CCl_3CHO was therefore transferred to a trap under a nitrogen atmosphere to exclude water vapour. All samples were degassed and trap-to-trap distilled prior to storage on the vacuum line.

3. Results

3.1. Room temperature measurements

Measurements of CF_3COCl , CF_3COF , CH_3COF , CCl_3CHO and CF_3COOH absorption spectra were made in the wavelength range 200–360 nm at several different pressures up to somewhat lower than the saturated vapour pressure. Inaccuracies in the cross-section measurements in the short wavelength region (less than 220 nm) arose because of the low light levels transmitted by the optical fibres at shorter wavelengths. In the longer wavelength region, the residual absorbance was not significantly greater than the baseline drift of approximately ± 0.0005 absorbance units. The ab-

sorbance showed good agreement with the Beer-Lambert Law provided the absorbance was less than 0.80. The absorption cross-section data are shown in log form (base 10) in Figs. 2-6. Absolute cross-sections, averaged over 5 nm intervals, are listed in Tables 1-4.

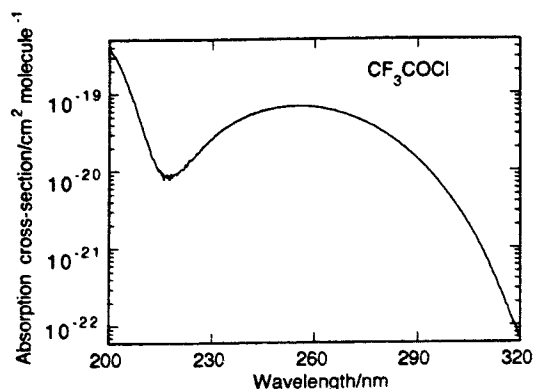


Fig. 2. Absorption spectrum of CF_3COCl at 296 K.

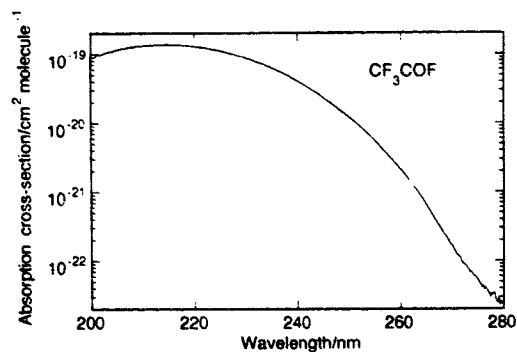


Fig. 3. Absorption spectrum of CF_3COF at 293 K.

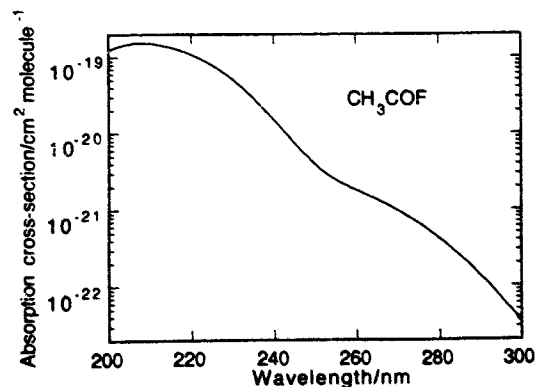


Fig. 4. Absorption spectrum of CH_3COF at 296 K.

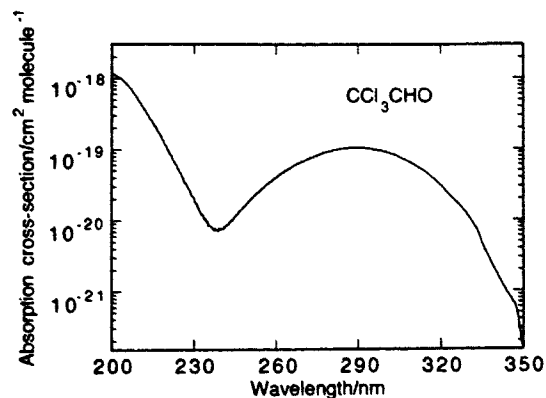


Fig. 5. Absorption spectrum of CCl_3CHO at 296 K.

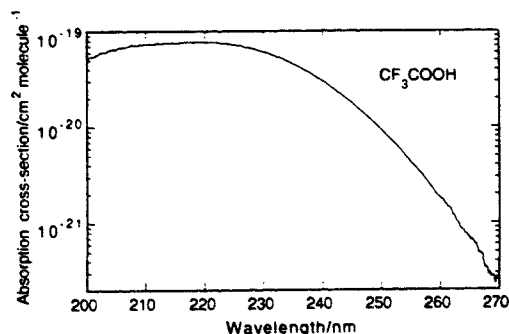


Fig. 6. Absorption spectrum of CF_3COOH at 296 K.

3.1.1. CF_3COCl

Trifluoroacetyl chloride absorbs strongly in the 200–215 nm region with a second, somewhat weaker, broad absorption band between 215 nm and 330 nm with a maximum absorption cross-section of $6.80 \times 10^{-20} \text{ cm}^2 \text{ molecule}^{-1}$ at 255 nm (Fig. 2).

3.1.2. CF_3COF

Trifluoroacetyl fluoride has a broad absorption between 200 nm and 300 nm with maximum absorption cross-section of $13.8 \times 10^{-20} \text{ cm}^2 \text{ molecule}^{-1}$ at 214 nm (Fig. 3).

3.1.3. CH_3COF

Acetyl fluoride appears to have two overlapping absorption bands in the UV, the first one with a maximum absorption cross-section of $12.4 \times 10^{-20} \text{ cm}^2 \text{ molecule}^{-1}$ at 207 nm, and a second band appearing as a shoulder near 260 nm and extending out to 310 nm (Fig. 4).

TABLE 1. Absorption cross-section for CF_3COCl

Wavelength (nm)	Cross-section $\times 10^{20}$ cm^2 molecule $^{-1}$		
	296 K	253 K	233 K
200	37.98	33.83	31.88
205	14.75	12.81	12.02
210	3.526	2.678	2.560
215	1.041	0.711	0.695
220	1.106	0.910	0.834
225	1.687	1.621	1.578
230	2.871	2.744	2.674
235	4.009	3.966	3.874
240	5.092	5.074	4.975
245	5.972	5.947	5.845
250	6.571	6.520	6.414
255	6.796	6.676	6.553
260	6.606	6.433	6.317
265	5.967	5.742	5.625
270	5.126	4.890	4.785
275	4.217	3.978	3.878
280	3.111	2.901	2.817
285	2.166	1.985	1.914
290	1.386	1.249	1.197
295	0.809	0.706	0.668
300	0.425	0.358	0.334
305	0.198	0.159	0.145
310	0.077	0.056	0.048
315	0.024	0.016	0.012
320	0.007	0.005	0.004
325	0.002	0.001	0.001
330	0.0	0.0	0.0

TABLE 2. Absorption cross-section for CF_3COF

Wavelength (nm)	Cross-section $\times 10^{20}$ cm^2 molecule $^{-1}$	
	293 K	238 K
200	9.354	9.456
205	11.47	11.63
210	13.14	13.16
215	13.63	13.69
220	12.87	13.09
225	11.11	11.40
230	8.775	9.106
235	5.299	6.551
240	4.074	4.179
245	2.348	2.298
250	1.220	1.157
255	0.552	0.491
260	0.216	0.179
265	0.070	0.047
270	0.026	0.010
275	0.010	0.003
280	0.003	0.001
285	0.002	0.000
290	0.001	0.000
295	0.000	0.000

TABLE 3. Absorption cross-section for CH_3COF and CF_3COOH at 296 K

Wavelength (nm)	Cross-section $\times 10^{20}$ cm^2 molecule $^{-1}$	
	CH_3COF	CF_3COOH
200	11.26	5.201
205	12.16	6.484
210	11.96	7.229
215	10.53	7.585
220	8.345	7.760
225	5.974	7.209
230	3.829	6.025
235	2.186	4.463
240	1.135	2.892
245	0.566	1.685
250	0.311	0.870
255	0.206	0.390
260	0.158	0.155
265	0.120	0.050
270	0.090	0.013
275	0.056	0.006
280	0.029	0.000
285	0.016	
290	0.008	
295	0.004	
300	0.002	
305	0.001	
310	0.000	

3.1.4. CCl_3CHO

Trichloroacetaldehyde exhibits strong absorption between 200 nm and 230 nm, and a second, somewhat weaker, absorption between 230 nm and 355 nm with a maximum absorption cross-section of 10.4×10^{-20} cm^2 molecule $^{-1}$ at 289 nm (Fig. 5).

3.1.5. CF_3COOH

Trifluoroacetic acid exhibits a single absorption band with a broad maximum near 215 nm, extending out to approximately 275 nm (Fig. 6).

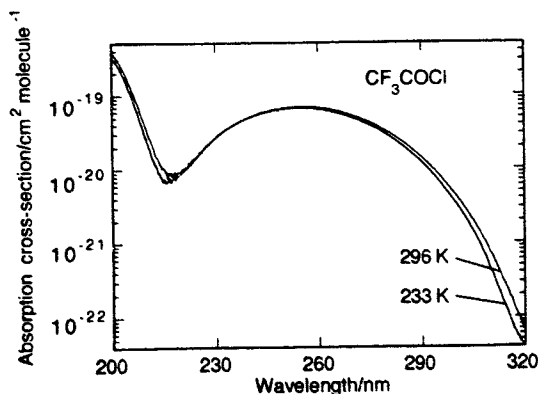
3.2. Temperature dependence of cross-sections

Absorption measurements of CF_3COF , CF_3COCl and CCl_3CHO in the wavelength range 200–360 nm were made at several temperatures in the range 296–233 K. At each temperature at least five spectra were recorded and the data averaged to produce the absorption cross-section at 0.15 nm intervals. The standard deviations on the cross-sections for CF_3COCl at 296 K were approximately 2% at wavelengths less than 300 nm increasing to 70% near the limit of measurable absorbance at 325 nm. At 233 K the standard deviation was 4% at wavelengths less than 300 nm increasing to 80% at 325 nm. Figures 7–9 illustrate the temperature dependence of the cross-

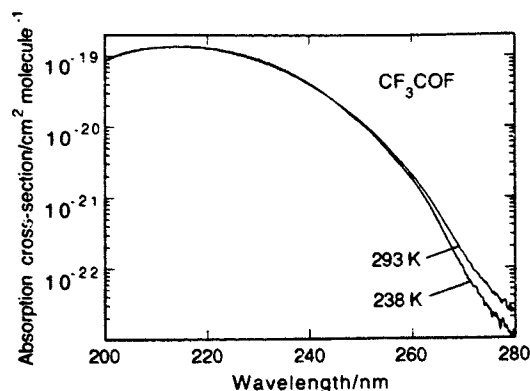
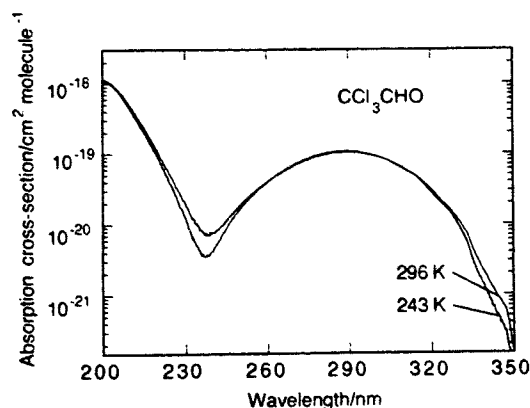
0075

TABLE 4. Absorption cross-section for CCl_3CHO

Wavelength (nm)	Cross-section $\times 10^{20}$ cm^2 molecule $^{-1}$	
	296 K	243 K
200	115.1	110.7
205	86.14	81.89
210	48.19	43.20
215	23.88	20.32
220	10.92	9.179
225	4.759	3.527
230	2.034	1.264
235	0.944	0.430
240	0.774	0.418
245	1.135	0.882
250	1.827	1.633
255	2.799	2.659
260	3.977	3.910
265	5.360	5.388
270	6.722	6.878
275	8.012	8.368
280	9.318	9.625
285	10.08	10.35
290	10.32	10.62
295	9.886	10.06
300	9.019	9.245
305	7.671	7.602
310	6.074	5.942
315	4.572	4.446
320	3.063	2.790
325	1.901	1.741
330	1.121	0.951
335	0.498	0.322
340	0.194	0.114
345	0.086	0.043
350	0.020	0.004
355	0.002	0.000
360	0.000	0.000

Fig. 7. Temperature dependence of CF_3COCl absorption cross-section in the wavelength range 200–320 nm.

sections for CF_3COF , CF_3COCl and CCl_3CHO in the wavelength range 200–360 nm. The spectra show a clear temperature dependence which is

Fig. 8. Temperature dependence of CF_3COF absorption cross-section in the wavelength range 200–280 nm.Fig. 9. Temperature dependence of CCl_3CHO absorption cross-section in the wavelength range 200–350 nm.

different for each of the compounds investigated. The spectra for CF_3COCl (Fig. 7) show a decline in the cross-section with decreasing temperature over most of the longer wavelength absorption band (215–330 nm), the decline being more pronounced in the long wavelength tail of this band at wavelengths greater than 290 nm. The temperature dependence also extends into the shorter wavelength region of the spectrum particularly at wavelengths less than 215 nm. In the case of CF_3COF and CCl_3CHO (Figs. 8 and 9) the decline is mainly apparent in the wings of the absorption bands, the cross-sections show an increase with decreasing temperature around the band maxima.

A more detailed investigation was undertaken for CF_3COCl . Measurements of the cross-section were carried out at six different temperatures in the range 296–227 K. Figure 10 shows a plot of $\log_{10} \sigma$ vs. temperature (K) for selected wavelengths in the long wavelength tail. The data show a good

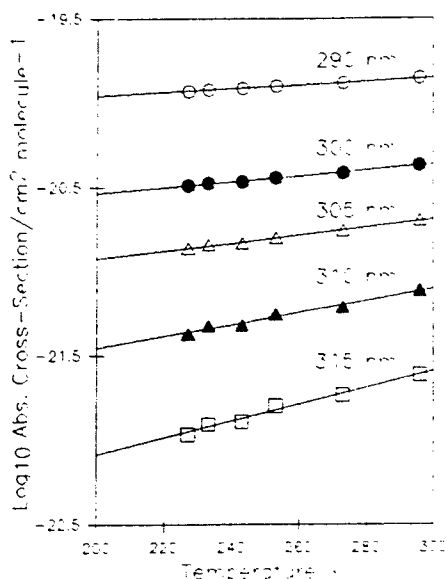


Fig. 10. Plot of logarithm of the absorption cross-section at selected wavelengths against temperature for CF_3COCl . Lines show least-squares linear regression slopes.

TABLE 5. Temperature dependence of CF_3COCl absorption cross-sections

Wavelength (nm)	$10^{21} (\sigma_0 \text{ cm}^{-2} \text{ molecule}^{-1})^a$	$(B/K^{-1} \times 10^3)^a$
290	6.866	1.028
300	1.346	1.672
305	0.424	2.253
310	0.070	3.457
315	0.9086	4.935
320	0.0042	6.370 ^b

^aIntercept and slope obtained from a plot of $\log_{10} \sigma = \log_{10} \sigma_0 + B/T$.

^bThe B value at 320 nm was extrapolated from a plot of $\log_{10} B$ vs. wavelength.

linear fit over the entire temperature range. In general the slopes of the plots show an increase with increasing wavelength as the temperature dependence becomes more marked, Table 5.

The spectrum for CH_3COF was found to change with time, possibly because of hydrolysis on the cell walls to form acetic acid. A fresh sample was used each time for absorption measurements. Because of this instability, the temperature dependence of the absorption cross-section was not investigated. Since the spectrum for CF_3COOH does not extend beyond 280 nm, photolysis is therefore relatively unimportant in the troposphere and hence the temperature dependence of the cross-section was not investigated.

4. Discussion

The absorption spectra of the halogenated carbonyls CX_3CXO show strong absorption in the UV, and by analogy with the aldehydes and ketones, bands caused by the $n \rightarrow \pi^*$ electronic transition of the $\text{C}=\text{O}$ group are expected. It appears that substitution of the halogen on the carbonyl carbon $\text{X}-\text{C}=\text{O}$ has the effect of shifting the absorption to shorter wavelengths. In CH_3COF , Fig. 4, the $n \rightarrow \pi^*$ band appears as a shoulder at 260 nm on the more intense absorption band centred around 207 nm. This may be compared with CH_3CHO where the $n \rightarrow \pi^*$ band centre is at 290 nm. Substitution of the halogen on the β -C atom also modifies the absorption spectrum significantly. Thus CF_3COCl , Fig. 2, has an absorption band, believed to be a result of the $n \rightarrow \pi^*$ transition, centred at 255 nm whereas in CF_3COF , Fig. 3, the band is blue shifted to 214 nm. In CCl_3CHO , Fig. 5, the $n \rightarrow \pi^*$ band has a maximum around 289 nm, extending out to 360 nm.

The UV absorption cross-sections for CF_3COCl and CF_3COF have previously been determined by Meller *et al.* [5] using a diode-array spectrometer. They report maximum absorption cross-sections of $6.87 \times 10^{-20} \text{ cm}^2 \text{ molecule}^{-1}$ at 255 nm and $14.1 \times 10^{-20} \text{ cm}^2 \text{ molecule}^{-1}$ at 212 nm for CF_3COCl and CF_3COF respectively, in excellent agreement with values of $6.80 \times 10^{-20} \text{ cm}^2 \text{ molecule}^{-1}$ at 255 nm and $13.8 \times 10^{-20} \text{ cm}^2 \text{ molecule}^{-1}$ at 214 nm from the present study. Jemi-Alade *et al.* [7] have measured the absorption spectrum of CF_3COCl between 220 nm and 290 nm, as part of their work on the chlorine-initiated oxidation of hydrohalocarbons. The shape of their absorption spectrum closely resembles that obtained in the present work, and they report a cross-section of $6.72 \times 10^{-20} \text{ cm}^2 \text{ molecule}^{-1}$ at 250 nm which is also in excellent agreement with the present work. Libuda *et al.* [6] and Gillotay *et al.* [2] have measured the absorption spectrum for CCl_3CHO . Libuda *et al.* [6] used a diode-array spectrometer and reported a maximum cross-section of $9.73 \times 10^{-20} \text{ cm}^2 \text{ molecule}^{-1}$ at 290 nm compared to $11.6 \times 10^{-20} \text{ cm}^2 \text{ molecule}^{-1}$ at 288 nm obtained by Gillotay *et al.* [2] in a dual-beam apparatus with a photomultiplier detector system. Our value of $10.4 \times 10^{-20} \text{ cm}^2 \text{ molecule}^{-1}$ at 289 nm is approximately midway between these two measurements.

4.1. Temperature dependences

Trifluoroacetyl fluoride, trifluoroacetyl chloride and trichloroacetaldehyde all showed a significant

variation in the absorption cross-section with temperature (Figs. 7–9) which was different for all three compounds. The variation was more pronounced in the long wavelength tail but the temperature dependence also extended into the shorter wavelength absorption bands. Gillotay *et al.* [2] have recently measured the temperature dependence of the UV absorption cross-sections for COCl_2 , CCl_3COCl and CCl_3CHO . They also observed a decrease in the cross-section in the tail of the absorption bands with declining temperatures whereas only a relatively minor change was observed at the band maximum. The magnitude of the temperature dependence for CCl_3CHO matches well with that of the present study.

The temperature dependence for CF_3COCl is illustrated in Fig. 10 where $\log_{10} \sigma$ is plotted against temperature for selected wavelengths in the tail of the UV absorption band. The intercepts and slopes of these plots, obtained by linear regression analysis, are given in Table 5. The slopes of these plots, B values, increase with increasing wavelength reflecting the increased importance of the temperature dependence at longer wavelengths. However, because of the large uncertainty (about 80%) in the cross-section at the lowest temperature in the longer wavelength region, the B value at 320 nm was extrapolated from a plot of $\log_{10} B$ vs. wavelength.

The temperature coefficients obtained from the plot of $\log_{10} \sigma$ vs. T can be used to obtain cross-sections outside the experimental range by extrapolation. This is particularly important for the purposes of calculating the photodissociation rate of CF_3COCl at temperatures relevant to the upper troposphere. The linearity of the plots in Fig. 10 allows the cross-section to be calculated for any temperature in the range 200–300 K from the equation:

$$\log_{10} \sigma = \log_{10} \sigma_0 + BT$$

It is believed that the decrease in the cross-section with decreasing temperature is caused by a reduction in the population of the vibrational and rotational levels of the ground electronic state of the molecule at the lower temperatures [8]. The shape of the UV absorption spectrum results from a Boltzmann-weighted average of the absorption spectra from each vibrational level in the ground electronic state. Absorption from higher vibrational levels have maxima at longer and shorter wavelengths than the maxima in the absorption from the ground vibrational level. As the temperature decreases, the contribution from higher vibrational levels decreases, which results in a

decrease in the cross-section in the wings of the absorption spectrum and a corresponding increase at the band maximum. This is apparent in both CF_3COF and CCl_3CHO (Figs. 8 and 9) where there is little overlap of the two absorption bands, but not in CF_3COCl (Fig. 7) because of the predominant influence of the tail of the strong absorption band centred at less than 200 nm. A similar effect has been observed in the spectra for HNO_3 and CH_3ONO_2 [9] which also have two overlapping absorption bands.

4.2. Atmospheric photolysis rates

Photodissociation of the HCFC degradation products is possible following absorption in their broad continuous UV absorption spectra. The solar radiation is strongly attenuated in the UV at wavelengths from 220–290 nm by absorption resulting from ozone. Two spectral regions therefore play a major role in the photolysis of the halogenated carbonyls. The first region, around 200 nm, becomes more important at higher altitudes, above 25 km, whereas the second region greater than 290 nm is dominant below 20 km [10]. Figure 11 shows a plot of \log_{10} (solar flux) vs. wavelength at 300 mbar (upper troposphere) [11] which

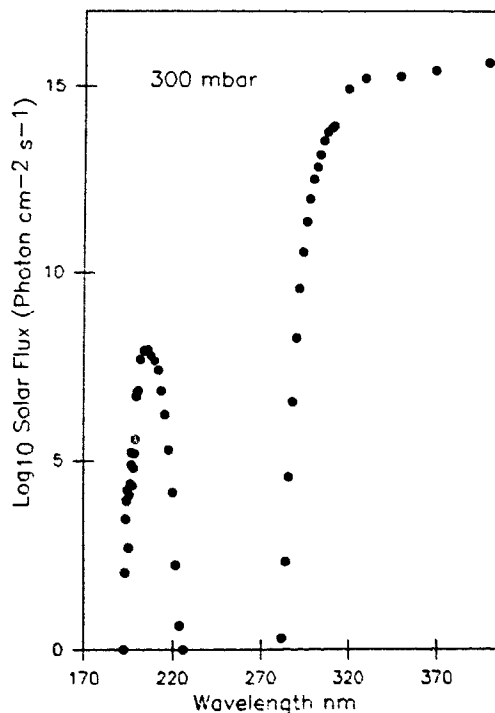


Fig. 11. Plot of logarithm of the solar flux vs. wavelength at 300 mbar.

clearly illustrates that wavelengths greater than 290 nm have the major contribution to photolysis in the troposphere.

The absorption cross-sections shown in Tables 1–4 were used to calculate globally averaged tropospheric photolysis lifetimes for CH_3COF , CF_3COF , CF_3COOH , CF_3COCl and CCl_3CHO (Table 6). These calculations were carried out using the Cambridge two-dimensional model [12]. An albedo of 0.35 was used, and a photodecomposition quantum efficiency of unity was assumed.

Table 6 lists the tropospheric lifetimes with respect to photolysis, reaction with OH and physical removal for CH_3COF , CF_3COF , CF_3COCl , CCl_3CHO and CF_3COOH . The OH lifetime for CCl_3CHO was calculated using the rate constant of $1.6 \times 10^{-12} \text{ cm}^3 \text{ molecule}^{-1} \text{ s}^{-1}$ determined by Scollard *et al.* [13]. For CH_3COF no rate data for the reaction with OH have been reported, thus the value for the reaction of OH with CH_3COCl [14] ($k = 0.91 \times 10^{-14} \text{ cm}^3 \text{ molecule}^{-1} \text{ s}^{-1}$) has been used. Since the Henry's Law solubilities for the acid halides are not well known, the removal rate by cloud water or deposition to the ocean is difficult to assess. Wine and Chameides [1] estimated that the hydrolysis lifetimes for acid halides are dominated by transport to the marine environment and cloudy regions, and are of the order of 1–2 months. Worsnop *et al.* [15] were unable to determine any significant uptake of gaseous acid halides into droplets, and thus removal by rainout was expected to be unimportant. However, recent modifications to their apparatus have enabled them to determine uptake coefficients and Henry's Law constants for COCl_2 , CF_3COCl and CF_3COF [16]. Their estimated lifetimes of these compounds because of removal in cloud water are approximately 20 d.

Both photolysis and reaction with OH are very slow for CH_3COF and CF_3COF (Table 6). Therefore, transport to the marine environment and cloudy regions with physical removal is likely to be their major loss process in the troposphere.

Hydrolysis products include CH_3COOH and HF from CH_3COF and CF_3COOH and HF from CF_3COF . The results from the present study suggest that photolysis of these acids is relatively unimportant and physical removal processes will therefore dominate.

For trifluoroacetyl chloride both photolysis (lifetime = 33 d) and uptake into cloud water (lifetime = 20 d) are the main loss processes. Hydrolysis of CF_3COCl will form CF_3COOH and HCl. These acids HCl and CF_3COOH are readily soluble in water and will be removed by precipitation.

Photolysis (lifetime = 3.4 h) and reaction with hydroxyl radicals (lifetime = 7 d) are the main loss processes for trichloroacetaldehyde. Therefore, provided the photolysis quantum yield is greater than or equal to that for CH_3CHO [17], photolysis is likely to be the major removal mechanism for trichloroacetaldehyde in the higher troposphere. The major photolysis products are COCl_2 and CO_2 [14]. COCl_2 is expected to be removed by hydrolysis in cloud water on a time scale of approximately 20 d [16].

5. Conclusion

The absorption cross-sections for CF_3COCl , CF_3COF , CH_3COF , CCl_3CHO and CF_3COOH have been measured over the wavelength range 200–360 nm. A significant temperature dependence in the absorption cross-sections was observed for CF_3COCl , CF_3COF and CCl_3CHO , which was particularly pronounced in the long wavelength tail of their absorption spectra. The calculated atmospheric photolysis lifetimes suggest that in the lower atmosphere, photolysis is an important removal process for CF_3COCl and CCl_3CHO but that physical removal processes in cloudy regions and in the marine environment are more important for CH_3COF , CF_3COF and CF_3COOH .

TABLE 6. Tropospheric lifetimes for the halogenated carbonyls

Removal	CH_3COF	CF_3COF	CF_3COCl	CCl_3CHO	CF_3COOH
*Photolysis	41 yrs	3×10^3 yrs	33 d	3.4 h	6×10^3 yrs
OH	3 yrs ^b	—	—	7 d	^c
Hydrolysis	1–2 mths ^d	20 d ^e	20 d ^e	120 d ^f	1–2 mths ^d

*Photolysis lifetimes are globally averaged tropospheric values.

^bOH lifetime CH_3COF calculated assuming $k(\text{OH}) \text{CH}_3\text{COCl}$ [14].

^cOH rate constant not determined.

^dHydrolysis lifetimes are upper estimates taken from Wine and Chameides [1].

^eWorsnop *et al.* [16].

^fAssumed the same as CH_3CHO [16].

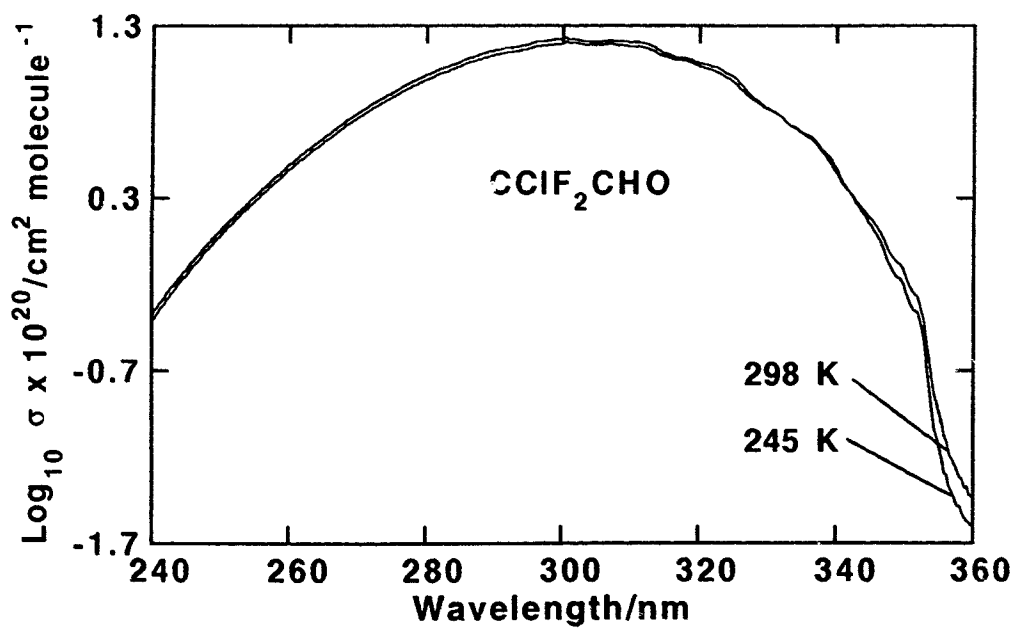
Acknowledgments

The authors wish to thank the Alternative Fluorocarbon Environmental Acceptability Study SPA-AFEAS, INC on contract (CTR90-2/P90-007) and the Department of the Environment, UK on contract (ref. PECD 7/12/47). OR wishes to thank the Commission of the European Communities for a post-doctoral fellowship award. Thanks are due to K. S. Law and E. Lutman for helpful discussion.

References

- 1 *Scientific Assessment of Stratospheric Ozone*, World Meteorological Organisation Report No. 20, Volume 2, 1989.
- 2 D. Gillotay, P. C. Simon and L. Dierickx, UV absorption cross-sections of some carbonyl compounds and their temperature dependence, *Quadrennial Ozone Symposium*, University of Virginia, June, 1992.
- 3 C. C. Chou, G. Crescentini, H. vera Ruiz, W. S. Smith and F. S. Rowland, Stratospheric photochemistry of CF₂O, CClFO and CCl₂O, *173rd Am. Chem. Soc. Meeting, New Orleans, LA*, 1977.
- 4 L. T. Molina and M. J. Molina, Chemistry of fluorine in the stratosphere, *182nd Am. Chem. Soc. Nat. Meeting, New York, August, 1982*.
- 5 R. Meller, D. Boglu and G. K. Moortgat, UV spectra of several halogenated carbonyl compounds and FTIR studies on the degradation of CF₃COCl, HCFC 123 and HFC 134a, *STEP-HALOCSIDE/AFEAS Workshop, Dublin, May, 1991*, University College Dublin.
- 6 H. G. Libuda, F. Zabel and K. H. Becker, UV spectra of some organic chlorine and bromine compounds of atmospheric interest, *STEP-HALOCSIDE/AFEAS Workshop, Dublin, May, 1991*, University College Dublin.
- 7 A. A. Jemi-Alade, P. D. Lightfoot and R. Lesclaux, *Chem. Phys. Lett.*, **179** (1991) 119.
- 8 H. Okabe, *Photochemistry of Small Molecules*, Wiley, New York, 1978.
- 9 O. Rattigan, E. Lutman, R. L. Jones, R. A. Cox, K. C. Clemitshaw and J. Williams, *J. Photochem. Photobiol. A: Chem.*, **66** (1992) 313.
- 10 F. Biau, *J. Photochem.*, **2** (1973) 139.
- 11 D. Lary, *Ph.D. Dissertation*, University of Cambridge, 1991.
- 12 R. S. Harwood and J. A. Pyle, *Quart. J. Roy. Met. Soc.*, **103** (1977) 319.
- 13 D. Scollard, M. Corrigan and H. Sidebottom, Kinetics and mechanisms for the oxidation of halogenated aldehydes, *STEP-HALOCSIDE/AFEAS Workshop, Dublin, May, 1991*, University College Dublin.
- 14 L. Nelson, I. Shanahan, H. W. Sidebottom, J. Treacy and O. J. Nielsen, *Int. J. Chem. Kinet.*, **22** (1990) 577.
- 15 D. R. Worsnop, G. N. Robinson, M. S. Zahniser and C. E. Kolb, Heterogeneous chemistry of alternative CFC oxidation intermediates, *STEP-HALOCSIDE/AFEAS Workshop, Dublin, May, 1991*, University College Dublin.
- 16 D. R. Worsnop, M. S. Zahniser, C. E. Kolb and P. Davidovits, The heterogeneous chemistry of carbonyl and haloacetyl halides, *AFEAS Workshop on Atmospheric Wet and Dry Deposition of Carbonyl and Haloacetyl Halides, Brussels, September, SPA-AFEAS, Washington, DC, 1992*.
- 17 D. L. Bauch, R. A. Cox, R. F. Hampson, Jr., J. A. Kerr, J. Troe and R. T. Watson, *J. Phys. Chem. Ref. Data*, **13** (1984) 1259.

Fig. 3



Temperature-dependent absorption cross-sections of gaseous nitric acid and methyl nitrate

O. Rattigan, E. Lutman, R. L. Jones and R. A. Cox[†]

Department of Chemistry, University of Cambridge, Lensfield Road, Cambridge CB2 1EW (UK)

K. Clemitshaw and J. Williams

School of Chemical Sciences, University of East Anglia, Norwich NR4 7TJ (UK)

(Received October 2, 1991; accepted February 6, 1992)

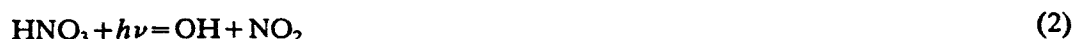
Abstract

Absorption cross-sections for HNO₃ and CH₃ONO₂ were measured in the wavelength region 220–340 nm, using a dual-beam diode array spectrometer, with a spectral resolution of 0.3 nm. The results at room temperature were in good agreement with earlier measurements. Absorption over most of the range showed a distinct temperature dependence, with a similar decline in cross-section with decreasing temperature in the range 295–239 K for both molecules. The results have quite large effects on the calculated photodissociation rate of HNO₃ in the lower stratosphere, especially at the low temperatures and high solar zenith angles (SZA) characteristics of the polar winter and spring. For example, at 20 km altitude, with an SZA of 80°, the photolysis rate at a temperature of 200 K is approximately a factor of 5 smaller than at 298 K.

1. Introduction

Nitric acid is the major reservoir for nitrogen oxides in the stratosphere. It is formed by the association reaction of the hydroxyl radical with NO₂ and by the heterogeneous reaction of dinitrogen pentoxide, N₂O₅, with water, on the surface of aerosol particles. The latter process is thought to be an important mechanism for the sequestration of stratospheric NO_x at high latitudes in winter time, especially during the polar night when polar stratospheric clouds form [1].

The release of nitrogen oxides from the HNO₃ reservoir occurs by reaction with hydroxyl radicals and by photodissociation of HNO₃:



Photodissociation of nitric acid occurs following absorption in its broad continuous UV absorption spectrum which starts near 330 nm and increases in intensity down to 190 nm. In the stratosphere, ozone absorption strongly reduces the photodissociation rate in the range 220–290 nm. Consequently, two spectral intervals play a major role in HNO₃ photolysis: the first interval around 200 nm is most important at high altitudes

[†]Author to whom correspondence should be addressed.

(above 25 km) and the second interval at around 300 nm, becomes dominant in the lower stratosphere at altitudes below 20 km [2].

Considering the importance of HNO₃ in stratospheric chemistry, there have been surprisingly few investigations of the absorption spectrum and photochemistry of HNO₃. The currently recommended values for the absorption cross-sections [3, 4] are based on the data of Molina and Molina reported in 1980 [5] as part of their study of the spectrum of HO₂NO₂. These data agree well with the earlier data of Biaueme [2] and those of Johnston and Graham [6], except near the long-wavelength tail of the absorption, where the uncertainty in all three studies is rather large. This uncertainty is due to the small HNO₃ cross-sections and also to the need to correct for the presence of small amounts of NO₂ impurity [2], which absorbs strongly in this region and seems to be unavoidably present in samples of pure HNO₃.

The need for accurate values for the HNO₃ photodissociation rates in the long-wavelength tail has recently become more important because of the critical role played by this process in the chemical changes in the lower stratosphere that are related to polar ozone depletion.

The extent to which the active chlorine species ClO can participate in photochemically driven ozone depletion cycles depends on the availability of NO₂, which converts ClO to the inactive chlorine reservoir, chlorine nitrate (ClONO₂):



Thus higher concentrations of NO₂ tend to suppress the ozone-depleting reactions of ClO. The availability of NO₂ is determined by the rate at which it is released from its major reservoir, HNO₃, which is primarily controlled by HNO₃ photodissociation in the high latitude springtime. Thus HNO₃ photodissociation exerts a controlling influence on the rate of "recovery" of the perturbed chemistry in air parcels which have been processed by exposure to polar stratospheric clouds (PSCs) in the north or south polar wintertime vortex [7]. The conditions for this recovery involve high solar zenith angles and low temperatures. We have therefore reinvestigated the UV spectrum of HNO₃ in the range 200–345 nm, with particular emphasis on determination of the temperature dependence of the absorption cross-sections near the long-wavelength tail of absorption in the near-UV region.

The alkyl nitrates have significance for tropospheric chemistry [8] and these molecules also exhibit a broad continuous UV absorption spectrum similar to HNO₃, which leads to photodissociation in the atmosphere, *e.g.*



There have been three recent studies devoted to the measurement of the absorption cross-sections of the alkyl nitrates [8–10]. There is reasonably good agreement between the results of these studies in the wavelength regions where they overlap, including the important long-wavelength tail, but all studies were restricted to room temperature. To extend the data for the purposes of calculating atmospheric photolysis rates, we measured the absorption cross-section for methyl nitrate over the range 200–340 nm as a function of temperature in the range 233–294 K. Analogous measurements for several C₂ to C₅ alkyl nitrates will be the subject of a separate report.

2. Experimental details

Absorption measurements were taken using a dual-beam diode array spectrometer. A well collimated beam from a deuterium lamp (Hamamatsu 30 W, L 1636) was

passed through a beam splitter (Oriel Scientific, model 78150) and the two beams, reference and sample, were collected in optical fibre couplers either directly (reference) or after passage through a 1 m long jacketed quartz sample cell (sample). The temperature of the cell could be regulated in the range 230–300 K by circulating cooled ethanol through the jacket. Evacuated double end-window assemblies prevented condensation on the optical faces. The light beams from the two optical fibres were directed one above the other into the 500 μm wide inlet slit of a 275 mm Czerny-Turner spectrograph (ARC, Spectropro) using a fibre optic adapter (Princeton Instrument Co., model OFA X1S). The spectrograph contained three indexable holographic gratings mounted on a turret under software control. A 600 groove mm^{-1} grating giving a spectral resolution of 0.3 nm and a range of 75 nm in each spectrum was used for the present study. The detector consisted of two 512 channel unintensified silicon diode arrays (Reticon), one above the other, in a cooled (-20°C), evacuated housing, mounted at the focal plane of the spectrograph. The detector function was controlled by an SI-180 0-SMA detector controller (Spectroscopy Instruments GmbH) which incorporated a 14-bit ADC, coupled to a Dell 316 SX computer. Software packages (Spectroscopy Instruments GmbH, POSMA) were used for calibration and linearization of the wavelength scale, for background subtraction and averaging of the data, and for calculation of absorbance using the reference spectrum to correct for changes in the source lamp intensity.

The main limitation of accuracy in the absorbance measurements for broad band spectra was the drift with time of the baseline, due apparently to inhomogeneities in the source output affecting the "reference" and "sample" beams differently. This baseline drift affected measurements at the 0.0005 absorbance unit level for continuous absorption: discrete absorption features, e.g. NO_2 at approximately 340 nm, could be detected at the 0.0001 absorbance level. Poor transmission of the optical fibres for light below 220 nm limited the accuracy of absorption measurements at the short-wavelength end of the range.

Gases were introduced to the sample cell from a conventional Pyrex glass vacuum line, with Youngs greaseless taps. Pressures were measured on calibrated Baraton gauges (100 Torr MKS 222, A 1000 Torr MKS 122 AA).

Pure HNO_3 was vacuum distilled from a 3:2 mixture of previously cooled sulphuric acid (Fisons 98%) and nitric acid (Kock-Light 70%) held at 273 K, into a trap cooled in liquid nitrogen. Several successive distillations were then performed, a middle fraction being retained in a trap cooled to 195 K (solid CO_2). The product was a white crystalline solid at this temperature.

When HNO_3 vapour was introduced to the sample cell from the reservoir, variable amounts of NO_2 impurity were found to be present, the amount relative to HNO_3 tending to decrease in successive samples. Clearly some decomposition of the HNO_3 occurred both in the sample and in the transfer process. Absorption cross-sections were determined from data collected with relatively low levels of NO_2 present, typically of the order of 0.5%. Even so, NO_2 absorption accounted for at least 50% of the sample absorbance at 320 nm.

Some absorption measurements were made at room temperature using HNO_3 vapour taken from a sample of reagent grade concentrated HNO_3 which had not been distilled from a mixture with sulphuric acid. These samples contained lower amounts of NO_2 (approximately 0.02%) compared with the "pure" HNO_3 . Absolute cross-sections could not be determined from these measurements because the samples contained an unknown amount of water vapour, together with HNO_3 . However HNO_3 spectra obtained from these samples showed no systematic difference from those derived after subtraction of larger amounts of NO_2 .

A reference sample of NO_2 was prepared by reaction of NO (Cambrian Gases, Research grade) with O_2 (B.O.C., Research grade) and stored in a blackened 3 l bulb.

Methyl nitrate was synthesized by the low temperature nitration of methanol [11]. The authenticity of the liquid product after vacuum distillation was verified by ^1H nuclear magnetic resonance and from Fourier transform IR spectroscopy. The purity of the sample was assessed at greater than 99%; no NO_2 could be seen in the gas phase UV spectra.

3. Results

3.1. Nitric acid

Measurements of HNO_3 absorption spectra in the wavelength ranges 200–275 nm and 269–344 nm were made at several different temperatures in the range 238–297 K. At each temperature, several pressures of HNO_3 were used up to a maximum somewhat less than the vapour pressure of HNO_3 at that temperature. This limited the HNO_3 pressure to approximately 0.8 Torr at the lowest temperature (238 K) and to about 35 Torr at room temperature. Consequently, the accuracy with which small absorptions in the long-wavelength tail could be measured was considerably reduced at the lower temperatures. However, the very large absorption cross-sections in the short-wavelength region (less than 220 nm) could not be determined accurately because of the difficulty in the measurement of the small partial pressures of HNO_3 required, together with inaccuracies related to the low light levels transmitted by the optical fibres at shorter wavelengths. Consequently, we do not report cross-section measurements at wavelengths below 220 nm.

All HNO_3 spectra in the 269–344 nm region required correction for the NO_2 present in the sample. This correction was based on scaled subtraction of a reference spectrum of NO_2 , utilizing the characteristic vibrational structure in the NO_2 absorption near 340 nm. In these corrections, account had to be taken of the presence of N_2O_4 which is in equilibrium with NO_2 . Based both on the known equilibrium constant [12] and on measurements of the NO_2 reference spectrum at different NO_2 partial pressures, the amounts of NO_2 were generally too small for significant N_2O_4 absorption in this region, even at the lower temperatures. Nevertheless, reference spectra were recorded at each temperature to match as closely as possible the actual amounts of NO_2 present in the samples so that any N_2O_4 absorption could be accounted for.

Figure 1 illustrates a typical HNO_3 spectrum recorded at 294 K with $P(\text{HNO}_3) = 29.8$ Torr in the long-wavelength region, together with the scaled NO_2 reference and the residual after its subtraction. At HNO_3 pressures below approximately 5 Torr, the residual absorbance at greater than 340 nm was not significantly greater than the baseline drift of approximately ± 0.0005 absorbance units. At higher pressures of HNO_3 , a small continuous level of absorption, which generally increased with HNO_3 pressure, could be detected up to at least 370 nm. A similar effect was noticed with high pressures of methyl nitrate, and is thought to be due to the presence of a low level of UV light of shorter wavelengths scattered within the spectrograph. This residual continuous absorption, which was of the order of 0.001 absorbance units, was subtracted assuming that HNO_3 absorption near 345 nm was negligible.

At each temperature, data from at least five experiments at different HNO_3 pressures were averaged to give the absorption cross-sections at 0.15 nm intervals. The standard deviations on the average values at 293 K were approximately 2.5% for

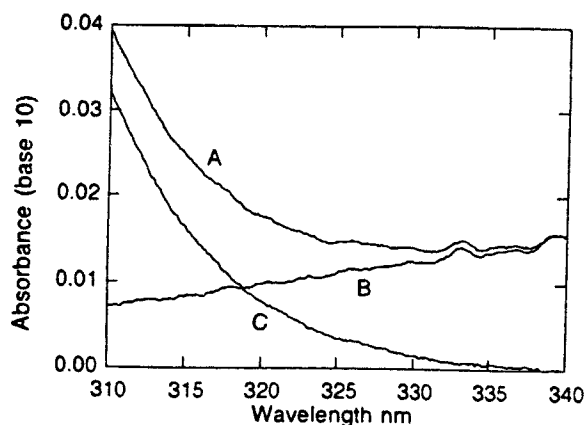


Fig. 1. Absorption spectrum of HNO_3 in the region 310–340 nm: A, spectrum from 29.8 Torr HNO_3 at 294 K; B, reference spectrum for 0.017 Torr NO_2 at 294 K; C, residual after subtraction of B from A.

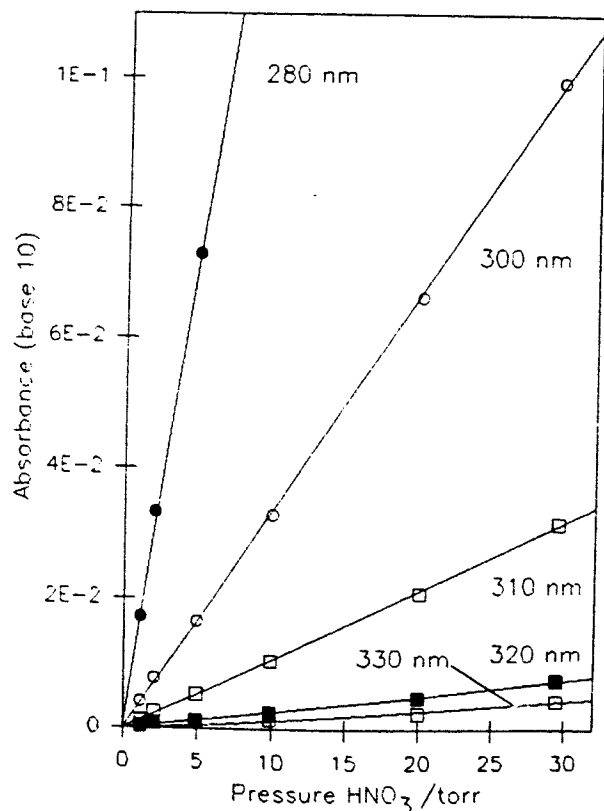


Fig. 2. Beer-Lambert law plot of nitric acid absorbance at 294 K after correction for the NO_2 component.

wavelengths less than 300 nm, increasing to 95% near the limit of measurable absorption at about 335 nm. At 239 K the standard deviation was 6.5% at 300 nm increasing to 95% at 320 nm. Conformity with the Beer-Lambert law was excellent provided the absorbance was less than unity; selected data are presented in Fig. 2. Figure 3 illustrates the temperature dependence of the HNO_3 cross-sections recorded in the 269–344 nm

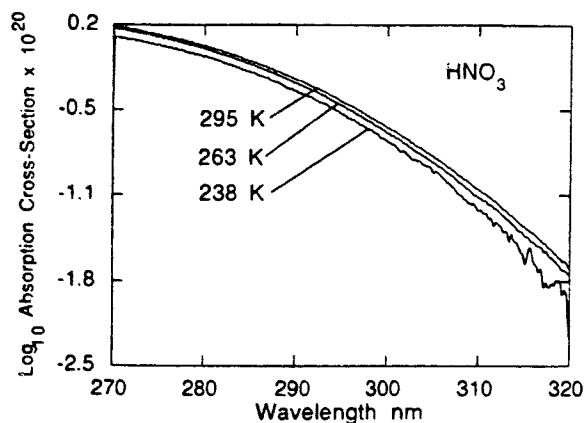


Fig. 3. Temperature dependence of the nitric acid absorption cross-section in the wavelength region 270–325 nm.

TABLE 1

Absorption cross-sections for HNO_3 and CH_3ONO_2

Wavelength (nm)	Cross-section σ ($\times 10^{20}$ cm ² per molecule)			
	HNO_3		CH_3ONO_2	
	293 K	239 K	294 K	238 K
220	12.34	9.92	66.8	52.9
225	7.73	6.23	29.3	26.23
230	5.15	4.28	15.7	13.1
235	3.44	3.29	9.00	7.28
240	2.43	1.87	5.57	4.40
245	2.00	1.54	4.07	3.16
250	1.88	1.52	3.68	2.67
255	1.82	1.55	3.27	2.56
260	1.84	1.55	3.08	2.37
265	1.73	1.47	2.76	2.12
270	1.55	1.29	2.31	1.89
275	1.36	1.13	1.96	1.56
280	1.08	0.885	1.55	1.22
285	0.821	0.668	1.17	0.914
290	0.587	0.471	0.842	0.639
295	0.394	0.311	0.562	0.410
300	0.247	0.190	0.357	0.250
305	0.145	0.109	0.207	0.140
310	0.0794	0.055	0.155	0.0761
315	0.0407	0.025	0.0584	0.0352
320	0.0198	0.011	0.0279	0.0118
325	0.0092	0.0052	0.0118	0.0054
330	0.0042	0.0010	0.0052	0.0020
335	0.0014	—	0.0015	—

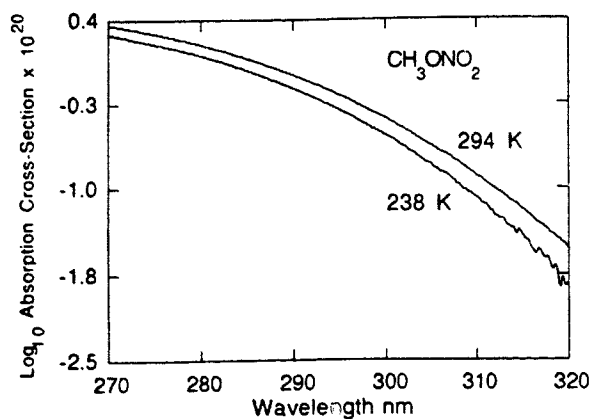


Fig. 4. Temperature dependence of the methyl nitrate absorption cross-section in the wavelength region 270–320 nm.

region, using the data at 238 K, 263 K and 295 K. The spectra show a clear decline in the cross-section with decreasing temperature throughout the region, the effect being particularly noticeable near the long-wavelength tail. The temperature dependence also extends into the shorter-wavelength region, as can be seen from the cross-sections at 293 K and 239 K listed in Table 1.

3.2. Methyl nitrate

Measurements of methyl nitrate absorption spectra were made in the wavelength ranges 200–276 nm and 269–344 nm at 233, 238, 248 and 294 K. As with HNO_3 the maximum pressures that could be used were limited by the vapour pressure of CH_3ONO_2 at each temperature. However, the higher vapour pressures and absence of NO_2 contamination allowed more accurate measurements of the weak absorption in the long-wavelength tail, compared with HNO_3 . The temperature dependence of the CH_3ONO_2 spectrum is illustrated in Fig. 4 using the data at 238 K and 294 K listed in Table 1. The absorption cross-section decreases with decreasing temperature throughout the wavelength range; the magnitude of the temperature effect is similar to that of nitric acid.

4. Discussion

4.1. Comparison with previous work

The HNO_3 absorption cross-sections measured at 294 K in the present work are compared with previously reported values in Fig. 5. At wavelengths less than 300 nm they show very good agreement with those reported by Molina and Molina [5], Biauume [2] and Graham and Johnston [6]. Table 2 shows a comparison of the values in the long-wavelength tail. The values obtained in the present work are higher than those reported by Biauume [2] and those of Molina and Molina [5], but are lower than those reported by Graham and Johnston [6]. It is difficult to state how significant these differences are in view of the uncertainty arising from the need to correct for absorption due to NO_2 at these wavelengths. The present experimental technique provides more spectral information for making this correction, but our samples apparently contained

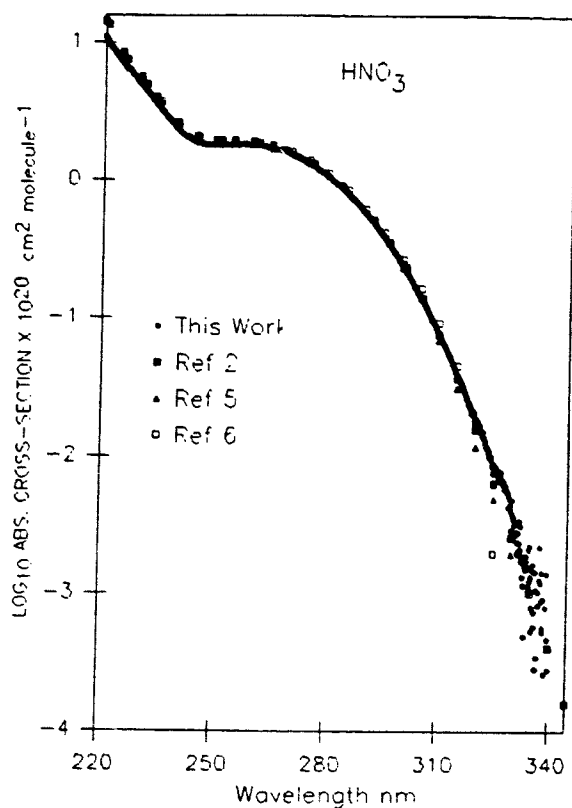


Fig. 5. Absorption spectrum of HNO_3 at room temperature; comparison of present results (\bullet) with those of Molina and Molina [5] (\blacktriangle), Biaueme [2] (\blacksquare) and Graham and Johnston [6] (\square).

TABLE 2

Comparison with cross-sections from previous work

Wavelength (nm)	Cross-section σ ($\times 10^{20}$ cm^2 per molecule) at 298 K					
	HNO_3				CH_3ONO_2	
	This work	Ref. 2	Ref. 5	Ref. 6	This work	Ref. 8
270	1.55	1.59	1.59	1.63	2.31	2.43
300	0.247	0.241	0.241	0.276	0.357	0.354
310	0.079	0.079	0.071	0.095	0.115	0.123
320	0.020	0.016	0.012	0.018	0.028	0.035
330	0.004	0.003	0.002	0.0002	0.005	0.012

more NO_2 than those measured by Biaueme [2]. Molina and Molina [5] did not report details of any corrections they made. The consistency of the cross-sections determined in the present work with differing amounts of NO_2 gives us some confidence in the values we report, which suggest a slightly higher absorption at wavelengths greater

than 310 nm than is recommended in the NASA and IUPAC evaluations [3, 4], which were based on the data of Molina and Molina [5].

Figure 6 shows a comparison of the present absorption cross-section measurements for methyl nitrate with literature values. They show excellent agreement with those reported by Roberts and Fajer [8] in the region of atmospheric interest, *i.e.* at wavelengths greater than 270 nm. The earlier data of Taylor *et al.* [9] are significantly higher in this region, by up to a factor of 2. At shorter wavelengths all the reported data are in reasonably good agreement.

4.2. Temperature dependencies

There are apparently no previous measurements of the temperature dependence of either the HNO_3 or CH_3ONO_2 absorption spectra with which to compare our results. The present results show that both molecules have similar spectra, their absolute cross-sections are comparable and their temperature dependences match well. This is not altogether surprising since the $-\text{ONO}_2$ chromophore is responsible for absorption in both molecules. The similarity in the temperature dependences is illustrated in Fig. 7 where $\log_{10} \sigma$ is plotted against temperature for selected wavelengths in the "tail" of the UV absorption band. The intercepts and slopes of these plots, obtained by linear regression analysis, are given in Table 3. The slopes of these plots are similar and increase with increasing wavelength. There is more scatter on the HNO_3 data owing to the smaller absorptions and the necessity to correct for NO_2 interference. At less than 270 nm the temperature coefficients remained fairly constant down to

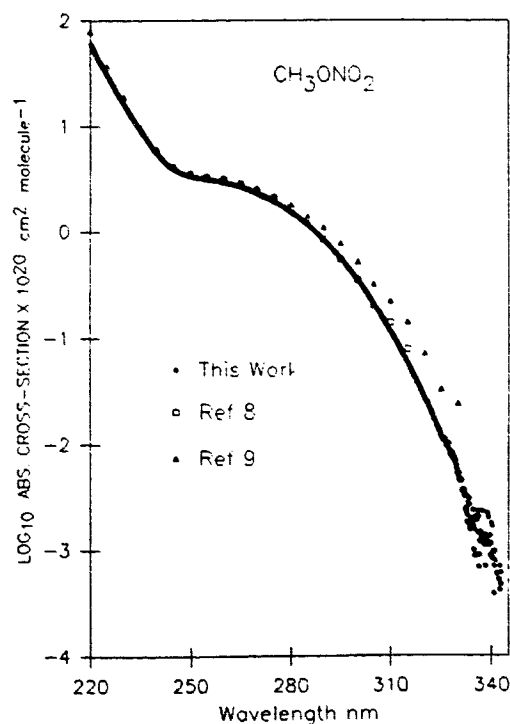


Fig. 6. Absorption spectrum of CH_3ONO_2 at room temperature; comparison of present results (\bullet) with those of Roberts and Fajer [8] (\square) and Taylor *et al.* [9] (\blacktriangle).

0 0 4 0

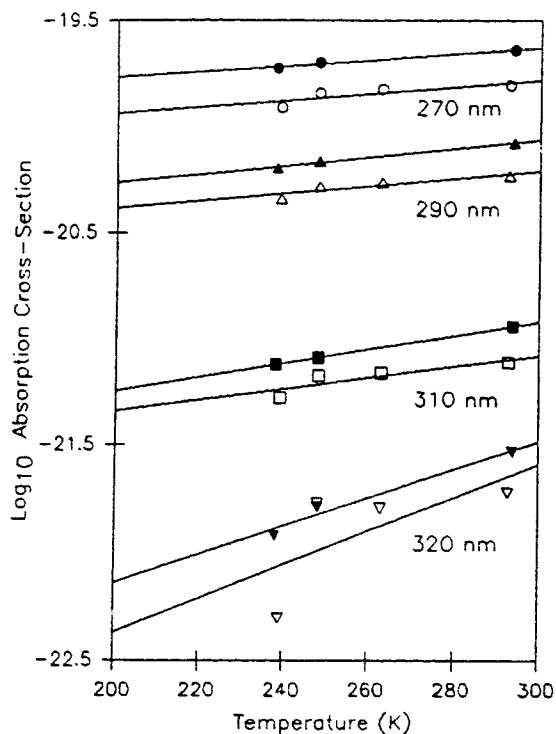


Fig. 7. Plot of the logarithm of the absorption cross-section at selected wavelengths against temperature for methyl nitrate (closed symbols) and nitric acid (open symbols). The lines show least squares linear regression slopes.

TABLE 3

Temperature dependence of HNO_3 and CH_3ONO_2 absorption cross-sections

Wavelength (nm)	σ_0 ($\times 10^{21}$ cm ² per molecule) ^a		B ($\text{K}^{-1} \times 10^3$) ^a	
	HNO_3	CH_3ONO_2	HNO_3	CH_3ONO_2
270	6.35	8.75	4.16	3.31
280	4.31	4.85	3.54	3.95
290	1.39	2.17	5.33	4.62
300	0.73	0.63	4.64	5.90
310	0.088	0.129	9.23	7.42
320	0.0012	0.0035	17.8	15.1
330	—	0.0009	—	13.7

^aIntercept and slope of plot of $\log_{10} \sigma = \log_{10} \sigma_0 + BT$

the start of the second absorption band near 230 nm, whereafter the temperature dependence declined.

The temperature coefficients from the plots of $\log_{10} \sigma$ vs. T can be used to obtain cross-sections outside the experimental range by extrapolation. This is particularly important for the purposes of calculating the photodissociation rate of HNO_3 at

temperatures relevant to the polar stratosphere. Table 4 shows recommended cross-sections at 298 K, which were obtained by averaging the data from the present work with those from refs. 2, 5 and 6, together with the recommended temperature coefficients based on the present work. The absorption cross-section can be calculated for any temperature from the equation:

$$\log_{10} \sigma = \log_{10} \sigma_{298} + B[T - 298]$$

The linear dependence of the cross-section used for extrapolation does not have any theoretical basis. The shape of the nitrate spectra indicates that two or more electronic transitions are involved, with overlapping absorption bands. The integrated absorption in a single band is expected to show little temperature dependence on theoretical grounds [13]. The increase in cross-section in the wings of the band is compensated for by a decrease at the band maximum, as the band broadens with increasing temperature, owing to the increasing number of rotational-vibrational states available. In regions of overlap these effects can act in opposite directions. Thus the positive temperature dependence of the HNO_3 and CH_3ONO_2 cross-sections in the "shoulder" region near 260 nm could be due to the predominant influence of the tail of the strong absorption band centred at less than 200 nm.

4.3. Calculation of atmospheric photolysis rate

Atmospheric photolysis rates of HNO_3 were computed using the absorption cross-sections shown in Table 4, over a range of temperatures, altitudes and solar zenith angles (SZAs). For these calculations, which were carried out using the photolysis model of Lary [14], atmospheric profiles of temperature and ozone appropriate to 70° N in winter were used. The model includes the effects of multiple scattering in a spherical horizontally stratiform atmosphere. The calculations were performed for a ground albedo of 0.3, although the effects of clouds were not considered. The quantum

TABLE 4
Recommended cross-sections for HNO_3

Wavelength (nm)	Cross-section at 298 K ($\times 10^{20} \text{ cm}^2 \text{ molecule}^{-1}$)	B ($\text{K}^{-1} \times 10^3$)
190	1560.0	0
200	661.0	0
210	105.0	2.5
220	14.1	2.5
230	5.45	3.5
240	2.44	3.5
250	1.92	3.5
260	1.86	3.5
270	1.59	3.5
280	1.10	3.5
290	0.613	4.5
300	0.243	6.0
310	0.081	9.0
320	0.017	18.0
330	0.003	> 18.0

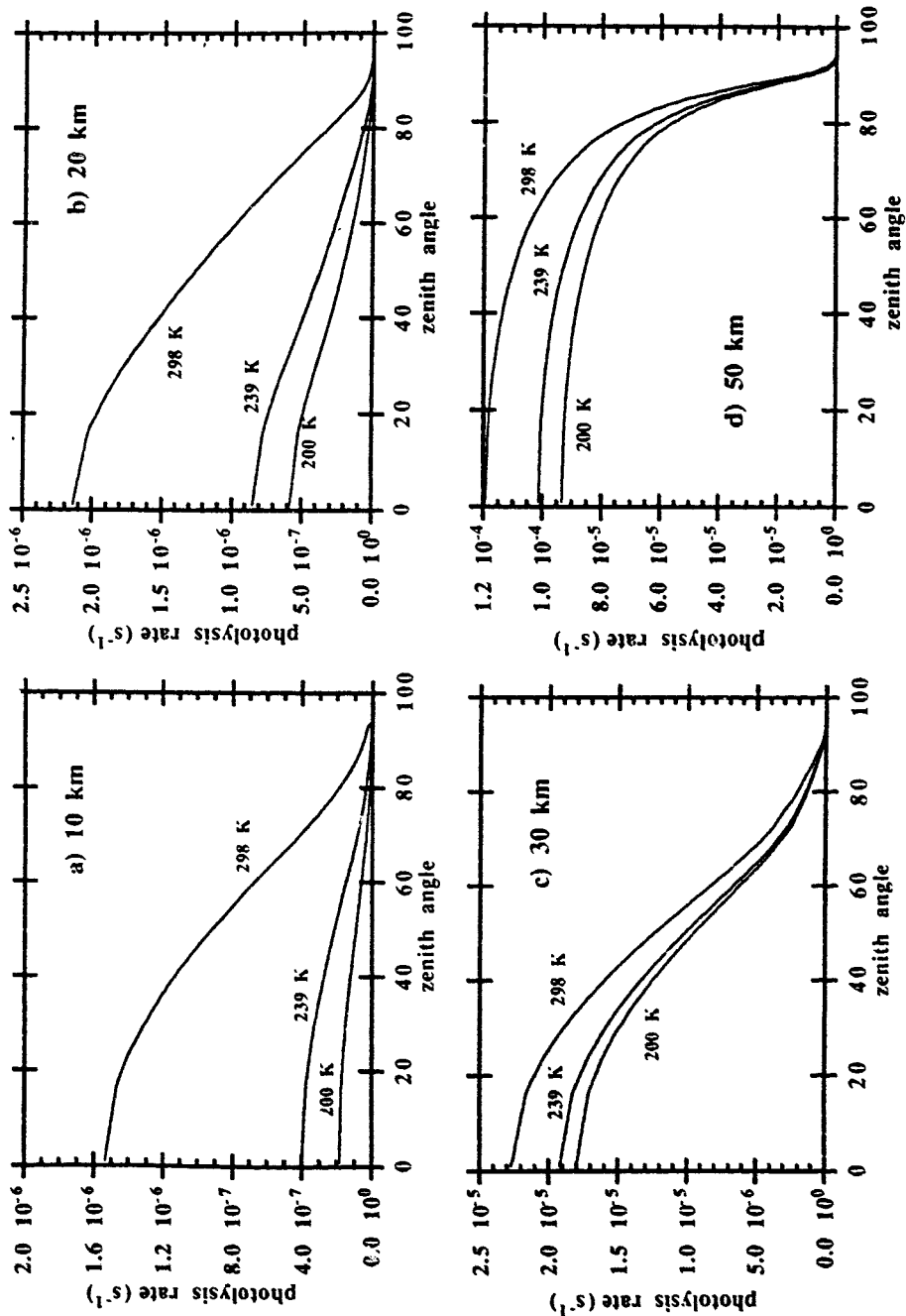


Fig. 8. Dependence of the atmospheric photodissociation rate of HNO_3 on SZA and temperature at four different altitudes.

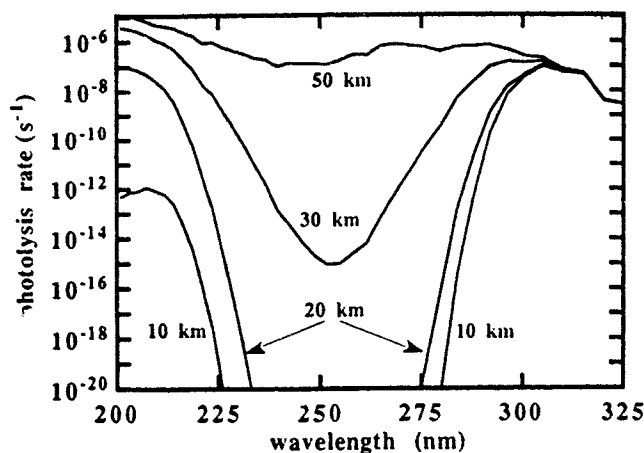


Fig. 9. Contribution of different wavelength intervals to HNO_3 photolysis as a function of altitude: $J(\text{HNO}_3)$ is given for a temperature of 200 K and an SZA of 0° .

yield for HNO_3 photodissociation was assumed to be unity throughout the wavelength region of interest.

The results are shown in Figs. 8 and 9. In Fig. 8 the calculated HNO_3 photolysis rates for SZAs between 0° and 100° at 10, 20, 30 and 50 km altitude, and at temperatures between 200 and 298 K, are presented. At all altitudes and SZAs the photolysis rates show a significant monotonic decrease at colder temperatures. However, the decline is more marked at lower altitudes with a 25% difference between $J(\text{HNO}_3)$ at 298 K and 200 K at 50 km and 0° SZA, increasing to 85% at 10 km. This difference increases at higher SZAs.

These features can be explained as follows. The temperature dependence of the HNO_3 cross-section is more marked at longer wavelengths, see Fig. 7. At both lower altitudes and higher SZAs the stratospheric absorption, due primarily to ozone, shifts the wavelengths which contribute to photolysis of HNO_3 to longer wavelengths, at which the absorption shows greater temperature dependence.

The relative contribution at different wavelengths to the total photolysis of HNO_3 is illustrated in Fig. 9. The data shown are calculated for a solar zenith angle of 0° and a temperature of 200 K. It is evident that at high altitude (50 km) the contribution of light absorption near 200 nm is greater than 300 nm. At altitudes of 20 km and below, photolysis predominantly results from absorption at wavelengths longer than 300 nm. Peak photolysis occurs at 310 nm for 0° SZA and the peak moves to even longer wavelengths at larger SZAs. As absorption at longer wavelengths becomes more important, the significance of the temperature dependence increases. An implication of these results is that the lifetime of HNO_3 with respect to photodissociation releasing NO_2 (reaction 2), at the low temperatures prevalent in the lower stratosphere, is longer than calculated using currently recommended values for the HNO_3 absorption cross-sections [3, 4]. Consequently the rate of "recovery" of the perturbed chemistry in air parcels which have been exposed to PSCs or sulphate aerosols is expected to be slower. This would allow a greater extent of ozone depletion to occur in these air parcels, through the established photochemical reaction mechanisms involving ClO.

These results highlight the need to determine accurately the temperature dependence of the absorption cross-sections in the long-wavelength tail. Unfortunately, the absorption of HNO_3 and other molecules of atmospheric significance is very weak in this region and accurate cross-section measurements present a considerable challenge,